Wissenschaftszentrum Weihenstephan für Ernährung, Landnutzung und Umwelt

Molecular interactions in chocolate and their impact on rheology – a molecular dynamics approach

Moritz Kindlein

Vollständiger Abdruck der von der Fakultät
Wissenschaftszentrum Weihenstephan für Ernährung, Landnutzung und Umwelt
der Technischen Universität München zur Erlangung des akademischen Grades
eines Doktor-Ingenieurs
genehmigten Dissertation.

Vorsitzende/-r: Prof. Dr. Horst-Christian Langowski

Prüfende/-r der Dissertation:

1. Prof. Dr.-Ing. Heiko Briesen

2. Prof. Dr. Julija Zavadlav

Die Dissertation wurde am 17.04.2019 bei der Technischen Universität München
eingereicht und durch die Fakultät
Wissenschaftszentrum Weihenstephan für Ernährung, Landnutzung und Umwelt
am 30.03.2020 angenommen.

Acknowledgments

At first I would like to express my sincere gratitude to my supervisor Heiko Briesen for giving me the opportunity to do the research presented in this dissertation. He always had an open ear and helped out immediately when his guidance was required. Not only did he give direct input to the asked questions but often gave a new perspective on the presented problem itself. He managed to build up a great team spirit and friendly atmosphere at his institute, making it a familiar and enjoyable workplace.

Exceptional gratitude goes to Ekaterina Elts and Maximilian Greiner who always were available for help during their daily business over the years of the work on this thesis.

Special thanks goes to Michael Kuhn, Frederik Luxenburger, Philip Schmid, and Stefan Schmideder who helped in proof reading of the presented thesis. In addition to the already mentioned, I would like to thank all further colleagues I had the honor to work with.

I further thank all the students I had the opportunity to supervise during their theses. Many fruitful discussions contributed to the presented dissertation. Special thanks goes to Melanie Portz, who contributed to the simulation studies presented in Section 5.3.3 during her master's thesis.

Finally, I would like to thank my family and my friends: my parents, who always have supported me during my whole life; my twin brother Julian, who is just the best brother one could imagine; my friends, who are always there for me; my wife Theresa and my daughter Josefine, I simply couldn't imagine life without you.

Parts of this research project were carried out in the framework of the industrial collective research programme (AiF 19745 N). It was supported by the Federal Ministry for Economic Affairs and Energy (BMWi) through the AiF (German Federation of Industrial Research Associations eV) based on a decision taken by the German Bundestag. The author gratefully acknowledges the compute and data resources provided by the Leibniz Supercomputing Centre.

Abstract

The presented dissertation explores different molecular interactions in chocolate in order to give mechanistic explanations for the rheological behavior of chocolate. This is done by performing molecular dynamics simulations of the relevant components of the molecular complex food system chocolate.

In the first study, different phospholipids, which are the main molecular components of lecithin, are examined in terms of their strength of interaction with crystalline sucrose at the interface to cocoa butter. Phospholipids are known to lower yield stress and viscosity when they are attached at this interface. Non-equilibrium pull-code simulations are used to detach six different phospholipids from the sucrose crystal surface in order to calculate the detachment work for the hydrophilic head groups of the phospholipids. The forced detachment models the reversed process of lecithin adsorption on sucrose crystal surfaces during chocolate conching. The related detachment work is thus a characteristic magnitude for the different phospholipid head groups. The detachment work of phospholipids with the head groups phosphatidylcholine, phosphatidylethanolamine, and phosphatidylinositol from the (100) sucrose crystal surface is calculated. Molecules with phosphatidylinositol head group are shown to require the biggest detachment work, followed by phosphatidylcholine with medium detachment work, and phosphatidylethanolamine with the lowest detachment work. The number of hydrogen bonds between the head group and sucrose is shown to correlate with the detachment work and the detachment mechanism is analyzed in detail.

In the second study, concentration-dependent phospholipid structures are calculated and used to give mechanistic explanations for known rheological behavior of chocolate. The increase of yield stress after adding an excessive dose of lecithin could be linked to specific micellar structures of phospholipids in chocolate. It is shown that phospholipids that are not adsorbed in the monolayer between sucrose particles and cocoa butter assemble in spherical, cylindrical, and wormlike micelles in cocoa butter, depending on the phospholipid concentration. The possibility of formation of hydrophilic bridges between sucrose particles is shown and further linked to the sucrose particle shape, as these bridges are primarily observed on kinks and edges of the sucrose particles. The influence of the degree of saturation of the phospholipid aliphatic chains on the area per lipid in the monolayer between sucrose particles and cocoa butter is investigated. Unsaturated phospholipids are shown to have a higher area per lipid.

In the third study, cocoa butter immobilization on sucrose crystal surfaces, which is assumed to be a reason for the high viscosity of chocolate, is explored by investigating the molecular interactions between cocoa butter triglycerides and crystalline sucrose. Lateral diffusion coefficients for cocoa butter triglycerides on a crystalline sucrose surface are compared to those of pure cocoa butter triglycerides. It is shown that the diffusion coefficients of cocoa butter triglycerides on the surface of crystalline sucrose are lower than of pure cocoa butter triglycerides. The mobility of single cocoa butter triglycerides in direct contact to the sucrose surface is compared to those not in direct contact. It is shown that the cocoa butter triglycerides are immobilized when the glycerol backbone is adsorbed at the sucrose surface.

Throughout the thesis, the usage of molecular dynamics simulations for investigation of complex food systems in order to gain food process engineering relevant insights is promoted. Typical methodological restrictions and challenges for the usage in a food related context are discussed and possible solutions are shown.

Kurzfassung

In der vorgelegten Dissertation werden verschiedene molekulare Interaktionen in Schokolade untersucht, um mechanistische Erklärungen für das rheologische Verhalten von Schokolade geben zu können. Dazu werden molekulardynamische Simulationen der relevanten Bestandteile des molekular komplexen Lebensmittels Schokolade durchgeführt.

In der ersten Studie werden unterschiedliche Phospholipide, welche die hauptsächlichen molekularen Bestandteile von Lecithin darstellen, hinsichtlich der Stärke ihrer Interaktion mit kristalliner Saccharose an der Grenzfläche zu Kakaobutter untersucht. An dieser Grenzfläche angelagert, reduzieren Phospholipide die Fließgrenze und Viskosität von Schokolade. Sogenannte pull-code Simulationen außerhalb des thermodynamischen Gleichgewichts werden durchgeführt, um sechs unterschiedliche Phospholipide von der Saccharoseoberfläche abzulösen und die Ablösearbeit der hydrophilen Kopfgruppen der Phospholipide zu berechnen. Das gezielte Ablösen stellt den umgekehrten Prozess der Lecithinanlagerung an Saccharoseoberflächen während des Conchierens dar. Die dazugehörige Ablösearbeit ist somit ein charakteristisches Maß für die verschiedenen Phospholipidkopfgruppen. Die Ablösearbeit wird für Phospholipide mit den Kopfgruppen Phosphatidylcholin, Phosphatidylethanolamin und Phosphatidylinositol von der (100) Saccharoseoberfläche berechnet. Moleküle mit Phosphatidylinositolkopfgruppen benötigen die größte Ablösearbeit, gefolgt von Phosphatidylcholin mit mittlerer Ablösearbeit und Phosphatidylethanolamin mit der niedrigsten Ablösearbeit. Die Anzahl an Wasserstoffbrückenbindungen zwischen den Kopfgruppen und der Saccharose korreliert mit der Ablösearbeit und der Ablösemechanismus wird im Detail analysiert.

In der zweiten Studie werden konzentrationsabhängige Strukturen von Phospholipiden berechnet und verwendet, um mechanistische Erklärungen für bekanntes rheologisches Verhalten von Schokolade zu geben. Der Anstieg der Fließgrenze nach Zugabe einer überhöhten Menge von Lecithin wird mit spezifischen mizellaren Phospholipidstrukturen in Schokolade in Verbindung gebracht. Es wird gezeigt, dass sich Phospholipide, welche nicht in der Monoschicht zwischen Saccharosepartikeln und Kakaobutter adsorbiert sind, zu sphärischen, zylindrischen und wurmartigen Mizellen in Kakaobutter zusammenlagern, abhängig von der Lecithinkonzentration. Die Möglichkeit zur Bildung von hydrophilen Brücken zwischen Saccharosepartikeln wird gezeigt und darüber hinaus mit der Form der Saccharosepartikel in Verbindung gebracht, da diese Brücken vor allem an Kanten und Ecken der Saccharosepartikel

beobachtet werden. Der Einfluss des Sättigungsgrads der aliphatischen Ketten der Phospholipide auf die Fläche pro Phospholipid in der Monoschicht zwischen Saccharosepartikeln und Kakaobutter wird untersucht. Es wird gezeigt, dass ungesättigte Phospholipide eine höhere Fläche pro Phospholipid einnehmen.

In der dritten Studie wird die Kakaobutterimmobilisierung an Saccharosekristalloberflächen, welche als ein Grund für die hohe Viskosität von Schokolade angesehen wird, untersucht, indem die molekularen Interaktionen zwischen Kakaobuttertriglyceriden und kristalliner Saccharose untersucht werden. Laterale Diffusionskoeffizienten der Kakaobuttertriglyceride an der Oberfläche von kristalliner Saccharose werden mit dem von reinen Kakaobuttertriglyceriden verglichen. Es wird gezeigt, dass die Diffusionskoeffizienten der Kakaobuttertriglyceride an der Oberfläche von Saccharosekristallen niedriger sind als der von reinen Kakaobuttertriglyceriden. Die Mobilität von einzelnen Kakaobuttertriglyceriden in direktem Kontakt zu der Saccharoseoberfläche wird mit denen verglichen, welche nicht in direktem Kontakt sind. Es wird gezeigt, dass die Kakaobuttertriglyceride stark immobilisiert sind, wenn das Glycerinrückgrat an der Saccharoseoberfläche adsorbiert ist.

Durchgehend durch die Arbeit werden die Möglichkeiten von molekulardynamischen Simulationen für die Untersuchung von komplexen Lebensmittelsystemen gezeigt, um lebensmittelverfahrenstechnisch relevante Einblicke zu bekommen. Typische methodische Einschränkungen und Herausforderungen für die Verwendung in einem lebensmittelbezogenen Kontext werden diskutiert und mögliche Lösungen werden aufgezeigt.

Contents

List of Figures

List of Tables

Symbols and abbreviations

Latin Symbols

$\boldsymbol{a}$	Acceleration
A	Arbitrary system property
b	Herschel–Bulkley model parameter
d	Average inter-atomic spacing
D	Diffusion coefficient
e	Euler's number
E	Energy
f	Dimensionless empirical parameter
F	Helmholtz free energy
$\boldsymbol{F}$	Force
g	Radial distribution function
G	Gibbs free energy
i	Imaginary unit
k	Particle shape factor
k_B	Boltzmann constant
K	Force constant
m	Mass
M_R	Mapping operator
n	Number of particles
n	Multiplicity
N	Number of particles
N_f	Number of the degrees of freedom
p	Pressure
$\boldsymbol{p}$	Momentum
q	Electric charge
$\boldsymbol{q}$	Generalized coordinate
Q	Partition function
r	Distance
$\boldsymbol{r}$	Cartesian coordinate
r_i	Radius of inner space of a molecule
R_i	Van der Waals radius
$\boldsymbol{R}_{CG}$	Position of coarse-grained beads

S	Entropy
SA	Solvent accessible surface area
t	Time
T	Temperature
$\boldsymbol{v}$	Velocity
V	Volume
var	Variance
w_{ens}	Non-normalized probability density
W	Non-equilibrium work

Greek Symbols

α	Born radius
β	Reciprocal of the product of Boltzmann constant and Temperature
γ	Empirical surface tension parameter
Γ	Phase space
$\dot{\gamma}$	Shear rate
$\dot{\gamma}^*$	Model parameter of the Windhab model
δ	Orientation parameter of non-spherical particles
δ	Kronecker delta
δ	Dirac delta
ε	Permittivity
ε_{ij}	Lennard-Jones potential parameter
η	Viscosity
$[\eta]$	Intrinsic viscosity
Θ	Angle
Λ	De-Broglie wave length
ρ_{ens}	Normalized probability density
ρ_0	Average particle number density
σ_{ij}	Lennard-Jones potential parameter
τ	Shear stress
τ_0	Yield stress
φ	Dihedral angle
Φ	Particle volume fraction
Ψ	Changes in surface and volume immobilized fluid volume before and after shearing
$\Psi^{(c,e)}$	Wave function that describes the quantum state of the cores c and the electrons e

Other

$\hbar$	Planck constant
$\mathscr{H}$	Hamiltonian
$\mathscr{K}$	Kinetic energy
$\mathscr{L}$	Lagrangian
$\mathscr{V}$	Potential energy

Accents

$\langle\rangle$	Averaged quantity
$\dot{}$	Time derivative

Chapter 1

Introduction

1.1 Motivation

Chocolate is probably one of the most passionately and emotionally consumed foods in the world. It is well tasting and with its fine sweetness and its tender melt appreciated by many. Among foods, it has the unique property that it is solid at room temperature and melts almost immediately in the mouth with a very distinct melting point, leaving a gentle cooling sensation. Typical aromatic descriptors of chocolate range from roasted and nutty to fruity and floral and can be more or less pronounced, depending on the ingredients and the manufacturing process [69]. Although chocolate has been properly manufactured with a great background of knowledge and a lot experience for several decades, there is still room and urge for research in many chocolate-related topics. These range from health aspects of chocolate consumption [90], over understanding and improvement of process steps of manufacturing [51] and keeping the product stable for a long shelf live [67], to developing heat resistant chocolate for the tropic and subtropic parts of the world [127, 128]. Like many other food process engineering related questions, the majority of these problems is governed by molecular interactions leading to certain macroscopic effects. Unfortunately, due to the high complexity of the molecular scale and the difficult experimental accessibility of phenomena on this scale, it is often not in the direct focus of food process engineers [56, 78]. This thesis is driven by the desire to understand the molecular behavior of lecithin during chocolate manufacturing, especially during the conching process, and the phenomenon of cocoa butter immobilization, which both influence chocolate rheology and final product properties. It is a step towards molecular tailoring or purposeful choice of emulsifiers in chocolate manufacturing. Further, this thesis is driven by the desire to promote the use of molecular dynamics simulations to gain food process engineering relevant insights. Besides the presented results that can be seen as an example of how to use molecular dynamics simulations for answering questions in the field of food process engineering, crucial aspects of employing the method in this field are elucidated and different approaches to overcome typical problems, such as limitations in time and length scales, are shown.

1.2 Fundamental interactions in chocolate with impact on rheology

1.2.1 Process–structure–property relationship in chocolate rheology

From a food process engineering point of view, chocolate is a lipophilic suspension with a high concentration of particles during its manufacturing process. The continuous matrix is molten cocoa butter, consisting mainly of triglycerides, the dispersed particles are sucrose and cocoa particles, in the case of dark chocolate [12]. Lecithin, a mixture of surface active molecules, is added to adjust the flow properties of liquid chocolate mass and is the active ingredient, which is in the main focus of the investigations of this thesis.

Many phenomena and processes in food process engineering can be described by the *process–structure–property* relationship, which is shown in Figure 1.1. In the specific case of lecithin usage in chocolate manufacturing, the *process* can differ in the type and amount of used lecithin. This leads to different molecular *structures* in the liquid chocolate mass especially at hydrophilic–hydrophobic interfaces, depending on type and amount of lecithin. This again leads to different *properties* of the system, such as the change in viscosity and yield stress.

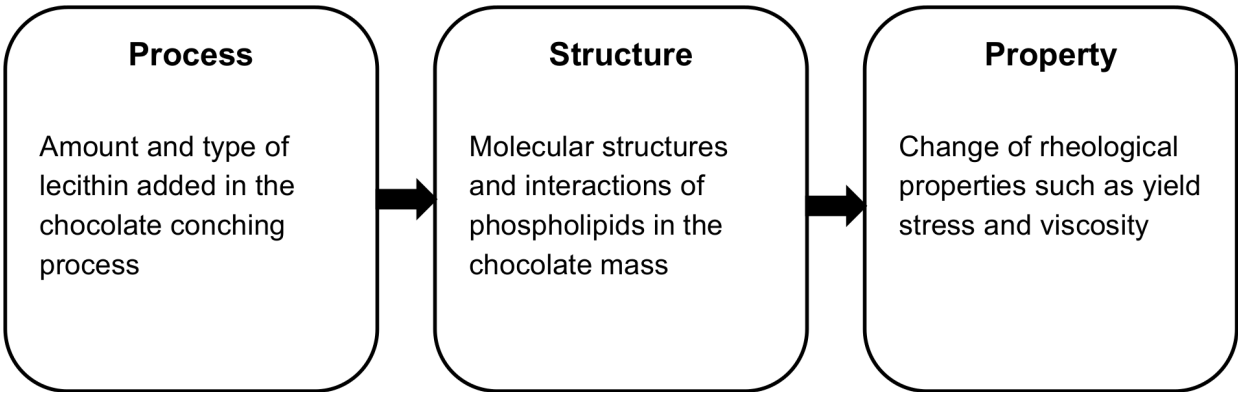

Figure 1.1: *Process–structure–property* relationship for the usage of lecithin in chocolate manufacturing.

Reducing viscosity and yield stress of liquid chocolate mass during the manufacturing process of chocolate is the main reason for using lecithin [12]. Lecithins are mixtures of phospholipids, mono- and diglycerides, triglycerides and other minor components. It is commonly agreed upon that phospholipids are the most important components of lecithin as they are strongly amphiphilic molecules that are known to adsorb at hydrophilic–hydrophobic interfaces. The most important hydrophilic phospholipid head groups of lecithins are phosphatidylcholine, phosphatidylethanolamin, phosphatidylinositol, and phosphatidic acid as they are the major part of phospholipid head groups [81, 101]. The aliphatic tail groups consist of a mixture of saturated, monounsaturated, and polyunsaturated fatty acids [101], where chain lengths of 16 to 18 carbon atoms are most common [99]. Traditionally, lecithin from soybeans is used in

chocolate manufacturing [12]. As soybean is more and more grown as a genetically modified organism the demand for alternative lecithin sources, such as sunflower and rapeseed, has grown steadily in the past decades on the European market. While all these sources primarily contain the same molecular components, they can vary in their concentration [101]. Further, weather and climatic influences are suspected to have an impact on the molecular composition of lecithins, indicated by the different phospholipid compositions published in literature [81, 101, 136]. As these changes can lead to different technological effects [9], it is desirable to understand the underlying molecular mechanisms. When the technological effects of different lecithin components are known and characterized, it will be possible to define optimal lecithin compositions eventually and maybe even purposeful tailoring of surface active molecules might come into practical reach.

Although lecithin usage in chocolate, with respect to different compositions, and their interaction with dispersed particles in chocolate as well as the resulting influences on rheology were already discussed broadly in literature (see Section 2.4.4), it is still not completely understood. The interface between hydrophilic sugar particles and partly hydrophilic cocoa particles and the surrounding cocoa butter medium has a high surface tension and is thermodynamically undesirable. This leads to hydrophilic particle interactions and the tendency to form aggregates, which results in unfavorable flow properties [12]. Also cocoa butter immobilization on the particle surfaces is supposed to have a rheological impact, as the immobilized fat is not available as liquid continuous medium . The usage of lecithin in supposed to prohibit the described behavior as it leads to improved flow properties [12].

1.2.2 Multiscale framework of chocolate rheology

Besides treating chocolate as a concentrated lipophilic suspension, researchers are more and more investigating chocolate on multiple time and length scales, in order to understand rheological behavior. With that, the molecular scale of chocolate comes into focus. In that terms, chocolate is like most foods, a complex mixture of a wide diversity of molecular components. In general, the different main molecular components of foods are either water, proteins, carbohydrates, or lipids, the latter three are the energy providing substances in human metabolism. Cocoa butter is composed of different triglycerides, which are mainly composed out of the three fatty acids palmitic acid, stearic acid, and oleic acid [47]. During the biggest part of the chocolate manufacturing process, cocoa butter is in its molten liquid state and finally crystallizes into the continuous solid chocolate matrix during the cooling process, right before demolding and packaging [12]. Sucrose particles consist almost exclusively of sucrose molecules, which are in a crystalline state when they are added to the cocoa mass. Although sucrose particles might become amorphous to a certain degree during the refining process of chocolate, they are chemically well-defined particles. In the case of cocoa particles, it is much more difficult to define the chemical structure, as they are composed of carbohydrates, proteins, and lipids. All these components, together with lecithin, result in complex molecular structures with several relevant characteristics on a

broad range of length scales and effects on different time scales and thus require a broad range of experimental and modeling techniques to be analyzed.

This broad range of time and length scales that are of relevance for simulations as well as experimental approaches, compared to the time and length scales that are mostly relevant for manufacturing are shown in Figure 1.2. Phenomena and characteristics on the different scales with impact on rheology are elucidated in the following and examples of research are given. The description starts from the manufacturers point of view going down to the molecular scale, where the focus of the presented thesis is. On the macroscopic scale, chocolate is produced from raw cocoa beans over a lipophilic suspension

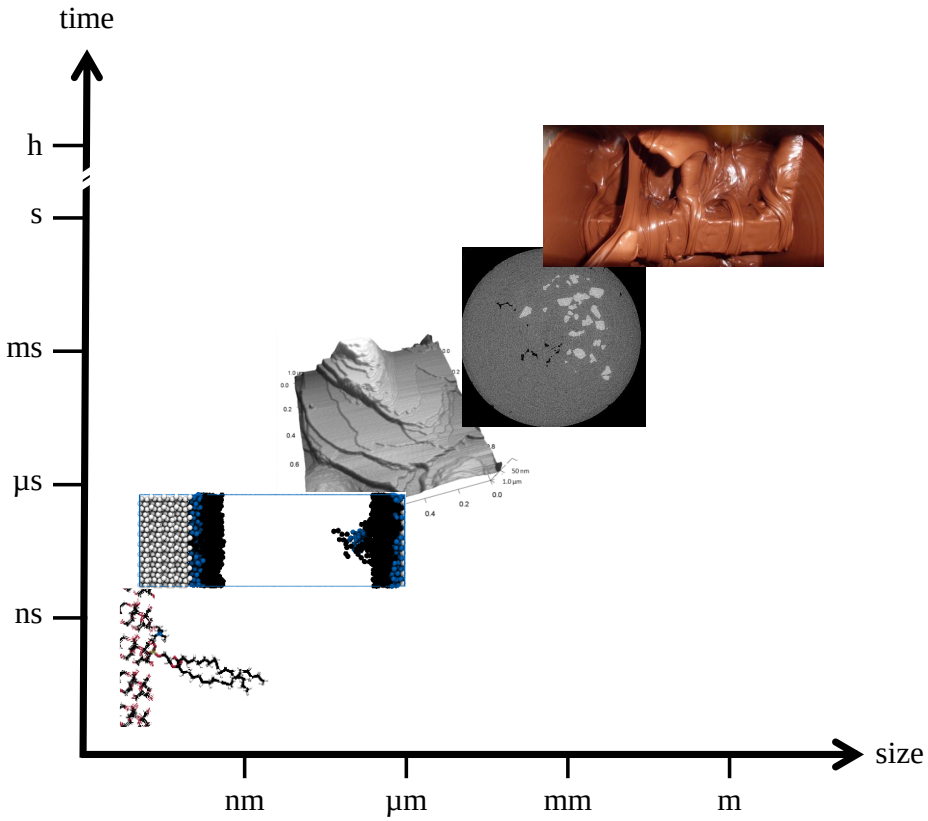

Figure 1.2: Phenomena that are relevant for chocolate conching and rheology occur on different time and length scales: all-atom (left) and coarse-grained (second from the left) molecular dynamics simulations; atomic force microscopy of sucrose particle surfaces (middle); microtomographic image of the microstructure of chocolate (second from the right); picture of the conching process (right). Permission to print the atomic force microscopy picture was kindly given by Dana Middendorf (Deutsches Institut für Lebensmitteltechnik). Permission to print the conching picture was kindly given by Isabell Rothkopf (Fraunhofer Institut für Verfahrenstechnik und Verpackung IVV). All figures of molecular snapshots throughout this thesis are created with the software VMD: Visual molecular dynamics [62].

to the final product by being subject to different manufacturing steps, such as fermentation, roasting, grinding, heating and stirring during conching, pumping, cooling, and demoulding [12]. These processes normally happen in length scales of millimeters to meters and time scales of minutes to hours.

The conching process, which is depicted in Figure 1.2 on the right, is the chocolate manufacturing step where the rheological behavior is defined and takes several hours. Standard rheological measurements of chocolate are performed on this length scale, where volumes of about $1\,\mathrm{cm}^3$ are examined. While standard rheological measurements and characterizations can be done without further insight into the systems, the origin of the flow properties has to be explained on smaller scales. In a suspension such as chocolate, rheological behavior is mainly influenced by the mass fraction of particles and cocoa butter, the particle size distribution and the physico-chemical interactions of these different phases. An overview of related literature is given in Afoakwa et al. [2]. Particle sizes are in the micrometer scale, which is shown in Figure 1.2 by a microtomographic image (second from the right), where sucrose particles are dispersed in cocoa butter. The sucrose and cocoa particles are in a length scale typically smaller than $30\,\mu\mathrm{m}$ in the final chocolate product. To understand phenomena such as cocoa butter immobilization, techniques on the next smaller scale can be used for investigations. Atomic force microscopy allows to investigate the particles on a micrometer to nanometer scale, and is shown in the center of Figure 1.2 by the example of the surface topography image of a sucrose particle extracted from chocolate mass after refining. Atomic force microscopy was used to investigate the layer thickness of immobilized fat at the particle surfaces [93], to study the role of polyglycerol polyricinoleate in chocolate rheology [91], as well as the effects of different lecithins [92]. In the nanometer to ångström scale, lecithin layers are adsorbed on the hydrophilic particles. By attaching side by side on the surface of sucrose or cocoa particles, they form a hydrophobic layer on these particles, which is investigated by coarse-grained molecular dynamics simulations in this thesis (second from the left in Figure 1.2). Further, single hydrogen bonds between phospholipids and sucrose molecules in the ångström length scale and the nanosecond to picosecond time scale are investigated by all-atom molecular dynamics simulations in this thesis (on the left of Figure 1.2). The phospholipid layers influence the rheological behavior of the lipophilic suspension chocolate, as they lower hydrophilic interactions and by getting adsorbed at the particle surfaces, less cocoa butter is immobilized and available as a flowing matrix. These microscopic mechanisms define the flow behavior for all bigger time and length scales of chocolate manufacturing. The given examples show the necessity of investigating foods, such as chocolate, on multiple time and length scales to understand the behavior in the macroscopic manufacturing scale. This thesis focuses on the smallest end of the presented scales, before quantum and relativistic effects become relevant.

1.3 Focus and outline

1.3.1 Focus and thesis statement

In this chapter, different characteristics of chocolate, which are relevant for its rheological behavior, were introduced. Despite several studies that already investigated chocolate on different time and

length scales and a lot of experience in manufacturing, there is still a lack of knowledge of the exact molecular mechanisms that occur and are the basis for characteristic behavior and properties of chocolate. Without getting a detailed understanding of the molecular phenomena that govern the rheological behavior, new process development approaches and adaption to different raw materials or technological parameters will always be based on trial and error.

Two main goals are set for this thesis.

- The first goal is to deliver understanding of specific molecular phenomena, interactions, and mechanisms that govern the rheology of chocolate by employing molecular dynamics simulations.
- The second goal is to promote the usage of molecular dynamics simulations in investigations of complex food systems in order to gain food process engineering relevant insights, to discuss the methodological restrictions and to show possible solutions.

The specific research questions as well as the focus of the theoretical background and the literature review are given in the following outline.

1.3.2 Outline

Chocolate conching and rheology
Chapter 2 gives an overview of the basics of chocolate manufacturing with a focus on the conching process. Commonly used rheological models for chocolate are reviewed. Further, a literature review on lecithin structures in hydrophobic solvents and its usage in chocolate, with a focus on the influences of different phospholipid fractions on chocolate rheology, is given.

Molecular dynamics simulations
Chapter 3 starts with a short introduction to the simulation method molecular dynamics. Two methods, which allow to extend the investigated time and length scale, the so-called coarse-graining and implicit solvation, are introduced. Additionally, molecular dynamics is reviewed regarding its general use in food science with a focus on food process engineering. Restrictions and limitations of the method with respect to food science are shown and possible approaches to overcome those are elucidated.

Interactions of different phospholipid head groups with sucrose crystals
Chapter 4 presents the first study of this thesis and aims at answering the question if different phospholipids interact differently with sucrose. The interactions of single phospholipids with sucrose at the interface to cocoa butter are investigated with detailed atomistic resolution. Non-equilibrium molecular dynamics simulations are performed to calculate the detachment work, which is an upper estimation of the free energy difference of phospholipid adsorption. Differences in the strength of interaction of different prominent phospholipid head groups of lecithin with sucrose are shown. A

correlation of the number of hydrogen bonds with the detachment work is shown and the analyzed mechanisms of detachment give further insights into the interaction of phospholipids with sucrose crystals.

Phospholipid structures surrounding sucrose particles
Chapter 5 presents the second study of this thesis and aims at answering the question if concentration-dependent molecular phospholipid structures at the sucrose–cocoa butter interface can explain rheological behavior of chocolate. The formation of phospholipid structures in the liquid cocoa butter medium is a slow process in terms of the achievable time scales of molecular dynamics simulations. This would result in high computational costs, especially when all-atom force fields are used. To reduce the computational costs a coarse-grained force field is used for this purpose. Phospholipid structures at the sucrose–cocoa butter interface are investigated and linked to rheological phenomena of chocolate. Formation of wormlike micellar structures and their ability to build hydrophilic bridges between sucrose particles is shown. The effect of the degree of saturation of the aliphatic chains on the area per lipid in the phospholipid monolayers is studied.

Cocoa butter structures and immobilization on sucrose crystal surfaces
Chapter 6 presents the third study of this thesis and aims at answering the question if cocoa butter immobilization at the sucrose surfaces is based on molecular interactions. Cocoa butter behavior regarding its structures and dynamics in presence of sucrose crystals is investigated and compared to pure cocoa butter bulk behavior. The strength of cocoa butter immobilization at sucrose interface through molecular interactions at perfect crystal interfaces is calculated by accessing the mobility of triglycerides at the interface.

Conclusion and Outlook
Chapter 7 gives a conclusion of the presented results and summarizes the presented thesis. Additionally, an outlook on non-classical rheological models for the description of chocolate flow behavior, on the role of water in chocolate rheology, and a short suggestion on how to treat cocoa particles in molecular dynamics simulations is given.

Please note that throughout the thesis, some central points of the theoretical background as well as basic hypotheses are mentioned redundantly to a certain extent. This is done intentionally, in order to avoid excessive referencing but to enable a self-contained reading of single chapters. The main restriction of this thesis is the pure simulational approach to the research questions. Although the used force field are soundly validated and numerous simulation results are compared to experiments from literature, no further experimental measurements are performed in this thesis. If applicable, further possible experimental approaches to validate the presented simulation results are proposed directly in the results sections.

Chapter 2

Chocolate conching and rheology

In this chapter chocolate is at first described by means of its molecular composition and second by its relevant characteristics in its liquid state as a rheological fluid. The conching process and its key role in chocolate production is discussed and different rheological models that are used for chocolate are presented in detail. Finally, the characteristics of the most commonly used surfactants in chocolate manufacturing, vegetable lecithins, are introduced and recent research is reviewed. This chapter is intended to give readers, who are unfamiliar with the topic, with basic understanding of chocolate and its rheology. The level of detail of the theoretical background is chosen to allow the reader to follow the argumentative lines of the presented thesis.

2.1 Chocolate

2.1.1 Molecular composition of chocolate

Chocolate is a product that is obtained from cocoa beans. Cocoa beans are the seeds from the fruit of the cocoa tree *Theobroma cacao*. The main ingredients of manufactured dark chocolate are sucrose, cocoa butter, cocoa particles, and lecithin as an emulsifier [131]. Cocoa butter forms the continuous matrix of chocolate, has special rheological, structural, and organoleptic properties [80] and is the decisive ingredient for many desired chocolate properties. The characteristics of cocoa butter are unique and no other edible fat has similar properties, which leads to a wide variety of different applications for cocoa butter in the food, cosmetic, and pharmaceutical industry [131]. These desired properties directly result from the molecular composition. The brittleness of chocolate, which accounts for the characteristic snap when chocolate breaks [123], the sharp melting point at body temperature, which provides the typical cooling effect in the mouth [80], as well as the smooth textural feeling of molten chocolate in the mouth are all cocoa butter specific properties. The exact composition of vegetable fats,

such as cocoa butter, depends on the age of the plants and the growing conditions. Foubert et al. [47] investigated 20 different cocoa butter samples and give detailed data on the molecular composition. Triglycerides are the main molecular components, followed by free fatty acids and diglycerides. The following composition of cocoa butter is given for one of the 20 cocoa butter samples (sample N) of Foubert et al. [47]. It is described as standard factory product, produced in a batch by Barry Callebaut in Wieze, Belgium [47]. The main fatty acids in chocolate are stearic acid (S) with 37.7 wt%, oleic acid (O) with 33.6 wt%, palmitic acid (P) with 25.0 wt%, linoleic acid (L) with 2.72 wt%, and arachidic acid with 1.01 wt%. Triglyceride names are in the following given by three of the introduced capital letters, for example POS, which would indicate a triglyceride composed of the three different fatty acids palmitic acid, oleic acid, and stearic acid. The chemical structure of a triglyceride is shown on the example of POS in Figure 2.1. All triglycerides have a glycerol backbone, which is shown on the right side in

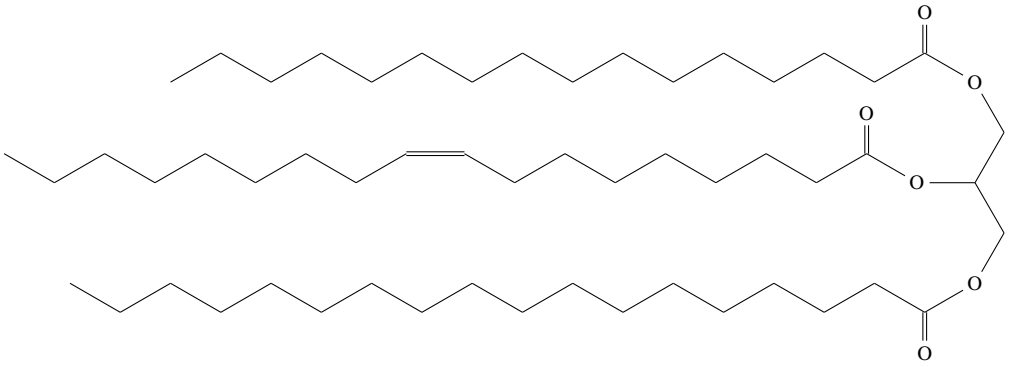

Figure 2.1: Structural formula of 1-palmitoyl-2-oleoyl-3-stearoylglycerol (POS), which is the most abundant triglyceride in cocoa butter.

Figure 2.1 and is connected to three fatty acids via ester bonds. The glycerol backbone is more polar than the fatty acids, due to the ester bonds. The fatty acids can vary in their chain length and degree of saturation. In the case of POS the chain lengths are 16 or 18 carbon atoms and either no bond or one bond is unsaturated. In Table 2.1 the triglyceride composition of cocoa butter is shown exemplarily on sample N of Foubert et al. [47]. The high number of triglycerides with oleic acids at the second

Table 2.1: Triglyceride composition of cocoa butter on the example of a standard factory product [47].

Triglyceride	Fraction (wt%)	Triglyceride	Fraction (wt%)	Triglyceride	Fraction (wt%)
PPP	0.192	PSS	0.525	SSS	0.252
MOP	0.222	POS	41.1	SOS	25.0
PPS	0.656	POO	2.53	SOO	3.17
POP	18.4	PLS	3.01	SLS+OOO	1.51
PLP	1.82	PLO	0.424	SOA	1.21

position of the triglyceride is typical for cocoa butter and is key for the valuable melting and crystallization behavior. Minor components of cocoa butter are shown in Table 2.2. The amount of free fatty acids is given as well as the amount of diglycerides, which shows the further lipid components besides

triglycerides. The amount of phosphorus is equivalent to the amount of phospholipids present in cocoa butter. The peroxide value gives information about the degree of oxidation, the unsaponifiable matter contains higher sterols, aliphatic alcohols, pigments, and hydrocarbons. Soap content gives information about the degree of alkalizing of cocoa nibs and traces of iron are due to old machinery and abrasion [47]. Beside the minor components, the composition of a typical industrially used cocoa butter shows

Table 2.2: Minor components of cocoa butter on the example of a standard factory product (sample N) [47].

Free fatty acids (wt% oleic acid)	Diglycerides (wt%)	Phosphorus (ppm)
1.38 ± 0.01	0.72	41.6 ± 0.2
Unsaponifiable matter (wt%)	Soap (ppm sodium stearate)	Iron (ppm)
0.39 ± 0.05	195.0 ± 53.0	2.71 ± 0.04
Peroxide value (meq/kg)		
1.1 ± 0.1		

that triglycerides are the main components of cocoa butter. Thus, their characteristics should mainly account for the bulk behavior of cocoa butter.

The solid parts of cocoa, the so called cocoa particles, are the remaining part of the cocoa beans after the cocoa butter is extracted. They are the second major chocolate ingredient from cocoa beans. Torres-Moreno et al. [131] analyzed the chemical composition of unroasted cocoa beans, which is given in Table 2.3. The composition of unroasted cocoa beans also contains information about the chemical

Table 2.3: Chemical composition of unroasted cocoa beans from Ecuador and Ghana [131].

	Ecuador	Ghana
Moisture (g)	59.51 ± 0.04	51.12 ± 0.03
Ash (g)	40.32 ± 0.03	35.65 ± 0.19
Total protein (g)	127.91 ± 0.03	128.25 ± 0.05
Carbohydrate (g)	337.85 ± 0.24	365.81 ± 0.15
Total dietary fibre (g)	194.74 ± 0.28	113.02 ± 0.17
Total fat (g)	434.56 ± 0.25	419.32 ± 0.13

composition of cocoa particles in chocolate. Changes in composition due to the subsequent processing steps have of course to be taken into account. Torres-Moreno et al. [131] further analyzed the chemical composition of chocolate. Combining the results of these two experiments, and due to the fact that the cocoa butter and sucrose parts in chocolate are very well-defined, the chemical composition of cocoa particles, as they are present in chocolate, can be deduced. Water, ash, protein, carbohydrates, dietary fiber, and fat are all present in chocolate. A main part of the carbohydrates and fats in chocolate are present in form of sucrose and cocoa butter. Nevertheless, the fat that remains in the cocoa particles after separating most of the cocoa butter during manufacturing and the carbohydrates should still be part of the cocoa particles in chocolate. Protein and dietary fiber are not present in cocoa butter and also not in sucrose, given it has standard industrial quality. This means that the major shares of them

are part of the cocoa particles in chocolate. Nevertheless, the absolute content in dietary fibres gets significantly reduced, when unroasted cocoa beans are separated from their shells after the roasting process.

Sucrose, which is added as a bulk sweetener during chocolate production, is a disaccharide composed of one glucose and one fructose monomer. It is added in its crystalline state, the structural formula is given in Figure 2.2. The presented section is intended to give an overview of the molecular composition

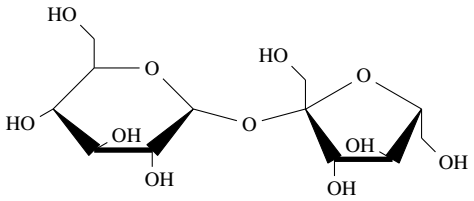

Figure 2.2: Structural formula of sucrose.

of chocolate. So far, lecithin has been left out and will be separately treated in Section 2.4.1, due to its central role in this thesis.

2.1.2 Chocolate – a concentrated suspension

From a rheological point of view, dark chocolate is a concentrated suspension of sugar and cocoa particles in a continuous cocoa butter matrix with non-Newtonian flow behavior. A schematic representation of the microstructure is given in Figure 2.3. The rheology of concentrated suspensions is governed by the volume fraction of particles and the volume fraction of the continuous matrix respectively, the particle size distribution, particle shape, particle surface, particle–particle interactions, particle interactions with the continuous matrix, and flow properties of the continuous matrix. In this chapter chocolate is treated as a concentrated suspension and its rheological properties are characterized from this point of view. Rheological models that are able to describe the rheological behavior and the influence of surfactants on rheology are discussed in depth in Sections 2.3 and 2.4 due to their central relevance for this thesis.

Particle size distribution and particle shape

Afoakwa et al. [2] differentiates between two main influences on chocolate rheology. First, the particle size distribution and second, compositional effects of the chocolate. Influencing rheological properties by defined particle size distributions is especially of interest due to the fact that rheology is otherwise controlled by addition of extra cocoa butter or emulsifiers, which represent the most expensive ingredients of chocolate [41]. Controling the particle size distribution was the subject of several studies. It is a crucial task due to the fact that particles coarser than about $30\,\mu m$ are responsible for perceived

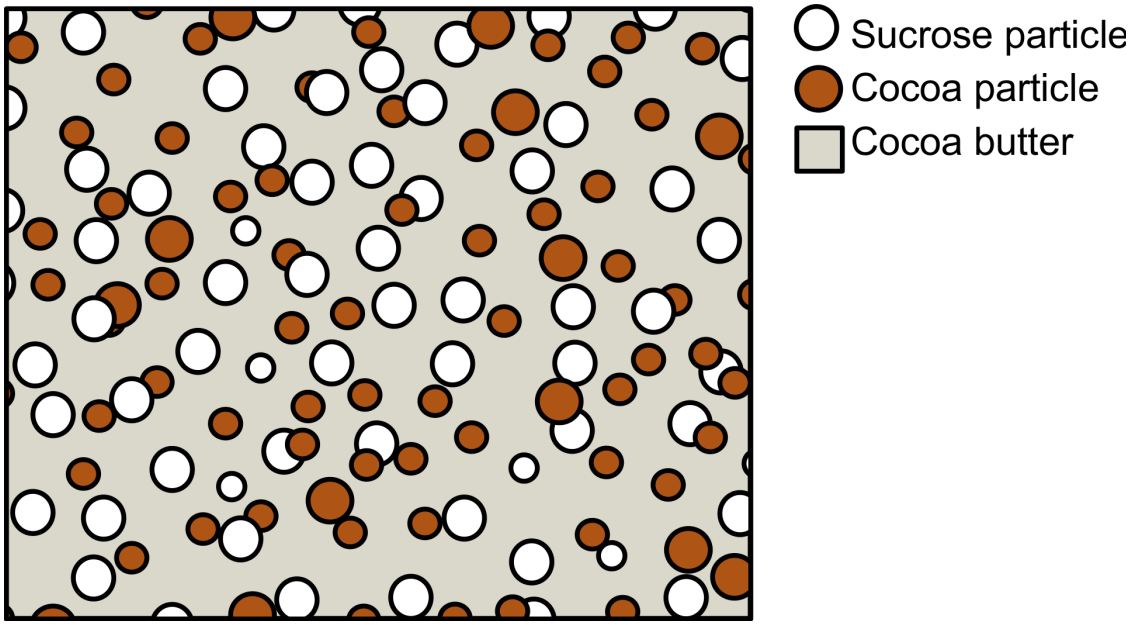

Figure 2.3: Schematic representation of chocolate as a concentrated suspension. Particles are presented as circles for sake of simplicity.

grittiness of chocolate, while a finer particle size has a negative effect on rheological behavior. Afoakwa et al. [3] shows that different aspects of the particle size distribution, the specific surface area, the size of the largest particle, the Sauter mean diameter, and the mean particle diameter influence the rheology of dark chocolate. Increasing the particle size generally results in lower viscosity and yield stress and both effects are stronger pronounced when lecithin and fat content is low [3]. Chevalley [26] reports several studies and industry case studies in his review about the rheology of chocolate that investigated the influence of particle size on rheology. It is reported that the Casson viscosity is 1.2 to 2 times higher and the Casson yield stress is 2 to 14 times higher for finer chocolate compared to a coarse one. The strongly increased viscosity indicates the high relevance of the particle size distribution on chocolate rheology. Chevalley [26] reports a further study in which the effect of the particle size in sugar–cocoa butter mixtures and on cocoa mass–cocoa butter mixtures was investigated. While particle size reduction led to increased viscosity in the first case, the reverse was true for the second case. A similar result was found in a further study listed by Chevalley [26]. Nevertheless, those studies are not further elucidated and are treated as exceptions. To the best of the authors knowledge, those study are the only ones obtaining this result.

In general, particle suspensions tend to become more viscous the higher the amount of dispersed solids in the continuous phase becomes. This effect can be influenced by the particles size distribution. Do et al. [41] showed that an intentionally designed multimodal particle size distributions with constant mass fractions of the components can positively influence the rheological behavior of chocolate, which means lowering the yield stress and the viscosity. This can be explained by the packing density of multimodal particles. For the particles to flow past each other it is commonly assumed that their surface

has to be covered with cocoa butter. Thus, a higher amount of fat leads to better flowability. The amount of available fat for particle coating can be influenced by displacement of trapped fat in the voids between big particles, due to enhanced packing density of multimodal particle size distributions. Do et al. [41] showed a resulting lower viscosity for wide monomodal particle size distributions and multimodal particle size distributions.

The influence of particle shape on chocolate rheology is a poorly investigated phenomenon. Do et al. [41] examined particle shape by light microscopy with the aim to investigate its rheological impact as the shape influences the packing density of particles. The Krieger Dougherty equation gives the relation between the viscosity of the suspension η_s and the suspending medium η_m

$$\frac{\eta_s}{\eta_m} = \left(1 - \frac{\Phi}{\Phi_M}\right)^{-[\eta]\Phi_M}, \tag{2.1}$$

where $[\eta]$ is the intrinsic viscosity, Φ the particle volume fraction, and Φ_M the maximum particle volume fraction that can be reached by dense packing. The equation shows that an increase in the maximum particle volume fraction would lower the suspension viscosity. While the maximum particle volume fraction can be increased by multimodality or by a broader monomodal distribution, it could also be influenced by the particle shape. Do et al. [41] showed that sugar particles are not spherical. They argue that rounder particles would in theory lead to a higher maximum packing density. This is at least not true for monomodal particles, where for example ellipsoids and cubes would have a higher maximum packing density. While the study makes clear that the particle shape can influence rheology, no further studies have been published, to the best of the authors knowledge.

Particle interactions

It is commonly agreed that particle interactions in chocolate should be minimized in order to prohibit formation of aggregates and immobilized cocoa butter within the aggregates. Only recently, it was shown that the surface characteristics of sucrose might have an influence on rheology. Middendorf et al. [93] showed that flow properties of model chocolate masses, which consist only of sucrose and cocoa butter, manufactured in different types of mills, namely a ball mill and a roller refiner, can lead to different flow properties despite very similar particle size distributions. It was shown that the differences in flow properties are related to different surface characteristics of the sucrose particles. It was shown by local thermal analysis in an atomic force microscope that sucrose particles that were refined in a roller refiner have more amorphous surface parts than sucrose particles refined in a ball mill. While sucrose tends to recrystallize very quickly when the relative air humidity is high enough, it is hypothesized that, due to the coverage with cocoa butter, recrystallization does not – or only very slowly – occur in chocolate [93]. Properties of sucrose are supposed to play a key role in chocolate rheology and are still a subject under investigation. Further, it needs to be examined whether the surface characteristics still have an

influence on particle interactions after lecithin, which is supposed to cover the surface, is added.

Fat content

Obviously, the continuous fat phase, cocoa butter, has a big influence on the rheology of chocolate. Final chocolate products have as mass fraction of about $30\,\mathrm{wt}\%$ fat. Increasing the fat content of chocolates has varying effects on chocolate viscosity depending on the initial fat content [12]. Below $23\,\mathrm{wt}\%$ fat content, chocolates have a pasty texture. In this area, increasing fat content has a dramatically viscosity lowering effect. At around $28\,\mathrm{wt}\%$, an increase of $1\,\mathrm{wt}\%$ in fat content decreases viscosity about $50\,\%$. Above $32\,\mathrm{wt}\%$, there is very little change in viscosity when the fat content is increased [12]. It is hypothesized that extra fat is only added to the free flowing fat around particles where it is not improving the lubrication between particles any further and thus their flow behavior in the continuous matrix [12]. The yield stress of the chocolate mass depends mainly on particle–particle interactions. That means that change in fat content should only affect yield stress when it changes the mean distance between particles on very narrow distances. Intermolecular forces decrease very strongly with distance in the nanometer range.

Moisture content

Water is strongly increasing the viscosity of chocolate, even if only a few weight percent are present. As a rule of thumb, it is given that an extra $0.3\,\mathrm{wt}\%$ of water required about $1\,\mathrm{wt}\%$ more cocoa butter to account for the negative rheological effects [12]. It is argued that water adsorbs on the hydrophilic sucrose surfaces and dissolves the first few layers of sucrose molecules, which makes the crystals more sticky, interacting more strongly with each other. Beckett [12] states that lecithin can prohibit this effect. Probably due to the fact that lecithin molecules are present at the sucrose surface and prohibit water to adsorb on the surface or water is prohibited to have a negative effect, by being trapped in the hydrophilic parts of lecithin molecular structures, such as micelles.

2.2 Conching

This section is intended to give an overview about different practical aspects of chocolate conching. First the reasons for conching are stated, followed by a description of the basic mechanisms of conching, the phases of conching, and conching machines. More detailed information and original sources are given in the textbook by Beckett [12], which is a well established reference book in chocolate manufacturing and research.

2.2.1 Reasons for conching

The two main reasons for chocolate conching are flavor development and the adjustment of flow properties. Flavor development is one of the most crucial and complex tasks of the chocolate manufacturer because it is influenced on many levels during manufacturing. It starts with choosing the right raw materials because no high quality chocolate can be produced from low quality cocoa beans. Mistakes in early chocolate manufacturing steps, for example development of off-flavors due to wrong fermentation, drying, or roasting, cannot be compensated for by conching. Though conching is the last and most crucial step in flavor development, it can only work on a solid basis.

The transition from a powdery dry mass to a viscous liquid during conching shows the drastic influence of conching on the flow properties of chocolate. During grinding, a huge amount of cocoa and sucrose particle surfaces is formed and are not fully covered by cocoa butter in the beginning of the conching process. The particles form aggregates, possibly trapping lipid droplets, thus being not available for forming the continuous matrix where the particles can flow in. The mechanical mixing and temperature control during conching redisperse particle aggregates and melt the cocoa butter. Additionally, further cocoa butter and lecithin get added during conching to adjust the flow properties as desired. Influences of emulsifiers are elucidated in Section 2.4.

2.2.2 Mechanisms of conching

Removal of volatiles is the first key mechanism of chocolate conching. Acidic volatiles, such as acetic acid, lactic acid, and also short chain fatty acids, have to be removed as they have strong undesirable sensory attributes. In modern processes a big part of these components gets already removed from cocoa liquor in a pre-treatment phase, which is usually a thin-film degassing process and allows to reduce subsequent conching time. Removal of volatile acids from cocoa liquor is easier than from chocolate mass as higher temperatures can be used without introducing further undesirable flavors due to heating. The slightly higher water content of cocoa liquor facilitates the degassing of undesired volatiles. The removal of undesirable flavor compounds leads to a more pronounced effect of desirable flavors and allows the manufacturing of well tasting chocolates, eventually. The total acid content decreases continuously over conching time, involving the danger of so-called over-conching, which would result in very bland tasting chocolate. Removal of the volatile component water from chocolate is very important due to its viscosity increasing effect. The water content starts to decrease rapidly at the beginning of the conching process as most of the water comes from milk ingredients and once they are coated by fat, water removal becomes more difficult and slower. Water removal depends on the conching temperature. The manufacturer has to make sure that the temperature is high enough to obtain fast moisture removal to save production time, and low enough to prohibit high free water contents, which cannot escape to the surrounding atmosphere in time, leading to sugar agglomerates

and gritty chocolate instead. Thus, sufficient air ventilation is also of high importance in chocolate conching.

Mechanical mixing is the second key mechanisms of chocolate conching and has multiple effects in the chocolate mass. At first, the freshly ground cocoa and sucrose particle aggregates get separated, the cocoa butter melts and covers the particle surfaces. As that happens, the chocolate mass transforms from its powdery and crumbly state to a liquid state. Further, mechanical mixing has also a big influence on the chocolate flavor. Ziegleder et al. [150] found that a redistribution of aromatic components happens during conching. In the beginning of the conching process the aromatic components are mainly present in the cocoa particles and in the cocoa butter. The sugar is only poorly coated with cocoa butter and no aromatic components are on its surface, leading to a very prominent and sharp sweet taste of the chocolate without further aromatic depth. Ziegleder et al. [150] showed that the amount of aromatic components in the cocoa butter phase decreases during chocolate conching while only a low proportion of aromatic compounds gets lost through evaporation. At the same time the chocolate has a more balanced and fine taste with less dominant sweetness. From that Ziegleder et al. [150] derived the theory that the aromatic components get distributed evenly in the chocolate mass, caused by concentration gradients, and aromatic components are also present at the sucrose surfaces.

2.2.3 Phases of conching

Conching is commonly divided in three different phases that are defined by the macroscopic appearance of the chocolate mass. First, there is the *dry phase*, where the chocolate mass is powdery in the beginning as a result of the previous grinding, soon turning into a crumbly mass due to mixing and increasing temperature. In this phase it is easy to remove water from the chocolate mass when the conche is ventilated sufficiently. The water takes a high amount of unwanted volatiles with it. During the filling of the conche the drawn electrical current increases and keeps increasing in the beginning of the dry conching when the powdery mass turns crumbly. At first small balls are formed, followed by formation of big lumps while the mass gets more pasty. The manufacturer has to make sure that the mass is mixed sufficiently and does not completely move with the mixing elements, by regulating the temperature. Second, there is the *pasty phase*, in which the chocolate is a highly viscous non-Newtonian fluid. In this phase, the energy input is very high. The conche needs to be cooled with help of a water jacket to keep the desired conching temperature. As the temperature has a strong effect on sensory properties of the product, controlling the temperature must be done very carefully. After the chocolate turned into a pasty substance, the viscosity falls steadily due to the decreasing water content and the proper coating of sucrose and cocoa particles with liquid cocoa butter. As this phase exhibits the largest energy input, it is proposed that this phase is vital for many conching mechanisms. For example the redistribution of aroma compounds is argued to happen in this phase. Third there is the *liquid phase*, during which the chocolate becomes a less viscous non-Newtonian fluid due to the final cocoa butter addition and addition of lecithin or other emulsifiers. After adding these ingredients, a certain time is

required for the chocolate to reach an equilibrium viscosity. After that, the conching is finished and the chocolate can be used for moulding or enrobing. Regarding production time, chocolate conching is a very time-consuming process. The complete process is usually performed in 6 to 24 hours in modern conching machines, the traditional longitudinal conching process takes up to 72 hours.

2.2.4 Conching machines

Rudi Lindt invented the longitudinal conche in Switzerland in 1878, where a granite roll in a longitudinal shell pushes the chocolate mass back and forth. Lindt found that through the long stirring of the chocolate mass, it was possible to produce a smoother and better tasting chocolate. The smoother mouthfeel was probably a result of further particle breakage due to poor milling equipment back then. The longitudinal conche is not commonly used industrially anymore because it has several disadvantages, such as the lack of being able to dry conche, which results in much longer conching times, due to poor water removal ability in liquid conching. Modern dry conching designs can be divided in batch and continuous designs. Most commonly batch conches are used, which exist in a large number of different designs and can mainly be divided into two groups. Horizontally stirred rotary conches and vertically stirred rotary conches. Both have in common that they usually have round chambers with mixers or scrapers, which rotate about either horizontal or vertical shafts. Both types are designed to produce a sufficient large surface area that is exposed to the surrounding air, in order to remove water and undesirable volatiles.

2.3 Rheological models for chocolate

Rheological properties of liquid chocolate are very important for two reasons. First, for manufacturing and second, for the sensory value of the final product [12]. Manufacturing steps, such as pumping, moulding, and enrobing, can only be performed sufficiently well when the flow properties are appropriate. For example, when the viscosity is too low, enrobing is not possible. When the viscosity is too high, air bubbles may remain in the chocolate or the desired shape of chocolate products cannot be achieved [12]. Sensory value is linked to the rate of contact of chocolate saliva mixtures with different flavor receptors in different parts of the mouth, which again is strongly linked to rheological properties of the chocolate mass [12]. This chapter gives an overview of the different rheological models that are commonly used for describing the flow properties of chocolate. At first several models are treated that simply fit the rheological data to mathematical functions without giving insight to underlying physical properties of the system. Later on, models will be discussed that aim to give more detailed physical insights.

2.3.1 Casson, Bingham, and Herschel–Bulkley model

From 1973 to 2000 the Casson model was used for rheological characterization of chocolates, proposed by the International Confectionery Association (ICA), which was called International Office of Cocoa, Chocolate and Sugar Confectionery (IOCCC) before 2002. The Casson model is given by

$$\sqrt{\tau} = \sqrt{\tau_{CA}} + \sqrt{\eta_{CA}} \cdot \sqrt{\dot{\gamma}}, \tag{2.2}$$

where τ is the shear stress, τ_{CA} the Casson yield stress, η_{CA} the Casson plastic viscosity, and $\dot{\gamma}$ the shear rate [4]. τ_{CA} and η_{CA} are model parameters that are used for the rheological characterization of chocolate. They can be obtained in the proposed method, after measuring the shear stress over an unspecified range of shear rates within the boundaries of $5\,s^{-1}$ and $60\,s^{-1}$, by ploting the square root of the shear stress $\sqrt{\tau}$ over the square root of the shear rate $\sqrt{\dot{\gamma}}$, which should follow the linear relation of Equation 2.2. $\sqrt{\tau_{CA}}$ is the extrapolated axis section and $\sqrt{\eta_{CA}}$ is the slope of the linear fit [1].

An international inter-laboratory study by Aeschlimann and Beckett [1] showed that using the Casson model does not give reproducible results. The Casson model only has two parameters and it is known that especially at lower shear rates the model is not capable to describe the flow behavior of chocolate well. Especially the Casson yield stress, which is obtained through extrapolation in the low shear rate area, can often not be measured reproducibly. Therefore, extrapolation with rheological models should be avoided when reproducible data of rheological properties are required. Interpolation between data is usually valid [4]. Due to the flaws of the Casson model, ICA recommends now to measure shear stress and viscosity at well-defined shear rates after pre-shearing and simply to report the measured values. The exact method is available from CAOBISCO in Brussels. It was shown that this strategy is accurate and easily applicable to different chocolates [4, 119].

Similar empirical models that have been used in chocolate rheology are the Bingham model and the Herschel–Bulkley model [124]. The Bingham model is given by

$$\tau = \tau_0 + \eta \cdot \dot{\gamma}, \tag{2.3}$$

where τ_0 is the yield stress and η the plastic viscosity. The Herschel–Bulkley model is given by

$$\tau = \tau_0 + \eta \cdot \dot{\gamma}^b, \tag{2.4}$$

where b is a further model parameter. The only difference of the Herschel–Bulkley model and the Bingham model is the exponent of the shear rate. Thus, the Herschel–Bulkley model is able to fit all data that the Bingham model fits and has a broader spectrum of applicability. Sokmen and Gunes [124] found that the Herschel–Bulkley model fitted best, compared to Casson and Bingham.

2.3.2 Windhab model

A further important rheological model, which is less empirically and more physically motivated, is the structure based so-called $\tau_{0.1}$ model or Windhab model [147]. In this model the flow behavior of chocolate is described by a superposition of measured yield stress, a description of the flow behavior at higher shear rates, and the flow behavior in an intermediate region. The flow behavior is given by

$$\tau = \tau_0 + \eta_\infty \cdot \dot{\gamma} + (\tau_1 - \tau_0)\left(1 - e^{\left(\frac{-\dot{\gamma}}{\dot{\gamma}^*}\right)}\right). \tag{2.5}$$

The yield stress τ_0 is a result of molecular interactions between the particles of the suspension in their isotropic rest structure and represents the yield stress. τ_1 is the intersection of the ordinate and of an linear extrapolation of the high shear rate regime $\eta_\infty \cdot \dot{\gamma}$. In this high shear rate regime the flow behavior of the suspension is similar to that of the pure continuous suspension matrix cocoa butter. The intermediate region describes the transition from the isotropic rest structure to the anisotropic shear induced structure. The model parameter $\dot{\gamma}^*$ can be calculated from τ_0 and τ_1 by

$$\dot{\gamma}^* = \tau_0 + (\tau_1 - \tau_0)(1 - \frac{1}{e}), \tag{2.6}$$

where e is Euler's number.

2.3.3 Fluid immobilization model

A further model by Windhab [148], which is labeled the fluid immobilization model, describes the rheological behavior of concentrated suspensions. It is based on an equation of the form

$$\eta = \left(1 + \frac{\Phi}{\Phi_M}\right)^{-k\Phi_M}, \tag{2.7}$$

which is similar to Equation 2.1 and was shown to accurately describe the dependency of the viscosity on the solid volume fraction [73]. The particle shape factor is labeled k. The role of fluid immobilization in particles and particle aggregates as a structure related key mechanism for the rheological behavior of concentrated suspension, such as chocolate, is emphasized in this model. The effective solid volume fraction Φ_{eff} is introduced and contains the solid volume fraction Φ_s and three additional terms for immobilized fluid. It is given as

$$\Phi_{eff} = \Phi_s + \Phi_{sif} + \Phi_{vif} + \Phi_{hifi}, \tag{2.8}$$

with Φ_{sif} the immobilized fluid at the surface of particle aggregates, Φ_{vif} the immobilized fluid within the volume of the particle aggregates, and Φ_{hifi} the hydrodynamically immobilized fluid. Hydrodynamically immobilized fluid arises when particle aggregates move in the fluid phase in such a way that a part of the liquid is excluded from the continuous liquid matrix, for example by rotation of the aggregate. The

ratio Ψ is introduced and describes the changes in surface (ΔV_{fis}) and volume (ΔV_{fiv}) immobilized fluid volume before and after shearing and is given as

$$\Psi = \frac{\Delta V_{fis}}{\Delta V_{fiv}}. \tag{2.9}$$

Ψ is equal to one, when no net change of free fluid is given by aggregation or deaggregation. Depending on whether deaggregation or aggregation is happening and more or less fluid is availabe after the shearing, Ψ is smaller or bigger than one. The effective solid volume fraction is finally given as

$$\Phi_{eff} = \Phi_s \left(1 + \frac{1-\Phi_M}{\Phi_M}\left(1 + (\Psi - 1)\,\frac{3}{4} n^{-\frac{1}{3}} \Phi_M^{\frac{1}{3}}\right)\right), \tag{2.10}$$

where n gives the mean number of primary particles per aggregate. After deducing the dependency of n on shear time and rate from experiments, and fitting to a suitable mathematical equation, the resulting equation for shear viscosity calculation is given by

$$\eta(\Phi, \dot{\gamma}, t, \delta) = \eta_m \left[1 - \frac{\Phi_{eff}(\Phi, \dot{\gamma}, t, \delta)}{\Phi_M(\dot{\gamma}, t, \delta)}\right]^{-k(\delta)\Phi_M(\dot{\gamma}, t, \delta)}. \tag{2.11}$$

The additional parameter δ describes the degree of orientation of non-spherical particles and t is time.

By reviewing the rheological models that are used for describing the flow behavior of chocolate, it can be seen that there is a broad difference in the degree of physical and mechanistic motivation. Of course, the models of Casson, Bingham, and Herschel–Bulkley are valuable tools in describing flow behavior. Nevertheless, their parameters have only limited physical meaning and do scarcely give mechanistic understanding. A next step towards mechanistic understanding is given in the $\tau_{0.1}$ model. The superposition of different rheological regimes, given in Equation 2.5, allows for a mechanistic interpretation of how the microstructure of particles in the continuous cocoa butter matrix changes according to different shear rates. The fluid immobilization model finally allows for detailed mechanistic explanation through different immobilization processes of the flow medium in the aggregate void or on the surface of the aggregates. The level of detail and the physically meaningful parameters of the fluid immobilization model also opens it up for a possible multiscale modeling approach. As this works takes a closer look at nano-scaled mechanisms in the concentrated suspension chocolate, examples will be given of how the results from molecular dynamics simulations can be used in rheological models like the fluid immobilization model.

2.4 Lecithin and other surfactants

Surfactants play a crucial role in chocolate rheology. As amphiphilic molecules they adsorb on hydrophilic–hydrophobic interfaces in chocolate. In dark chocolate this is mainly the sucrose–cocoa

butter interface and further the cocoa particle–cocoa butter interface. There are several classes of surfactants that are used in chocolate manufacturing and they are listed below. Detailed molecular mechanisms leading to the rheological effects are elucidated later. Vegetable lecithin is the most prominent emulsifier. It is a by-product of oil production and the primary sources are soybean, rapeseed, and sunflower. It is a mixture of phospholipids, triglycerides, glycolipids, fatty acids, sterols, sphingolipids and carbohydrates, where the phospholipids are the main surface active component [101]. Polyglyceryl polyricinoleate is a further important emulsifier in chocolate manufacturing. It was shown to form pillow-like structures with cocoa butter triglycerides and is acting as buffer between sucrose particles [91]. YN is a synthetic lecithin and is produced from partially hardened rapeseed oil. It is more constant in its composition than soybean lecithin and also has a greater efficiency in improving flow properties [12]. Further less often used emulsifiers are citric acid ester, sucrose esters, calcium-stearoyl lactoyl lactate, and soritan tristearate [12].

2.4.1 Composition of lecithins

Phospholipids in lecithin have different head and tail groups. The four most prominent head groups in soybean, sunflower, and rapeseed lecithin are phosphatidylcholine (PC), phosphatidylethanolamin (PE), phosphatidylinositol (PI), and phosphatidic acid (PA). The variable parts of the head groups are shown in Figure 2.4. As phospholipids, the variable head groups from Figure 2.4 are connected to a

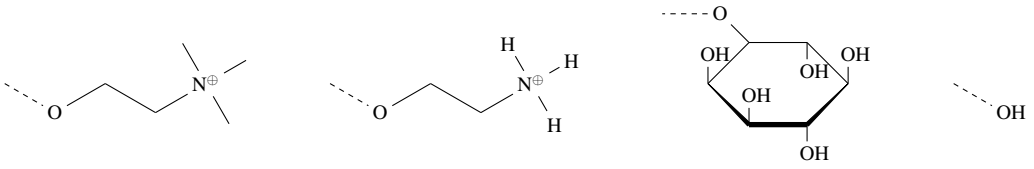

Figure 2.4: Structural formulas of the variable head group parts of the most prominent phospholipids PC, PE, PI, and PA (from left to right).

phosphate group, the glycerol backbone, and to two fatty acids, such as linoleic acid. This residual part of a possible phospholipid is shown in Figure 2.5. The composition of different head groups in lecithins was investigated in several literature studies. A comparison of two different studies [81, 136] is given in Table 2.4. Both studies show similar values in head group composition. For all three vegetable sources PC contributes the biggest part to the phospholipid fraction. While in soybean lecithin PE is the second biggest part, followed by PI and PA, in sunflower and rapeseed lecithin the second biggest part is PI followed by PE and PA. The total phospholipid content is similar for all three vegetable sources. Nguyen et al. [101] also compared phospholipid head group compositions for the same three different vegetable sources. Although they did not give explicit values, the findings can be compared with help of the given bar plots. In contrast to the studies by Loncarevic et al. [81] and van Nieuwenhuyzen and Tomas [136], PI was also the second biggest soybean phospholipid frac-

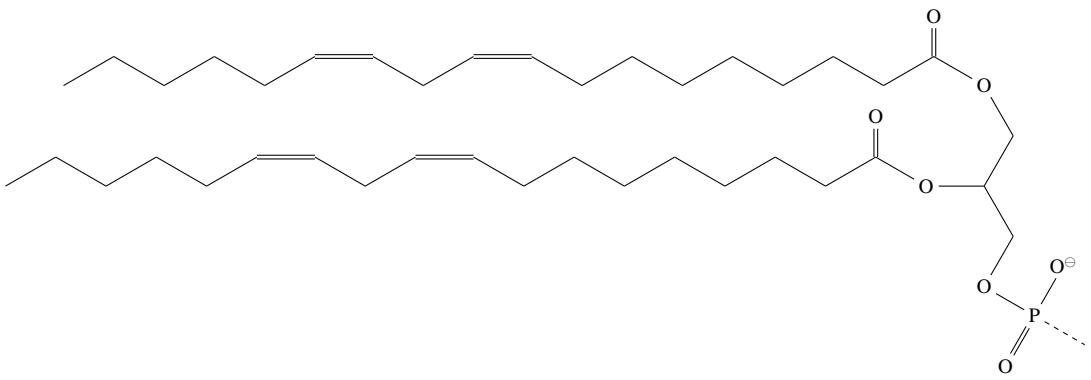

Figure 2.5: Exemplary residual part of a phospholipid that is connected to the head groups from Figure 2.4.

Table 2.4: Head groups composition of different lecithins from literature [81, 136].

Phospholipid (wt% of phospholipids)	Soybean		Sunflower		Rapeseed	
Literature source	[136]	[81]	[136]	[81]	[136]	[81]
PC	31.91	34.76	34.04	40.53	36.96	40.93
PE	23.40	24.6	17.02	14.40	19.57	16.93
PI	21.28	17.49	29.79	31.76	21.74	24.78
PA	8.51	11.0	6.38	3.28	8.7	6.75
All phospholipids (wt%)	47	45.79	47	42.02	46.0	44.61

tion in the study by Nguyen et al. [101]. All the other trends are comparable. Further, it has to be noted that these measurements are quite prone to measuring errors, which can be seen in the error bars given in the study of Nguyen et al. [101]. Loncarevic et al. [81] and van Nieuwenhuyzen and Tomas [136] did not calculate errors or performed a single measurement. Nguyen et al. [101] also investigated the content of saturated, monounsaturated, and polyunsaturated fatty acid of the acetone insoluble fraction of vegetable lecithins. The acetone insoluble value is supposed to represent the total amount of surface active components in the lecithin. This includes phospholipids, glycolipids and carbohydrates all together. Soybean lecithin and sunflower lecithin have a quite similar composition with 20 wt% to 30 wt% saturated fatty acids, 10 wt% to 20 wt% monounsaturated fatty acids and about 60 wt% polyunsaturated fatty acids. Rapeseed lecithin has only about 10 wt% of saturated fatty acid, about 50 wt% monounsaturated fatty acids and about 35 wt% polyunsaturated fatty acids. A quite similar composition is given by van Nieuwenhuyzen and Tomas [136]. Mukhamedova and Glushenkova [99] did the only study where the amount of single specific phospholipids was evaluated. The two biggest species for PC were found to be 1,2-dilinoleoyl-phosphatidylcholine (DLPC) (43.1 wt%) and 1-palmitoyl-2-linoleoyl-phosphatidylcholine (PLPC) (15.6 wt%). For PE it was found to be 1-palmitoyl-2-linoleoyl-phosphatidylethanolamine (PLPE) (21.3 wt%) and 1,2-dilinoleoyl-phosphatidylethanolamine (DLPE) (15.0 wt%). For PI it was found to be 1-palmitoyl-2-linoleoyl-phosphatidylinositol (PLPI) (34.3 wt%) and 1-stearoyl-2-linoleoyl-phosphatidylinositol (SLPI) (11.6 wt%). Further important species that are studied in this thesis are 1,2-dilinoleoyl-phosphatidylinositol (DLPI), 1,2-distearoyl-phosphatidylcholine

(DSPC), 1,2-distearoyl-phosphatidylethanolamine (DSPE), 1,2-distearoyl-phosphatidylinositol (DSPI), 1,2-distearoyl-phosphatidic acid (DSPA), and 1,2-dilinoleoyl-phosphatidic acid (DLPA).

2.4.2 Lecithin production

Van Nieuwenhuyzen and Tomas [136] give a detailed description of the lecithin production process. Only a short overview is given here and the interested reader is referd to the mentioned review [136]. This section intends to present the soybean lecithin production process in order to get an understanding of the natural product lecithin and how it is subject to several aspects that influence its molecular composition.

The world market for lecithin is estimated to be about 150.000 to 170.000 tons and soybeans have been the main source of lecithin in the last decades. Due to the increasingly limited availability of non genetically modified lecithin for the European market, the demand for alternative lecithins, such as high quality sunflower and rapeseed lecithins, is increasing [136]. Soybean oil contains about $800\,\mathrm{ppm}$ to $1200\,\mathrm{ppm}$ phosphorus, which is mainly present in the form of phospholipids. The phospholipids have to be separated from the oil in the so-called degumming step because crude oil with low phosphorus content is required in order to further refine it with low chemical input and low waste output. The lecithin production is divided into four unit operations. The first unit operation is the hydration of phospholipids. After mixing with $1\,\mathrm{wt\%}$ to $3\,\mathrm{wt\%}$ water at $50\,^{\circ}\mathrm{C}$ to $70\,^{\circ}\mathrm{C}$, the phospholipids hydrate and form a gum with higher specific density than the rest of the crude oil. While PC and PI are easily hydratable, PE and PA are only poorly hydratable. Thus, the commercial hydration process delivers a mix of different phospholipids. Water degumming usually gives a crude oil with $50\,\mathrm{ppm}$ to $100\,\mathrm{ppm}$ phosphorus and further treatment of the poorly hydratable phospholipids results in $5\,\mathrm{ppm}$ to $10\,\mathrm{ppm}$ residual phosphorus. The second unit operation is the separation of the gums, which is done by continuously operating centrifuges. This delivers a lecithin gum with an oil content of $30\,\mathrm{wt\%}$ to $39\,\mathrm{wt\%}$ dry oil. As the gums contain up to $50\,\mathrm{wt\%}$ water at that point, the lecithin has to be dried in the third unit operation. Moisture is reduced to less than $1\,\mathrm{wt\%}$, which enhances fluidity and long time shelf life. Film evaporators are used for the drying process and have a high capacity of $70\,\mathrm{kg\,h^{-1}\,m^{-2}}$ to $90\,\mathrm{kg\,h^{-1}\,m^{-2}}$ gum. As the heating during the drying process can lead to darkening through chemical reactions, cooling is necessary to prevent post-darkening and is the fourth unit operation in lecithin production. Therefore, a heat exchanger is used directly after the drier.

2.4.3 Micellar structures of lecithins in different solvents

Phospholipids are a very important class of molecules as they have several important functions in the human body and in several life science areas. They are a key element of cell membranes [102], have an important role in many cosmetic products [15], are a crucial ingredient for many food products [72, 136],

and are investigated for their ability to form liquid crystalline systems, which can be used as drug delivery systems in pharmaceutical applications [46] or for the formation of oleogels [85]. All the different roles that phospholipids have in life sciences are due to their amphiphilic nature and the corresponding ability to form diverse structures with long-range orders. For chocolate manufacturing, this behavior is also very important, and leads to the formation of molecular structures in two different settings. First, the behavior of phospholipids at solid–liquid interfaces, and second their behavior in non-polar solvents. While the behavior at interfaces is introduced with respect to chocolate in the next section, this section highlights their ability to form aggregates in non-polar solvents. To the best of the authors knowledge, no studies exist where the structural behavior of typical soybean lecithin phospholipid mixtures, as they are used in chocolate manufacturing, has been investigated in cocoa butter. Nevertheless, several studies exist where especially PC has been investigated in different non-polar solvents. So far, these studies have not been considered for the explanation of lecithin concentration-dependent rheological effects in chocolate, to the best of the authors knowledge.

Phospholipids are known to self-assemble in different structures, which are labeled lyotropic liquid crystalline mesophases [46]. Occurring structures are the inverse micellar or reverse micellar, reverse cubic micellar, reverse hexagonal, lamellar, and bicontinuous cubic phases [46]. Several system properties can have an effect on the resulting mesophase. The resulting structures are shown to be a concentration-dependent phenomenon. Thus, the phospholipid concentration has a crucial influence [6]. The exact type of phospholipid and hydrophobic organic solvent are key parameters for the resulting structure. So far, the main focus in the literature was on PC and a wide variety of organic solvents when the formation of the liquid crystalline structures was investigated. An overview is given in a literature review [120]. The molecular shape and thus the types of head groups, due to their different sizes as well as the degree of saturation of aliphatic chains, were shown to have an impact on resulting mesophases and are discussed by Shchipunov [120]. Nevertheless, the shape factor doesn't seem to be investigated extensively so far. For the case of chocolate, the phospholipid shape factor is highly relevant as a wide variety of different phospholipids are present in soybean lecithin. The four most prominent head groups have a big difference in their size, where PI is the biggest one, followed by PC, PE, and PA. The size difference is shown in Figure 2.4. The tail groups also have different shapes as unsaturated bonds lead to other angles between the carbon atoms and thus to other spacial configurations. Addition of trace amounts of small organic molecules, such as water, glycerol or ethylene glycol, were shown to enhance the formation of gels [120]. Due to the macroscopic gel-like properties of these systems, they are labeled lecithin organogels. Different PC based systems in hydrophobic solvents are reported to form big reverse cylindrical micelles, for more details the review by Shchipunov [120] can be taken as a starting point. Low concentrated PC in cyclohexane assembles in the reverse micellar phase and with increasing concentrations it changes to reverse hexagonal and lamellar phases [6]. A dilute solution of PC in isooctane with trace amounts of water was argued to form more rodlike than wormlike structures as the micelles are too short to form a three-dimensional network [28]. Mixtures of PC, fatty acids, and water were shown to form reverse hexagonal, reverse micellar, reverse cubic, and

lamellar phases depending on the concentration of the components [49]. Markina et al. [86] performed dissipative particle dynamics to investigate the molecular mechanisms of wormlike micelle formation in PC–cyclohexane mixtures after adding a bile salt. Vierros and Sammalkorpi [137] showed that simulations employing the CHARMM36 all-atom force field do not correctly predict reverse micellar structures of PC in organic solvents. To predict the right structure it has to be reparametrized with respect to its lipid-tail cyclohexane interaction.

A special type of organogel, so called oleogels, are quite similar to a cocoa butter–lecithin mixture. In a suitable composition, a cocoa butter–lecithin mixture with water should be able to form an oleogel. Oleogels are lipid based gels, which get its gel properties by adding organo-gelators, such as phospholipids, to the liquid oil. Depending on processing and environmental conditions as well as composition, the oleogels are firm gels with physical properties that are similar to solid fat [16]. Their potential physico-chemical properties are a high viscosity, plasticity, thermo-reversibility, and durability [16]. Bodennec et al. [16] investigated the microstructural organization of lecithin–canola oil oleogels depending on the water content, lecithin concentration, and temperature. In their study, the lecithin was a mixture of PC (24 wt%), PE (20 wt%), PI (14 wt%), and PA (8 wt%), quite similar to the lecithins investigated in this thesis. The microstructure of the systems was investigated by confocal laser scanning microscopy. In a canola oil based system with 30 wt% lecithin an arbitrary collection of lecithin aggregates was found. After addition of only 1 wt%, a well-developed network was visible. Below temperatures of about 55 °C, a wormlike micellar network was apparent, where small-angle X-ray diffraction strongly suggested a reverse hexagonal structure. While the shown studies give detailed insights into phospholipid structures, primarily PC, in different hydrophobic solvents, structures of soybean lecithin-like phospholipid mixtures in cocoa butter have not been investigated so far.

2.4.4 Lecithin behavior in chocolate and its impact on rheology

The best yield stress and viscosity reducing effects of lecithin in chocolate can be achieved at concentrations of 0.3 wt% to 0.5 wt%. Further addition of lecithin has only a minor viscosity reducing effect, while the yield stress increases again [12, 35, 118, 135]. Van Nieuwenhuyzen [135] compared the effects of different lecithins with certain enriched phospholipid fractions in chocolate. The PC enriched lecithin has the strongest viscosity reducing effect, while PE and PI enriched lecithins have a similar effect that was a little less pronounced. The PI enriched lecithin has the strongest effect in yield stress reduction at low lecithin concentrations (< 0.3 wt%). At higher concentrations (> 0.3 wt%) PE reaches the same yield stress reducing effect. Further, the yield stress increases for all chocolates with lecithins at higher concentration, with the PI enriched fraction showing by far the strongest effect. Unfortunately, it seems that the total amount of phospholipids in the lecithin mixtures differed for the investigated lecithins, leading to the fact that when the same amount of lecithin was used, the total amount of phospholipids differed and thus the effects have to be compared with care. Arnold et al. [9] compared the rheological effects of the specific phospholipids 1,2-dipalmitoyl-phosphoethanolamine (DPPE), 1,2-

dipalmitoyl-phosphocholine (DPPC), and 1,2-dipalmitoyl-phosphatidic acid (DPPA) on oil-based suspensions to that of a typical soybean mixture. The soybean lecithin was found to have the strongest viscosity reducing effects at low concentrations, the single fractions were more viscosity reducing at higher concentrations. Further, it was shown that the yield stress increases with increasing concentration of soybean lecithin but not with increasing concentration of the single fractions DPPC, DPPE, and DPPA. Arnold et al. [9] state that this different behavior of soybean lecithin might be explained by the additionally containing phospholipids and other minor fractions and the different composition of aliphatic chains.

It is commonly agreed that the basic principle for the rheological effects of lecithin in chocolate is the coverage of hydrophilic sucrose and cocoa particles with phospholipids. From a physical point of view this has one major effect: the interfacial tension is lowered due to the thermodynamically more desirable interface. Adsorption of phospholipids and the resulting lower surface tension lead to different effects in the liquid chocolate, which are hypothesized to improve rheological behavior. First, adsorption of phospholipids at particle surfaces leads to desorption of cocoa butter triglycerides that are immobilized at the particle surfaces. After desorption more cocoa butter triglycerides are available as liquid matrix for the particles to flow in. Immobilization is evident, due to the powdery state of cocoa mass after refining and can be measured by centrifugation experiments, where it is shown that not all triglycerides can be separated from sucrose particles after centrifugation [93]. Up to $0.33\,\mathrm{g\,m^{-2}}$ cocoa butter per sucrose surface are immobilized. Nevertheless, it has to be considered that this amount accounts for surface immobilized fat as well as fat that is immobilized in aggregate voids. Second, lecithin adsorption leads to a smoothing of particle surfaces by filling gaps and crevices, allowing the particles to pass each other more easily in flow. Third, rendering the particles hydrophobic, by adsorption of phospholipids, lowers the hydrophilic particle interactions, leads to less aggregation, better flow behavior, and further leads to a better wettability of the particles. All three mechanisms have been supported by studies from literature, which is shown in the following.

Johansson and Bergenstahl [68] investigated phospholipid adsorption on sucrose crystals in soybean oil. They found that the amount of adsorbed phospholipids is between the double to sixfold amount of the estimated monolayer formation. The estimate is given by measuring the surface and assuming an average area per lipid of $0.7\,\mathrm{nm^2}$. They assume a multiple layer formation of phospholipids or phospholipid aggregates near the interface. Further structural analysis was not performed in their study. The study supports the hypothesis for phospholipid effects in chocolate of reduction of cocoa butter immobilization at sucrose surfaces by showing adsorption of phospholipids at these surfaces. Another study investigated adsorption of 1-oleoyl-2-palmitoyl-phosphatidylethanolamine (OPPE) on mica and sucrose surfaces [37]. While the OPPE molecules adsorb in a monolayer on the mica surface, it was found that more than a monolayer adsorbs on the sucrose surface. The authors argue that it is does not seem likely for OPPE to form multiple layers as no further polar interaction can be satisfied by adsorbing in a second layer. They propose that another effect than polar head group interactions must be the reason for this. The excess OPPE might condense at the sucrose surface by filling crevices and

gaps, which could be promoted by the low solubility of OPPE in the oil. Filling of crevices and gaps was also observed by scanning electron microscopy and is consistent with the idea of condensing of phospholipids in crevices and gaps [61]. Due to phase separation the phospholipids fill crevices and gaps and allow the particles to slide past each other more easily. In that case the phospholipid phase might be in a reverse micellar, hexagonal or laminar phase. Dedinaite et al. [37] further measured adhesion forces between particles and showed that OPPE layers on mica particle surfaces influence the adhesion force between particles. Changes in the adhesion were present when water is added to the system, leading to reverse phospholipid aggregates in the apolar oil matrix. This study promotes the reduced cocoa butter immobilization hypothesis as well as the smoothing hypothesis and the reduced particle interaction hypothesis. The same group also showed that the most polar part of triglycerides, the glycerol backbone, adsorbs with its ester groups on hydrophilic mica particles [29]. This supports the hypothesis that immobilized cocoa butter gets replaced by phospholipids at the interface. Rousset et al. [114] showed by inversed gas chromatography that coating of sucrose particles with phospholipids leads to increased lipophilicity of sucrose particles. Recent atomic force microscopy studies give detailed insight into lecithin structures at sucrose–cocoa butter interfaces [92]. Soybean lecithin seems to be better suited for the chocolate conching process than sunflower lecithin as it leads to a higher total coverage of sucrose surfaces with thinner layers than sunflower lecithin. The study shows that sucrose surfaces are not completely covered by phospholipids and that the parts that are covered, are covered with relatively thick layers. The layers consist of a cocoa butter–phospholipid mixture and are between 34 and 36 nm thick.

The increase of the yield stress of chocolate after addition of an excess amount of lecithin, which is investigated in this thesis, is so far only partly understood, nevertheless a few explanations were proposed. The first approach argues that after reaching the phospholipid concentration that gives a monolayer of adsorbed phospholipids at the particles, further phospholipid layers are formed, which might also render the sucrose particle hydrophilic again. This hypothesis is promoted by Beckett [12] as well as by Johansson and Bergenstahl [68]. Johansson and Bergenstahl [68] argue, without further evidence that the outermost layer should always be directed with the aliphatic chains towards the cocoa butter phase. This explanation has already been a matter of debate in literature as it has a weakness [37]. For the formation of a second layer (and also each further layer with an even number) there is no polar driving force for adsorption. When the first monolayer is formed the next phospholipids have no driving force to connect their tails to the tails of the phospholipid monolayer and can as well simply interact with cocoa butter triglycerides. In fact a second layer would result again in a thermodynamically unfavorable hydrophilic–hydrophobic interface (between phospholipid head groups and hydrophobic cocoa butter triglycerides). To what extent the low solubility of phospholipids in oil, which was used as an argument for filling crevices and gaps by Dedinaite et al. [37], could be used an explanation for the formation of multiple layers, has not been investigated so far.

A second approach argues that the phospholipids might form some kind of micellar structures when present in an excessive dose and a first monolayer has already been formed. Micelle formation would

directly lead to a thermodynamically favorable configuration as the hydrophilic head groups would directly interact with each other and were not forced to build a hydrophilic–hydrophobic interface with cocoa butter like they would be during formation of a second layer. Arnold [8] and former co-workers [118] of the group argue that the formed aggregates could increase the particle interactions in the highly concentrated suspension and thus lead to an increase in the yield stress. When flow is induced, the formed structures and aggregates have to be broken and then do not further influence rheological behavior. This would explain increased yield stress while viscosity stays low at higher lecithin concentrations.

Chapter 3

Molecular dynamics simulations

Molecular dynamics is a simulation technique that allows to calculate the dynamic evolution of a system with atomistic resolution. The resulting molecular trajectories can be used to calculate different dynamic and thermodynamic system properties. Evolving molecular structures and the dynamic system behavior can be examined in detail. To perform molecular dynamics simulations several key aspects have to be considered.

- Classical mechanics of atomistic systems and solving equations of motion
- Development of a molecular model and corresponding interaction potentials
- Statistical mechanics and sampling from thermodynamic ensembles
- System analysis and calculation of macroscopic properties

This chapter is intended to give an overview of the theoretical background of molecular dynamics simulations for readers who are not familiar with the simulation method. More detailed information, together with original sources, are given in references [5], [48], and [52] and thus are omitted in this summary. Subsequently, two methods are introduced that help to overcome the limits of time and length scales of classical molecular dynamics simulations to a certain extent; the coarse-graining method and the implicit solvation method. Finally, a literature review on molecular dynamics simulations with food related applications is given.

3.1 Classical mechanics

In classical molecular models, which are used to perform molecular dynamics simulations, molecules are modeled with atomistic resolution. Generally, the dynamic behavior of atoms is governed by the

dynamics of their elementary particles, which is given in the Schrödinger equation as

$$-i\hbar\frac{\partial\Psi^{(c,e)}(\boldsymbol{r_c},\boldsymbol{r_e},t)}{\partial t} = \mathscr{H}\Psi^{(c,e)}(\boldsymbol{r_c},\boldsymbol{r_e},t), \tag{3.1}$$

with $\Psi^{(c,e)}$ being the wave function that describes the quantum state of the cores c and the electrons e of the molecules and depends on the position of the cores $\boldsymbol{r_c}$ and electrons $\boldsymbol{r_e}$, time t, Planck constant $\hbar$, imaginary unit i, and the Hamiltonian $\mathscr{H}$. The Hamiltonian gives the total energy of a system

$$\mathscr{H} = \mathscr{K}^c + \mathscr{K}^e + \mathscr{V}^c + \mathscr{V}^e + \mathscr{V}^{c,e}, \tag{3.2}$$

with $\mathscr{K}$ the kinetic energy and $\mathscr{V}$ the potential energy. To calculate the dynamic behavior of bigger molecular systems, such as chocolate in this case, the Born–Oppenheimer approximation and the classical approximation are used to avoid the necessity to solve the Schrödinger equation for the whole system. The Born–Oppenheimer approximation states that the mass of electrons can be neglected compared to the mass of the atomic cores, which means that the core movement is much slower than the electron movement, and thus electrons directly respond to core configuration changes. This results in a new formulation of the wave function, where only the state of the cores is time-dependent

$$\Psi^{(c,e)}(\boldsymbol{r_c},\boldsymbol{r_e},t) = \Psi^{(e)}(\boldsymbol{r_c},\boldsymbol{r_e})\Psi^{(c)}(\boldsymbol{r_c},t) \tag{3.3}$$

and means also that the dynamic behavior of atoms can be described by the dynamics of the cores alone. Together with the classical approximation, which states that quantum effects do not govern the system behavior as long as the average inter-atomic spacing is much bigger than the thermal De-Broglie wave length, the dynamics of the cores can be calculated with Newtonian mechanics. The thermal De-Broglie wave length Λ is given as

$$\Lambda = \sqrt{\frac{2\pi\hbar^2}{mk_BT}} \ll d, \tag{3.4}$$

with the Boltzmann constant k_B, the average inter-atomic spacing d, the mass m, and temperature T. Following the Born–Oppenheimer and classical approximation the dynamic behavior of atoms can be calculated employing classical mechanics. The above approximations are only valid as long as quantum effects do not affect the systems. Further, classical mechanics are only valid when relativistic effects do not affect the system. Hence, the following scenarios should be avoided in classical molecular dynamics simulations: particles with very small masses, temperatures near absolute zero, extremely high particle velocities, extremely small length scales, and processes where chemical reactions occur.

Commonly three different mathematical formalisms are used to describe classical mechanics and are briefly described in the following.

3.1.1 Newtonian mechanics

Sir Isaac Newton stated his three laws of motion in his most important work *Philosophiae Naturalis Principia Mathematica* from 1687. His laws describe the motion of physical objects and can explain Kepler's laws of planetary motion. The index i references the different objects of the system. The first law states that the net force acting on an object i with constant velocity is zero and is given as

$$\sum \boldsymbol{F}_i = 0, \tag{3.5}$$

where $\sum \boldsymbol{F}_i$ is the sum of all forces acting on the object.

The second law states that the force acting on an object is equal to the rate of change of momentum, both acting in the same direction. For constant masses the second law is given as

$$\boldsymbol{F}_i = \frac{d\boldsymbol{p}_i}{dt} = m_i \frac{d\boldsymbol{v}_i}{dt} = m_i \boldsymbol{a}_i, \tag{3.6}$$

where $\boldsymbol{p}_i$ is the momentum, m_i is the mass, $\boldsymbol{v}_i$ the velocity, and $\boldsymbol{a}_i$ the acceleration. Newton's third law states that all the forces that act between to physical objects are of equal magnitude with opposite directions and is given as

$$\boldsymbol{F}_1 = -\boldsymbol{F}_2. \tag{3.7}$$

3.1.2 Lagrangian mechanics

In the Lagrangian formalism the trajectory of a system of n particles is described as function of its energies rather than of the forces. In order to include system constraints, generalized coordinates $\boldsymbol{q} = (\boldsymbol{q}_1, \boldsymbol{q}_1, ..., \boldsymbol{q}_n)$ and their time derivatives $\dot{\boldsymbol{q}} = (\dot{\boldsymbol{q}}_1, \dot{\boldsymbol{q}}_2, ..., \dot{\boldsymbol{q}}_n)$ are usually introduced. The central quantity is the Lagrangian $\mathscr{L}$, which has the dimension of an energy and is given as

$$\mathscr{L}(\dot{\boldsymbol{q}}, \boldsymbol{q}) \equiv \mathscr{K}(\dot{\boldsymbol{q}}) - \mathscr{V}(\boldsymbol{q}). \tag{3.8}$$

The Lagrangian equation of motion for one particle is given as

$$\frac{d}{dt}\left(\frac{\partial \mathscr{L}}{\partial \dot{\boldsymbol{q}}_i}\right) - \left(\frac{\partial \mathscr{L}}{\partial \boldsymbol{q}_i}\right) = 0. \tag{3.9}$$

The kinetic energy $\mathscr{K}$ is given as

$$\mathscr{K}(\dot{\boldsymbol{q}}_i) = \frac{1}{2} m_i \dot{\boldsymbol{q}}_i^{\,2} \tag{3.10}$$

and depends only on the velocity. The potential energy $\mathscr{V}$ is defined by the interaction energies of the particle and is only a function of the position. The force is given as the negative spacial derivative of

the potential energy

$$-\frac{\partial \mathscr{V}}{\partial \boldsymbol{q}_i} = \boldsymbol{F}_i. \tag{3.11}$$

By combining Equations 3.9, 3.10, and 3.11 and using Cartesian coordinates for a system of atoms Newtons second law is obtained.

$$\frac{d}{dt}\left(\frac{\partial \mathscr{K}}{\partial \dot{\boldsymbol{q}}_i}\right) + \left(\frac{\partial \mathscr{V}}{\partial \boldsymbol{q}_i}\right) = \frac{d}{dt}(m_i \dot{\boldsymbol{q}}_i) - F_i = m_i \ddot{\boldsymbol{q}}_i - F_i = 0. \tag{3.12}$$

Equation 3.12 is a reformulation of Newtons equation of motion by explicitly giving the relationship between motion and potential and kinetic energy, which are in the framework of molecular dynamics usually given rather than the explicit forces. To solve this system of second-order ordinary differential equations in three dimensional space, two initial condition for each dimensions have to be given, which are initial velocity and position for each particle.

3.1.3 Hamiltonian mechanics

By using the Hamiltonian formalism the system of 3N second-order differential equations (Equation 3.12) can be expressed as a set of 6N first-order differential equations, where N is the number of particles. This gives the opportunity for the development of more efficient algorithms for calculating the system trajectories. The Hamiltonian is strictly defined as

$$\mathscr{H}(\boldsymbol{p},\boldsymbol{q}) \equiv \sum_i \dot{\boldsymbol{q}}_i \boldsymbol{p}_i - \mathscr{L}(\boldsymbol{q},\dot{\boldsymbol{q}}), \tag{3.13}$$

where the conjugate momenta $\boldsymbol{p}_i$ to the coordinates $\boldsymbol{q}_i$ are defined as

$$\boldsymbol{p}_i = \frac{\partial \mathscr{L}}{\partial \dot{\boldsymbol{q}}_i}. \tag{3.14}$$

The time evolution of the system and thus the equations of motion are given as

$$\dot{\boldsymbol{q}}_i = \frac{\partial \mathscr{H}}{\partial \boldsymbol{p}_i} \tag{3.15}$$

$$\dot{\boldsymbol{p}}_i = -\frac{\partial \mathscr{H}}{\partial \boldsymbol{q}_i}. \tag{3.16}$$

The Hamiltonian equations of motion for Cartesian coordinates can then be written as

$$\dot{\boldsymbol{r}}_i = \frac{\boldsymbol{p}_i}{m_i} \tag{3.17}$$

$$\dot{\boldsymbol{p}}_i = -\nabla_{\boldsymbol{r}_i} \mathscr{V} = \boldsymbol{F}_i, \tag{3.18}$$

which gives the mentioned system of 6N first-order differential equations.

3.1.4 Integrating the equations of motion

In order to compute the time evolution of the system, also called the system trajectory, the equations of motion 3.12 or 3.17 and 3.18 have to be solved. That means that the positions and velocities of the atomic components of the molecular system for a time $t + \partial t$ have to be calculated from the actual positions and velocities by integration of the equations of motion. The following requirements are imposed on a suitable integration algorithm: conservation of momentum and energy; time-invariance of the algorithm; possibility to use a long time step; moderate use of memory; only one calculation of forces per time step; efficient computation; easy implementation; delivery of accurate system trajectories. Different algorithms that fulfill these requirements are available, commonly the leap-frog algorithm or the velocity verlet algorithm are used in molecular dynamics simulations. For more details on integration algorithms the reader is again pointed to literature [5, 48].

3.1.5 Periodic boundary conditions and finite size effects

Macroscopic laboratory experiments are usually performed in test tubes, tanks, or some kind of containers, which suggests that molecular dynamics simulations should also be performed in some kind of container where the system under investigation is contained. However, due to the huge difference in system size between experiment and molecular dynamics simulations, wall effects would act much stronger on the system because the specific surface in small volumes is much higher. Atoms at the system boundaries would be exposed to other forces than in bulk due to the interaction with the container walls. Therefore, the principle of periodic boundary conditions is introduced. The simulation box is replicated in all spacial directions in order to form an infinite lattice of simulation boxes. During the simulation the trajectory of the replicated beads is exactly the same in all periodic boxes and has to be calculated only once for the original box and all coordinates and velocities also have to be stored only once. In the case that one molecule leaves the central box, the periodic image of the molecule will enter the box from the opposite side. This is schematically shown in Figure 3.1 and results in a system, which has no wall effects or surface molecules, and thus represents a system with infinite bulk properties. The molecule from the central box moves to the replicated box on the left, while simultaneously the periodic image of the molecule from the right enters the central box. The number density of the central box is conserved.

Nevertheless, it has to be checked if the simulation of a small infinitely replicated box is comparable to the behavior of a macroscopic bulk system. This depends on two things: the range of the potentials in the system and the phenomena to be studied. Thus, the system size has to be related to the short range interactions in the system. It has to be guaranteed that each atom only interacts pairwise with the nearest periodic representation of each atom. Interactions with all replicated particles are neglected. This is called the minimum image convention. Usually short range interactions are truncated with a cut-off distance, which defines the radius of the sphere wherein the short range interactions of each

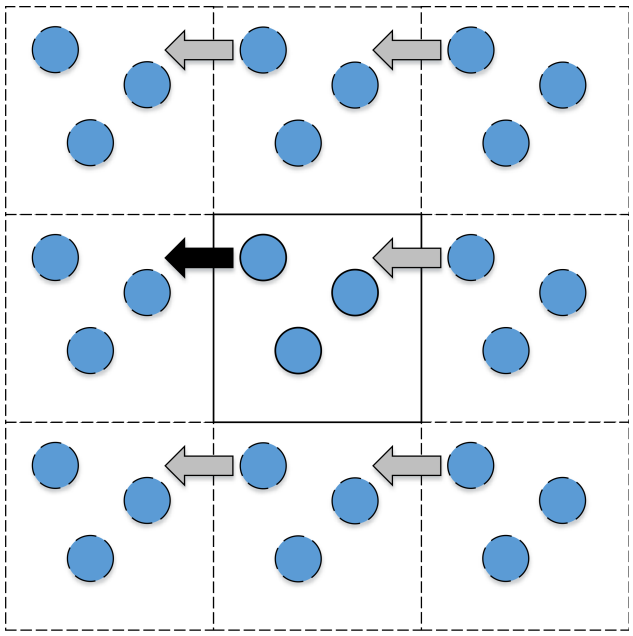

Figure 3.1: Two dimensional representation of the original box with its periodic boxes along two coordinates. Molecules can leave one box and enter the neighbouring periodic image.

atom are calculated. For consistency with the minimum image convention, the smallest box vector has to be at least twice the cut-off radius plus the longest dimension of the biggest molecule in the system.

Regarding the size of the system a further aspect has to be considered. In general, the thermodynamic limit has to be estimated, which means that the investigated macroscopic property has to be extrapolated for the number of particles $n \to \infty$ and the Volume $V \to \infty$ while the ratio $\frac{n}{V} = const.$. Periodic boundary conditions alone do not ensure thermodynamic limit behavior, they only avoid boundary effects. The simulation boxes have to be built big enough to make sure that all quantities are in the thermodynamic limit and no so-called finite size effects occur. For example a single molecule simulated with periodic boundary conditions would always look like a crystal, which would be a finite size effect.

3.2 Molecular models and interaction potentials

Molecular models usually describe bonded and non-bonded interactions between the beads of the investigated system in a pairwise additive manner, which is an approximation of the correct multi-body potential. The potential $\mathscr{V}(r)$ of the system depends on the position of all particles and is given as

$$\mathscr{V}(r) = \sum_{i=1}^{n} \sum_{j>i}^{n} \mathscr{V}(r_{ij}). \tag{3.19}$$

More details on the interaction potentials are given in the following section.

3.2.1 Bonded interactions

Bonded interactions are in general much stronger than non-bonded interaction and represent all interactions that are caused by covalent chemical bonds. They preserve the three dimensional molecular order of atoms and its structure within a certain range. The bonded interaction potential is zero in the equilibrium state of the molecule, which depends on the surrounding medium. Atomic motion in the investigated system leads eventually to disturbances of the equilibrium molecular structures and thus forces arise, which tend to get the atoms back to equilibrium. Three different bonded interactions are commonly included in molecular dynamics simulations and are schematically shown in Figure 3.2 These are the bond interaction controlling the bond length between two atoms, the angle-interaction

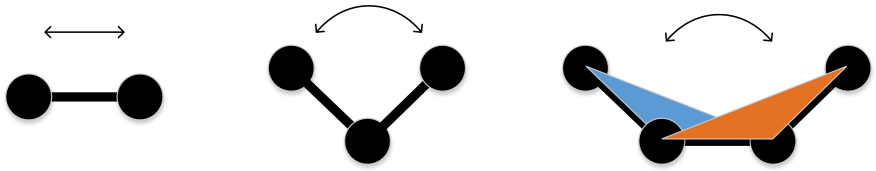

Figure 3.2: Bond- (left), angle- (middle), and dihedral- (right) interactions commonly represent covalent interactions in molecular dynamics simulations.

controlling the angle defined by three atoms, and the dihedral-interaction controlling the dihedral angle defined by four atoms. The specific formulations of these interactions depend on the used force field and thus only examples are presented here. The bond and angle potential are usually given by harmonic potentials. The potential of the bond length $\mathcal{V}_{bond}(r)$ is given by

$$\mathcal{V}_{bond}(r) = K_{bond}(r - r_0)^2, \tag{3.20}$$

with a equilibrium distance r_0, the actual distance r, and a force constant K_{bond}. The potential of the angles $\mathcal{V}_{angle}(\Theta)$ is given by

$$\mathcal{V}_{angle}(\Theta) = K_{angle}(\Theta - \Theta_0)^2, \tag{3.21}$$

with an equilibrium angle Θ_0, the actual angle Θ, and a force constant K_{angle}. The dihedral potential $\mathcal{V}_{dihedral}(\Phi)$ is given by

$$\mathcal{V}_{dihedral}(\varphi) = \sum_n K_{dihedral}(1 + (-1)^{n+1}\cos(n\varphi - \varphi_0)), \tag{3.22}$$

with the multiplicity n (number of potential minima between 0 and 2π), the dihedral angle of the first minimum of the potential φ_0, the actual dihedral angle φ, and a force constant $K_{dihedral}$.

3.2.2 Non-bonded interactions

Commonly two different non-bonded interactions are considered in molecular dynamics simulations: van der Waals interactions and electrostatic interactions. Non-bonded interactions act between molecules and also within molecules, when separated by a defined minimum number of bonds, which is shown in Figure 3.3. Van der Waals interactions are given by a Lennard-Jones potential energy function

$$\mathscr{V}_{LJ}(r) = 4\varepsilon_{ij}\left[\left(\frac{\sigma_{ij}}{r}\right)^{12} - \left(\frac{\sigma_{ij}}{r}\right)^{6}\right], \tag{3.23}$$

with σ_{ij} being the distance at which the Lennard-Jones potential is zero and ε_{ij} being the depth of the potential well. The potential is positive when the particles are very close to represent steric repulsion or negative after exceeding the distance σ_{ij} to account for attractive van der Waals effects, which represent electrical dipoles. The van der Waals potential reaches a minimum with the well depth of ε_{ij} and afterwards converges quickly to zero with increasing distance. A cut-off distance can be introduced easily, making the van der Waals interaction a short-range potential. The Lorentz–Berthelot-combination rule gives the parameters for the van der Waals interactions of different atoms i and j by

$$\sigma_{ij} = \frac{(\sigma_{ii} + \sigma_{jj})}{2} \tag{3.24}$$

$$\varepsilon_{ij} = \sqrt{\varepsilon_{ii}\varepsilon_{jj}}. \tag{3.25}$$

Electrostatic interactions result from the charge distribution within the investigated molecules. Besides real electric charges also different electronegativities of the atoms within the molecules lead to a charge distribution in the molecules. The resulting electrostatic interactions are calculated by a Coulombic potential energy function $\mathscr{V}_{el}(r)$

$$\mathscr{V}_{el}(r) = \frac{q_i q_j}{4\pi\varepsilon_0}, \tag{3.26}$$

with the electric charges q_i and q_j of the interacting beads and the permittivity of vacuum ε_0. Further, it is also possible to account for induced polarization effect in molecular dynamic simulations by introducing so-called virtual sites, which have an electric charge but no mass. Since this was not done in this thesis, it is not further described here. The overall potential energy of the force field is then given as the sum of all bonded and non-bonded interactions and is given as

$$\mathscr{V} = \mathscr{V}_{bond} + \mathscr{V}_{angle} + \mathscr{V}_{dihedral} + \mathscr{V}_{LJ} + \mathscr{V}_{el}. \tag{3.27}$$

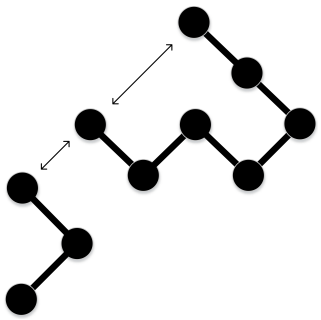

Figure 3.3: Non-bonded interactions act between molecules and also within molecules, when atoms are separated by a defined number of bonds.

3.3 Statistical mechanics

In the last two sections, a short overview was given on how atomistic systems can be treated as simple mass points, and how their dynamic behavior can be calculated by classical mechanics based on a typical set of interaction potentials. This results in trajectories of the atomistic systems, where the positions and velocities for all atoms of the system are calculated for a given time. In this section, the basic tools of statistical mechanics are discussed, which allow to calculate macroscopic thermodynamical properties, such as pressure, temperature, free energy, and entropy. Statistical mechanics is the link between microscopic trajectories and macroscopic system properties. The term statistical thermodynamics can synonymously be used.

3.3.1 Thermodynamic ensembles and the principle of ergodicity

The microscopic state of the investigated system is defined by the positions and velocities or momenta of all atoms in the system. All possible positions and momenta can be seen as the coordinates of a multidimensional space, the so-called phase space. Thus, the phase space is defined by the basis vectors of the position coordinates $\boldsymbol{r} = (\boldsymbol{r}_1, \boldsymbol{r}_2, ..., \boldsymbol{r}_n)$ and the momenta coordinates $\boldsymbol{p} = (\boldsymbol{p}_1, \boldsymbol{p}_2, ..., \boldsymbol{p}_n)$ and is a $6N$ dimensional space, with N the number of atoms in the system. The thermodynamic state of a macroscopic system in equilibrium is defined by a set of constant state variables, for example constant number of particles N, volume V, and energy E, which is called the microcanonical ensemble or *NVE* ensemble. The term ensemble describes all points in phase space that fulfill the defined macroscopic requirements of an ensemble, for example with certain constant *N*, *V*, and *E*. Further important ensembles are the *NVT* ensemble, where *T* means constant temperature, the so-called canonical ensemble and the *NPT* ensemble, where *P* means constant pressure, the so-called isothermal-isobaric ensemble. It can be assumed that a property of the system A, for example the potential energy, can be calculated for every single point in phase space as $A(\Gamma)$, where Γ is a certain point in phase space.

In experiments, all systems evolve in time, which means that Γ changes, and thus $A(\Gamma)$ changes. It is reasonable to assume that in a macroscopic experiment, the time average $\langle A(\Gamma)\rangle$ is observed, which is given as

$$A_{obs} = \langle A\rangle_t = \langle A(\Gamma(t))\rangle_t = \lim_{t_{obs}\to\infty} \frac{1}{t_{obs}} \int_0^{t_{obs}} A(\Gamma(t))dt. \tag{3.28}$$

The equations that govern the described time evolution of a system of atoms and molecules, are the already introduced equations of motion, which give a system of ordinary differential equations. The integration of Equation 3.28 cannot be performed for infinite time, but it is possible to average over a sufficiently long finite time. This is exactly what is done in molecular dynamics simulations.

Using time averages is not the usual approach for calculating thermodynamic properties in the means of statistical mechanics, where Gibbs suggested to use ensemble averages instead. Each point in a certain ensemble has a probability density $\rho_{ens}(\Gamma)$, which is defined by the macroscopic ensemble parameters (NVE, NVT, NPT). As the system evolves with time, according to Newtons equations of motion, in molecular dynamics simulations, $\rho_{ens}(\Gamma)$ also changes with time because Γ changes with time. However, during the time evolution of the trajectory in thermodynamic equilibrium, no points in phase space are destroyed or created and Liouville's theorem states that $\frac{d\rho_{ens}}{dt} = 0$, which is a conservation law for the probability density. When we take a look at one very long trajectory, it travels through the complete phase space and will visit every point in phase space eventually. By solving equations of motion for an infinitely long time, all possible points in phase space will be sampled. This is what is called an ergodic system and it becomes clear that replacing ensemble averages with time averages, which are calculated by molecular dynamics simulations, is valid. The ergodic hypothesis states that time averages equal ensemble averages when sufficient sampling of the phase space is ensured.

$$A_{obs} = \langle A\rangle_{ens} = \sum A(\Gamma)\rho_{ens}(\Gamma) = \lim_{t_{sim}\to\infty} \frac{1}{t_{sim}} \int_0^{t_{sim}} A(\Gamma(t))dt = \langle A\rangle_t. \tag{3.29}$$

$\sum$ indicates a summation over the complete phase space. Note that the probability density is not part of the time average and thus it is a requirement on molecular dynamics simulations to generate configurations in accordance with the probability distribution corresponding to a certain ensemble, which is described in Sections 3.3.2 and 3.3.3.

The so-called partition function Q_{ens} is the sum over all states $w_{ens}(\Gamma)$, where $w_{ens}(\Gamma)$ is a non-normalized form of $\rho_{ens}(\Gamma)$.

$$Q_{ens} = \sum w_{ens}(\Gamma) \tag{3.30}$$

$$\rho_{ens}(\Gamma) = \frac{w_{ens}(\Gamma)}{Q_{ens}} \tag{3.31}$$

The normalization is chosen in a way to set the integral of the density over phase space to one, where Q_{ens} is the normalizing factor. As Q_{ens} is a characteristic quantity that includes all states in the ensemble, it is the key quantity that is required to calculate thermodynamics properties from molecular systems. Of

course the summation over all possible states is generally not possible for a molecular systems of the size that is usually of interest. Fortunately, this is also not necessary as only points with high probability in phase space have a relevant contribution to Q_{ens}. The molecular dynamics approach to that problem is to use Newtons equations of motion and further temperature and pressure regulation algorithms in order to generate a trajectory of states in accordance with the density function ρ_{ens}.

3.3.2 Typical thermodynamic ensembles in molecular dynamics simulations

The previous section showed that it is necessary to sample a trajectory according to the probability density of the microstates. Therefore, it is necessary to explicitly know the mathematical form $\rho_{ens}(\Gamma)$ for each ensemble. Further Q_{ens} is the characteristic property of the ensemble that links it to classical thermodynamic properties. Due to the importance of these two quantities, they are given in this section. For the exact derivations of probability densities and partition functions and calculation of specific properties, the interested reader is again referred to the literature [5, 48].

The probability density of the microcanonical ensemble is $\rho_{NVE}(\Gamma) = \frac{1}{Q_{NVE}}$ for every $\mathscr{H}(\Gamma) = E$, indicating that every microstate is equally likely. The partition function of the microcanonical ensemble is given as

$$Q_{NVE} = \sum \delta(\mathscr{H}(\Gamma) - E) \tag{3.32}$$

$$Q_{NVE} = \int \delta(\mathscr{H}(\Gamma) - E) d\Gamma. \tag{3.33}$$

$\int d\Gamma$ stands for integration over the complete phase space. In the discrete case (Equation 3.32) δ is the Kronecker delta, in the continuous case (Equation 3.33) it is the Dirac delta. By using Heisenbergs uncertainty principle $d\boldsymbol{r}_i d\boldsymbol{p}_i \sim \hbar$ and by accounting for the indistinguishability of particles the dimensionless form of the partition function can be derived as

$$Q_{NVE} = \frac{1}{N!} \frac{1}{\hbar^{3N}} \int \delta(\mathscr{H}(\Gamma) - E) d\Gamma. \tag{3.34}$$

The characteristic function that links classical thermodynamics with statistical mechanics is the entropy S and can be derived from the most likely energy distribution of two systems in thermal contact.

$$S = k_B \ln Q_{NVE} \tag{3.35}$$

The probability density for the canonical ensemble is given as

$$\rho_{NVT}(\Gamma) = \frac{1}{Q_{NVT}} e^{\frac{-\mathscr{H}(\Gamma)}{k_B T}}. \tag{3.36}$$

The partition function is given an

$$Q_{NVT} = \frac{1}{N!}\frac{1}{\hbar^{3N}}\int e^{\frac{-\mathscr{H}(\Gamma)}{k_B T}} d\Gamma. \tag{3.37}$$

The characteristic function is the Helmholtz free energy F

$$F = -k_B T \ln Q_{NVT}. \tag{3.38}$$

The probability density for the isothermic-isobaric ensemble is given as

$$\rho_{NPT}(\Gamma) = \frac{1}{Q_{NPT}} e^{\frac{-\mathscr{H}(\Gamma)+pV}{k_B T}}. \tag{3.39}$$

The partition function is given an

$$Q_{NPT} = \frac{1}{N!}\frac{1}{\hbar^{3N}}\frac{1}{V}\int\int e^{\frac{-(\mathscr{H}(\Gamma)+pV}{k_B T}} d\Gamma dV, \tag{3.40}$$

where $\int dV$ indicates integration over all possible volumes. The characteristic function is the Gibbs free energy G

$$G = -k_B T \ln Q_{NPT}. \tag{3.41}$$

3.3.3 Controlling pressure and temperature

In order to sample configurations that are in accordance with the probability density functions of the canonical and isothermal-isobaric ensembles, it is not sufficient to solve Newtons equation of motion as energy is not constant in these systems. These are ensembles that are more similar to real experimental setups, where often temperature and pressure are constant, in contrast to the microcanonical ensemble. In the canonical ensemble an additional algorithm is required that controls the temperature, and in the isothermal-isobaric ensemble a pressure controlling algorithm is additionally required. Temperature controlling algorithms are called thermostats and pressure controlling algorithms are called barostats. A thermostat controls the temperature by controlling the associated kinetic energy $\mathscr{K}$. The relation between the temperature of a system and its kinetic energy is given as

$$\langle \mathscr{K} \rangle = \langle \sum_i \frac{\boldsymbol{p}_i^2}{2m} \rangle = N_f \frac{k_B T}{2}, \tag{3.42}$$

where N_f describes number of the degrees of freedom. Different more or less elaborate algorithms are available. In the easiest case the kinetic energy is only scaled accordingly; more elaborate methods introduce a further fictitious degree of freedom in form of a friction coefficient, which varies in its magnitude and can also be negative. Three different thermostats are usually used: the Berendsen thermostat

[14], the Nosè–Hoover thermostat [59, 103], and the velocity rescale [20] thermostat. The Berendsen thermostat does not sample correct ensembles but is very stable in a non-equilibrium state and thus can be used for equilibration purposes. Nosè–Hoover and velocity rescale thermostats sample correct ensembles and thus can be used for production runs.

A barostat regulates the pressure by scaling the coordinates of the atoms in the system and the simulation box, making the volume time-dependent. The relation between pressure and volume for molecular systems is given as

$$p = \frac{Nk_BT}{V} - \frac{1}{3V}\langle \boldsymbol{r}\frac{\delta \mathscr{V}}{\delta \boldsymbol{r}}\rangle. \tag{3.43}$$

Again, different more or less elaborate algorithms exist. Simple algorithms, directly couple the box size via a relaxation time constant to the desired pressure, while more elaborate algorithms introduce a further degree of freedom, where the volume of the box is described by a further equation of motion. Two different barostats are usually used: the Berendsen barostat [14] and the Parrinello–Rahman barostat [106]. The Berendsen barostat is again very stable but does not produce correct ensembles and thus can be used for equilibration purposes. The Parrinello–Rahman barostat produces correct ensembles and thus can be used for production runs.

3.4 Coarse-grained molecular dynamics simulations

From a molecular point of view, foods are often highly viscous systems, where complex molecular structures can be present. Therefore, the time and length scales that are accessible with classical molecular dynamics simulations are often not feasible. Two different methods are introduced to overcome these limitations to a certain extent. In this section, the method of coarse-grained molecular dynamics is introduced, which will be applied in the study of Chapter 5. In the subsequent section an alternative method to overcome the limitations in time and length scales, the so-called implicit solvation method is introduced as a further helpful tool in molecular simulations of foods, and preliminary results are presented.

From all-atom to united-atom to coarse-grained force fields

Classiscal molecular dynamics force fields, as described in Section 3.2, exist with different levels of detail. On the one end of the scale there are so called all-atom force fields, which describe each atom of the investigated molecules as a single mass bead, which interact via the stated bonded (length, angle, dihedral) and non-bonded (van der Waals, electrostatic) interactions with each other. These force fields are commonly used when a high accuracy of the simulation is required, detailed information about atomistic interactions are of interest, and when the size and time scales of interest are within a feasible computation time. For example, an all-atom force field is used in this thesis when the roles of

single atoms in the hydrogen bonding between two molecules are of interest. The detailed atomistic representation results in high computational costs as equations of motions have to be solved for each atom in the simulated system. When the position and dynamic behavior of single hydrogen atoms are of minor importance, so-called united-atom force fields are frequently used. In these force fields, each hydrogen atom is represented together with the heavy atom it is covalently bonded to. For example, these force fields are commonly used when properties of alkanes or other aliphatic hydrocarbons are studied. This type of modeling results in a big reduction of computational cost as the number of bead decreases drastically, at least in most organic systems. In a multitude of systems, it is often sufficient to examine the behavior of even coarser atomic beads. In this case, whole groups of atoms can be summarized to so-called coarse-grained beads. For example in the investigation of amphiphilic molecules, the focus is often on the behavior of the hydrophilic and hydrophobic parts of the molecules as a group, while the specific behavior of the single atoms can be neglected. The representation on different scales is shown for the typical cocoa butter triglyceride POP in Figure 3.4.

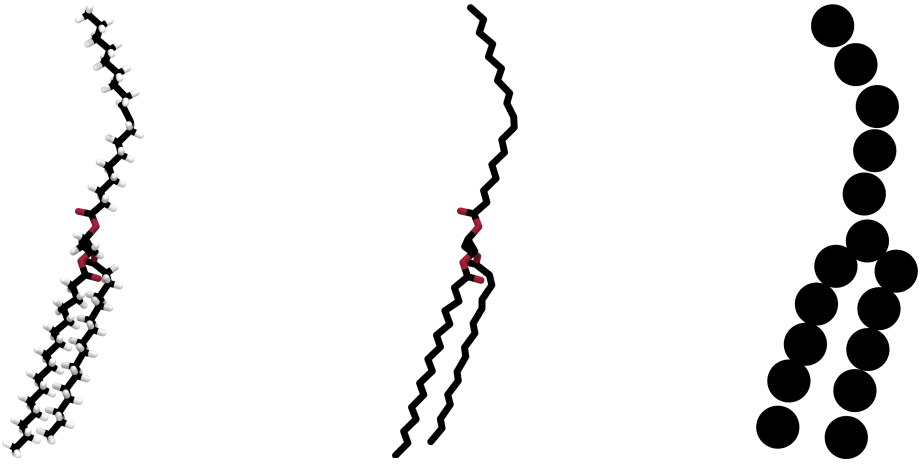

(a) POP in its all-atom representation.

(b) POP in its united-atom representation.

(c) POP in its coarse-grained representation.

Figure 3.4: Different degrees of detail of molecular models.

Several reviews have been published, describing the progresses of using coarse-grained molecular simulation methods and their relation to all-atom simulations. A general overview for biological systems is given [116] as well as with respect to food systems [107]; relevant aspects for this thesis are briefly described here. The three described molecular models with different levels of detail from above are all at the lower end of the multiscale framework, which was already shown on the example of chocolate in Figure 1.2. Nevertheless, it is desirable to have this detailed level of differentiation. Atomistic scale phenomena are linked to different mesoscale processes, which itself are linked to the continuum level. In this case the atomistic composition of phospholipids, gives molecules with hydrophilic head groups and hydrophobic tails. On the mesoscale, heads and tails can be considered on a coarser level and effects like adsorption at interfaces can be modeled. This is linked to continuum characteristics like

rheological properties. This means that details on the atomistic scale are crucial for even the largest continuum scale properties, eventually [116].

The coarse-grained simulations of lecithin structures at sucrose interfaces cover a range of time and length scales that is not feasible for atomistic simulations. In fact it is not even desirable as the gain of atomistic simulations, i.e. the detailed behavior of singular atoms over time, is not even of interest and would only produce unnecessary data. Coarse-grained simulations are on an intermediate level between atomistic detail and averaged macroscopic continuum and classical thermodynamics. Coarse-grained beads are by definition quasi particles that interact with each other more effectively (as interactions of several atoms are summarized) and thus also more computationally efficient than the atoms they represent. Together with the enormous reduction in degrees of freedom, due to the reduced amount of interaction sites, this results in a big leap on spacial and temporal scales. In the best case, coarse-grained simulations deliver substantially more and new insights in investigated systems, compared to atomistic simulations, by omitting the detailed resolution and simplifying the interactions, while simultaneously keeping physical key features. Coarse-grained simulations are mainly motivated by the need to bridge the atomistic and the mesoscopic scale. At the mesoscopic scale investigation of critical features of biological soft matter systems, which can be similar in their molecular components to chocolate, become feasible. For example self-assembly of complex structures, like phospholipid micelles in chocolate, can be investigated on the coarse-grained level, but not on the atomistic level (at least not in reasonable computation time).

However, there are several key aspects that have to be considered by the transition from the atomistic scale to a coarse-grained scale. The foundation of atomic scale molecular simulations is soundly established in the presented statistical mechanics framework of Chapter 3.3. Coarse-grained models can also be formulated with a sound connection to physical principles. Therefore, the same statistical mechanics framework can be used as for the atomistic models. While other approaches are possible, as will be shown later, coarse-grained models are at best developed in the context of the following statistical mechanics formula, which can be derived from Equation 3.38:

$$e^{(-\beta F)} \propto \int e^{(-\beta \mathscr{V}(\boldsymbol{r}))} d\boldsymbol{r}. \tag{3.44}$$

F is the Helmholtz free energy of the system, $\mathscr{V}(\boldsymbol{r})$ is the potential energy, $\beta = \frac{1}{k_B T}$, and $\int d\boldsymbol{r}$ stands for integration over all possible positions. Equation 3.44 links the atomistic scale potential energy function with the macroscopic thermodynamic quantity the Helmholtz free energy and all its derivatives, such as the entropy, internal energy, and heat capacity. The evaluation of the integral on the right hand side of Equation 3.44 is a crucial aspect of molecular dynamics simulations as the phase space has to be sampled sufficiently (compare Chapter 3.3). Coarse-graining aims at taking a short cut at this evaluation by replacing the variables in the following way:

$$\int e^{(-\beta \mathscr{V}(\boldsymbol{r}))} d\boldsymbol{r} \equiv \int e^{(-\beta \mathscr{V}_{CG}(\boldsymbol{R}_{CG}))} d\boldsymbol{R}_{CG} \; with \; (N_R \ll N_r). \tag{3.45}$$

$\boldsymbol{R}_{CG}$ is the position of the coarse-grained beads. The Helmholtz free energy is now written as an integral over N_R coarse-grained particle positions. Further, the effective coarse-grained potential $\mathscr{V}_{CG}$ is introduced. Thus, the computational cost is reduced because the number of particles is (often drastically) reduced ($N_R \ll N_r$) and the potential $\mathscr{V}_{CG}$ is simpler or smoother and thus easier to evaluate. Sampling of the phase space gets much more efficient. However, there are two substantial challenges in this framework: first, a feasible mapping of atoms to coarse-grained beads is unknown because the solution of Equation 3.44 is unknown and second, the potential energy function is not known and thus has to be somehow approximated. A mapping operator $M_R(r)$ can be defined, which maps the center of mass of a group of atoms to the coarse-grained beads. Due to the fact that integrals over the delta functions of all possible coarse-grained positions $\int \delta(M_R(\boldsymbol{r}) - \boldsymbol{R}_{CG}) d\boldsymbol{R}_{CG}$ is unity, the mapping operator can be introduced to Equation 3.45

$$\int e^{(-\beta \mathscr{V}(\boldsymbol{r}))} d\boldsymbol{r} = \int \int \delta(M_R(\boldsymbol{r}) - \boldsymbol{R}_{CG}) e^{(-\beta \mathscr{V}(\boldsymbol{r}))} d\boldsymbol{R}_{CG} d\boldsymbol{r}. \tag{3.46}$$

After rearranging, this delivers the formal definition of $\mathscr{V}_{CG}$

$$e^{(-\beta \mathscr{V}_{CG}(\boldsymbol{R}_{CG}))} \equiv \int \delta(M_R(\boldsymbol{r}) - \boldsymbol{R}_{CG}) e^{(-\beta \mathscr{V}(\boldsymbol{r}))} d\boldsymbol{r}. \tag{3.47}$$

With this derivation, it becomes clear that finding $\mathscr{V}_{CG}(\boldsymbol{R}_{CG})$ can be a difficult task. Certain degrees of freedom of the all-atom representation are integrated out by going from the right hand side of Equation 3.47 to the left hand side. This leads to the fact that $\mathscr{V}_{CG}(\boldsymbol{R}_{CG})$ also needs to contain entropic effects of the atomistic scale. Those entropic effects can be ill-defined and their behavior is hard to predict. This is one of the main challenge of coarse-graining [116].

While the presented procedure demonstrates a theoretically sound but very complex approach to derive coarse-grained models, the applied force field of this thesis uses an empirical approach and does not attempt to solve Equation 3.47 directly. In fact, it takes the opposite extreme by fitting simple functional forms, such as the Lennard-Jones potentials for beads from a previously chosen mapping scheme, to reproduce experimental values, such as partitioning free energies. Though it is without a doubt that empirically derived force fields give valuable results (compare Section 5.1), their connection to statistical mechanics is less clear. It is a common desire of the community to have coarse-grained force fields that are highly transferable. Equation 3.47 shows that this transferability is hard to achieve for soundly derived coarse-grained force fields as the effective coarse-grained potentials are depending directly on the all-atom potential. The more standardized approach of fitting interaction potentials to a broad database, as is done in the Martini coarse-grained force field for biomolecular simulations (Martini FF), which is used in Chapter 5 of this thesis, is superior in terms of transferability to other molecular systems, with less clear predictability at the same time.

To give an idea of typical computation times that are required for the presented simulations, the following frame of references is given. The major part of the computation is done on cluster nodes with two

Intel Xeon E5-2670 v3 processors. This results in 48 logical processors, which are available for each simulation. About 18 ns of simulation time can be calculated per day for the typical all-atom simulations and about 176 ns of simulation time can be calculated per day for the typical coarse-grained simulations.

Limitations of coarse-grained force field

Besides the already mentioned difficulties in coarse-grained force field development, which lead either to weaker predictive capabilities or to poor system transferability, further limitations, which were raised by the authors of the Martini FF [87] due to the reduction of degrees of freedom, have to be kept in mind and are discussed in the following. A first limitation directly results from the coarser resolution of the model itself. This can be made clear on the example of phospholipids. Through the four to one mapping, an aliphatic chain with 16 carbon atoms results in four beads and with twelve carbon atoms in three beads. Aliphatic chains with 14 carbon atoms fall in the middle. This means that molecules are not mapped uniquely and cannot be distinguished, despite the chain length difference would already result in different membrane layer thickness, stability, and melting points. A second limitation is the loss of effective time scales, which is well-defined in atomistic simulations, where for example diffusion coefficients can be calculated. This does not hold for coarse-grained simulations because the earlier described smoothing of the free energy surface results in more sampling in shorter time, which speeds up the dynamics of the system. While the efficient sampling is also a big advantage of coarse-grained simulations, kinetic and dynamic properties are not accurate and can only roughly be estimated. The best guess for a universal speed up factor in the Martini FF is 4, based on lateral diffusion coefficients of peptides and lipids in membranes. Nevertheless, the speed up factor has to be handled with care, as it was shown that the speed up factor varies for different systems between 1.2 and 22. A third important limitation is the balance between entropy and enthalpy. Martini reproduces free energies from atomistic simulations with a reduced number of degrees of freedom. Reduced degrees of freedom directly affect the entropy of the system, which gets compensated for by reduced enthalpic terms. Compensation of the enthalpic term directly leads to non-accurate temperature dependence of the model. While reproduction of free energy is achieved correctly, its break down in enthalpy and entropy is not correct. While this was shown to have a negative effect on water structures, Marrink and Tieleman [87] state that lipids and hydrophobic solvents, which are investigated in this thesis, are much less likely to be affected negatively.

3.5 Alternative approach: using implicit solvation methods

Section 3.4 emphasized the dilemma of slow dynamics and high complexity of typical food systems in combination with the short time and length scales that are accessible in molecular dynamics simulations. For future work in the field of molecular dynamics simulations of food, a further approach,

besides performing coarse-grained simulations, to overcome the stated dilemma is presented and was approached in the orientation phase of this thesis. The so-called implicit solvation approach completely omits the degrees of freedom of the solvent, which in the case of this thesis is cocoa butter, by representing it implicitly [115]. To mimic the interactions of solutes and solvents implicitly, the free energy of solvation is calculated for the specific solvent, depending on the solute conformation [130]. The free energy of solvation can be decomposed to the electrostatic contribution ΔG_{els}, the van der Waals contribution ΔG_{vdw}, and the energy that is required to form a cavity in the solvent ΔG_{cav}. These three contributions sum up to the free energy of solvation

$$\Delta G_{sol} = \Delta G_{els} + \Delta G_{vdw} + \Delta G_{cav}. \tag{3.48}$$

The electrostatic part describes the response of the solvent to the atomic charges and their distribution within the solute and is given with help of the generalized Born formalism in the following pairwise additive expression [126]:

$$\Delta G_{els} = \frac{1}{2}\left(\frac{1}{\varepsilon_p} - \frac{1}{\varepsilon_w}\right) \cdot \sum_{i=1}^{n}\sum_{j=1}^{n} \frac{q_i q_j}{\sqrt{r_{ij}^2 + a_i a_j \exp\left(-\frac{r_{ij}^2}{f\alpha_i\alpha_j}\right)}}. \tag{3.49}$$

ε_p is the dielectric constant of the solute cavity, ε_w is the dielectric constant of the solvent. r_{ij} is the distance between atoms i and j and α_i and α_j are the Born radii of atoms i and j. f is a dimensionless empirical parameter. The Born radii are commonly calculated with the Coloumb field approximation [10] by the solute volume integration approach, which is given as

$$\frac{1}{\alpha_i} = \frac{1}{R_i} - \frac{1}{4\pi}\int_{solute, r>R_i} \frac{1}{r^4} dV. \tag{3.50}$$

R_i is the van der Waals radius of atom i and r is the radius of the inner space of the molecule. Normally, approximations are introduced for this integration, in a way that only pairwise sums over atoms are involved; three different algorithms are commonly used [54, 105, 111]. The non-polar contributions to the free energy of solvation, ΔG_{vdw} and ΔG_{cav} are commonly approximated by an expression that depends linearly on the solvent-accessible surface area of the different atoms SA_i

$$\Delta G_{np} = \Delta G_{vdw} + \Delta G_{cav} = \gamma \sum_{i=1}^{n} SA_i. \tag{3.51}$$

γ is an empirical surface tension parameter. The solvent accessible surface area is approximated directly via the Born radii in Gromacs [117]. Studies showed that this approach represents the cavity part of the solvation energy quite well [42] while the van der Waals part is still subject to improvement [77].

First qualitative checks for the usage of an implicit solvent model are performed. The micelle formation

of 20 DLPC molecules, which is the main phospholipid of soybean lecithin, in two different dielectric environments is calculated, to check for qualitatively reasonable behavior. The dielectric constant of the solvent ε_s is set to 80 to represent water, and to three to represent non-polar cocoa butter. Qualitatively correct behavior is shown, as two different types of micelles were observed for the different dielectric constants, representing cocoa butter and water, respectively. They are shown in Figure 3.5. In the case

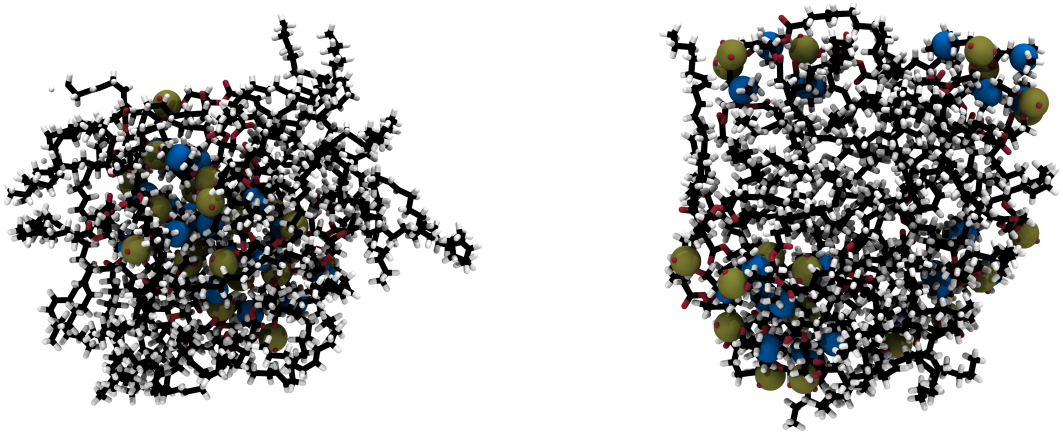

(a) (b)

Figure 3.5: DLPC micelle after 3 ns simulation in implicit solvent with a permittivity of 3, representing the solvent cocoa butter (Figure 3.5a), and after 3 ns simulation in implicit solvent with a permittivity of 80, representing the solvent water (Figure 3.5b).

of water, the hydrophilic parts of the DLPC molecules are oriented towards the outer implicit solvent, which shows the favorable hydrophilic interaction of the head groups with the surrounding solvent. In the case of the low dielectric solvent, the hydrophilic head groups are oriented to the inside of the spherical micelle, to maximize hydrophilic interactions with each other.

Implicit solvation opens up the possibility to perform molecular simulations with full atomistic detail of the molecules of interest, which are in many cases biological macromolecules, such as proteins, by representing the solvent as continuum. This means that the explicit characteristics of the solvent are completely lost, and not accessible in the simulations. It has to be considered if this is acceptable or if information about the explicit behavior of the solvent might be of interest. In the presented thesis the approach of implicit solvation was eventually dismissed as certain cocoa butter properties are in fact of interest. Coarse-graining, kind of takes the middle ground, by coarsening the resolution of the molecules of main interest as well as the solvent. To sum up, for food related topics that are approached with molecular simulations, several aspects have to be considered, regarding the treatment of the solvent. If the system under consideration can be represented by a relatively small simulation setup and can also be investigated on small time scales, all-atom simulations should be performed as they deliver the most precise results and allow the investigation of dynamic properties and kinetic processes. If the behavior of the solvent is of no further interest and size and time scales for explicit

treatment of the solvent are to big, implicit solvent models should be considered. If the properties of the solvent are of interest or if the solvent is a complex mixture of different components and size and time scales are to large for explicit treatment, coarse-grained approaches should be considered. Despite the presented scheme, it still has to be considered that finding suitable force fields for food systems is a difficult task due to the wide range of different molecular components of foods and their complex mixtures as well as phase behavior. This leads to the situation that choosing between all-atom models, implicit solvent models, and coarse-grained models might not be possible anyway.

3.6 Molecular dynamics in food process engineering – review, challenges, and limitations

Ho et al. [56] state in their review on multiscale modeling in food process engineering that food researchers did mathematical modeling to describe phenomena such as mass and heat transfer for several years. Nevertheless, foods are structured systems with several characteristics that occur on different time and length scales, reaching from molecular phenomena to macroscopic effects. While macroscopic continuum models, which describe a kind of averaged behavior of foods, have often been used, microscale processes were usually not modeled explicitly, which often led to poor understanding of phenomena at that scale. The main reasons for this are the high computational cost and complexity of microscopic models. The new modeling paradigm multiscale modeling, which emerged due to the Comprehensive Nuclear-Test-Ban Treaty in the late 1990s [60], where many countries agreed to ban nuclear testing, got increasingly more attention in food process engineering over the last years and is very useful to gain more detailed insights on the different time and length scales. It is basically a framework of models on different time and length scales that are connected via their different inputs and outputs [56]. Usually the output of the small scale models is used as input for the larger scale models. Thus, all contributing effects of the investigated macroscopic phenomenon are modeled on a physical basis and computational cost gets minimized. In a food process engineering context, molecular modeling is usually on the small end of the multiple scales as quantum mechanics models are scarcely used. A short review of molecular dynamics studies in a food process engineering context is given in the following.

Monosaccharide solutions regarding their translational and rotational dynamics were studied and an analogy between high sugar concentrations and low temperatures, which provides an explanation of bioprotective phenomena in living organism, was found [76]. Three different studies investigated amorphous saccharides. Microscopic mechanisms of water diffusion in glucose glasses were studied and two different mechanisms of transport were found [96]. On the one hand water diffuses by jumping to neighbor water positions and on the other hand water jumps to neighbor glucose positions that are coupled to the rotational dynamics of glucose molecules. Glass transition temperatures of amylose were investigated [97]. It was found that simulated temperatures match experimental data very good.

Structural and dynamic characterization of maltooligomers was performed [79]. Further, several studies investigated triglyceride properties. The influences of double bonds and additional ethyl groups as branches from the main chain on the viscosity of pure and mixed triglycerides were predicted [129]. Structural phenomena in liquid triglycerides and triglyceride crystallization were studied [53]. It was shown that the behavior of liquid triglyceride systems is clearly different from crystalline triglyceride systems in many aspects. Oil binding capacities of triglyceride crystal nanoplatelets were investigated [112] and it was found that oil between two fat particles, which are separated by a few nanometers, is expelled into the surrounding oil. Further, the temperature and pressure dependency of density and self diffusion of saturated triglycerides were calculated [50]. As triglycerides are a high viscous system, coarse-grained force fields have a big advantage in overcoming calculation time and thus simulation time limits and were developed by the Milano group [17]. They developed a coarse-grained force field with the aim to study crystallization processes of tridecanoin. They showed that crystallization starts from the clustering structures of the triglyceride backbones as they were also reported elsewhere [53]. Further, the Milano group [108] investigated crystallization of a binary mixture of the two saturated triglycerides of similar chain length, tripalmitin and tristearin. The crystalline structures they observed show a high number of the so-called tuning fork conformation, which corresponds to the crystalline α phase. The ability of ethylcellulose to form hydrogen bonds with sucrose in chocolate was shown, leading to a network structure that enables oil-trapping or fat immobilization and gives mechanical strength to the system [128]. Thus, ethylcellulose can be a key ingredient for manufacturing heat resistant chocolate. A food grade organogel was investigated by molecular dynamics simulations [89]. Sitosterol and oryzanol self-assemble in different organic solvents and build a gel. By adding glycerol instead of water, polar droplets can be included in the gel without significantly lowering the gel stability. Besides solid foods, beverages were also the subject of molecular dynamics simulations. Biophysical interactions of seven different green tea catechins with cell membranes were studied, in order to gain deeper understanding of their influence on cancer cell membrane structures [122]. All catechins were found to have an affinity to the cell membrane, three of them were absorbed underneath the membrane surface. Further, a brewing science related problem was investigated with molecular dynamics simulations. Molecular mechanisms behind gushing of carbonated beverages were investigated [36]. The given examples show that important food properties that are relevant for different manufacturing aspects, can be calculated with molecular dynamics simulations. Nevertheless, molecular dynamics is only helpful when the problem is well-defined on a molecular level and chemical composition as well as basic chemical structures are known. Only then a suitable force field can be chosen and the structural representation of the system can be designed. As an example from chocolate manufacturing, cocoa particles can be considered to emphasize this problem. They are a complex mixture of proteins, carbohydrates, and fats which get fermented, roasted, and ground before conching and thus it is very hard to analyze all occurring chemical structures and to define a representative model system. Further, food systems are often highly structured materials that form network-like systems, meaning that it is not enough to know the pure chemical components but also the structure they build, in order to have a realistic starting configuration for molecular dynamics simulations. As examples, a food gel, such

as yogurt, or a food foam, such as whipped cream, can be mentioned. Even when the exact network structure is known to an atomistic degree, the already discussed problem of strong limitations in time and length scales get relevant. When proteins are investigated with molecular dynamics simulations today, it is usually computational feasible to investigate one protein in solution for several nanoseconds. This should give a point of reference and show that simulations of a representative part of a complete protein network is often not possible.

Chapter 4

Interactions of different phospholipid head groups with sucrose crystals

The strength of interaction between different phospholipids, which are the most prominent components of lecithins used in chocolate manufacturing, and the (100) sucrose crystal surface at a cocoa butter interface are calculated and presented in this chapter. The major part of this chapter is based on the study by Kindlein et al. [70]. Lecithins that are used in chocolate manufacturing are commonly produced from vegetable resources, as described in Chapter 2.4.2. The different lecithin sources mainly contain the same phospholipids with the most prominent head groups PC, PE, PI, and PA and are connected to the same fatty acids but in different compositions. It is known from experimental studies that lecithins of different sources and thus with different molecular compositions have differences in their technological effects in the chocolate manufacturing process [9, 92]. Therefore, it can be concluded that the specific phospholipids behave differently in the complex molecular system chocolate. In this study, the interactions of single phospholipid molecules with a crystalline sucrose surface at the cocoa butter interface is calculated by applying the so called pull-code. The pull-code is a non-equilibrium molecular dynamics method, where an external force is applied to a molecule. In each of the presented simulations, a single phospholipid molecule gets pulled away from the sucrose surface with constant velocity and the force that is required to move the molecule is analyzed and a detachment work is calculated. Besides the calculation of the detachment work, this procedure gives information about the mechanisms of detachment and thus gives detailed insights about molecular interactions, which could hardly be accessed by experimental procedures. In this study it is not directly possible to deduce rheological insights from the molecular simulations, but it is possible to explain different behaviors from varying phospholipid compositions as it is shown that different phospholipids interact differently with sucrose.

4.1 Suitability of the general AMBER force field

The general AMBER force field (GAFF) [143] is designed to represent the possible broadest range of organic molecules and to be compatible with the existing AMBER force fields, which were developed for nucleic acids and proteins [30, 145, 146]. Most organic molecules that consist of H, C, N, O, S, P, and halogens can be modeled with GAFF and the parameters can be assigned automatically. Atom type definitions have to be handled very carefully in force field design and are key to success and transferability of the molecular model. Each additional atom type gives the possibility to cover subtle chemical differences between molecules but also needs to be parametrized. 35 *basic* atom types, five for carbon, eight for nitrogen, three for oxygen, five for sulfur, four for phosphorus, six for hydrogen, and one for each halogen, were defined. Further 22 *special* atom types were defined to accurately describe specific chemical environments of the atoms, such as conjugated single or double bonds, with the aim to cover a broader range of molecules. For the exact atom type definitions the interested reader is referred to the original paper by Wang et al. [143]. Atomic charges are key for the accurate description of non-bonded and conformational energies of the molecules and should be assigned in a transferable fashion. Therefore, a consistent approach should be used, such as the restrained electrostatic potential (RESP) [11, 27] approach, which is used in the AMBER protein force fields. Unfortunately, the RESP charge approach requires ab initio optimization using the Hartree-Fock method HF/6-31G* [55]. Especially when a force field is designed to be used generally for a wide number of different organic molecules, such as GAFF, an approach like this cannot be efficiently taken. Therefore, the alternative charge approach AM1-BCC [64] can be used, which does semi-empirical AM1 calculations [125] to obtain Mulliken charges, followed by a bond charge correction (BCC)[19]. This method closely resembles the charges obtained by HF/6-31G*. The same Lennard-Jones parameters as in other AMBER force fields are used. Bond and angle parameters are based on crystal structures, ab initio calculations, and the AMBER protein force field. Rotational angles are also based on ab initio calculations.

Since its development, GAFF was used in a very high number of molecular dynamics studies and the original paper was cited 5510 times as of July 2018. It was used for modeling molecules similar or equal to those investigated in this thesis, which are phospholipids, triglycerides, and sucrose. Foley et al. [45] give a comprehensive review of carbohydrate force fields. Several studies that employ the AMBER force field and GAFF for carbohydrates are given therein, showing the suitability of the force field. For example, Delbianco et al. [38] investigated structural characteristics of oligo- and polysaccharides. Similar lipids as in the systems of this study were also already investigated with GAFF. Dickson et al. [40] stress that standard GAFF molecular dynamics simulations yields good results of phospholipid membrane simulations in a wide variety of studies. Additional force field validation for the use of GAFF in chocolate simulations was done by co-workers [51]. As a static property the densities of the main bulk phases of the simulated systems, sucrose and cocoa butter triglycerides, were validated. Cocoa butter was validated for three different temperatures for which experimental values are available. All three temperatures of 313 K, 323 K, and 353 K are of interest in chocolate manufacturing. 313 K is near body

temperature, where chocolate melts when it gets consumed. 323 K and 353 K are temperatures that commonly occur in chocolate conching. The density of sucrose was calculated for its typical crystalline state at room temperature. That is the state in which sugar is commonly present in solid foods. Table 4.1 shows the predicted values of densities by molecular dynamics simulations employing GAFF and experimental values for according temperatures. The very high accuracy of calculated densities, which

Table 4.1: Calculated densities by molecular dynamics simulation with GAFF compared to corresponding experimental measurements [51].

Substance	Temperature [K]	Simulation [$\mathrm{kg\,m^{-3}}$]	Experiment [$\mathrm{kg\,m^{-3}}$]
Cocoa butter	313	897.8	894.8 [22]
Cocoa butter	323	893.8	888.5 [22]
Cocoa butter	353	875.0	868.1 [22]
Sucrose	293	1569.3	1586.2 [58]

deviate less than 1 % from experimental values for cocoa butter and less than 1.1 % for crystalline sucrose, shows the suitability of the force field. As a dynamic property, the micelle formation of DLPC in water was studied [51]. In a water environment DLPC is suspected to form micelles, where the hydrophilic head group is oriented to the surface of the micelles to maximize the hydrophilic interactions with water. The apolar aliphatic fatty acids are suspected to be oriented towards the inner part of the micelle, where van der Waals interaction between hydrocarbon chains are maximized. This behavior is clearly shown on exemplary snapshots at the beginning of a molecular dynamics simulation and after 20 ns [51]. This is a further qualitative validation of a dynamic property of lecithin micelles for GAFF molecular dynamics simulations. A corresponding simulation was performed for DLPC in cocoa butter. Due to the viscosity of cocoa butter, which is orders of magnitude higher than that of water, no micelle formation, which would be suspected to deliver reverse micelles due to the chemical nature of the solvent, could be shown. The simulation time is to short to enable the phospholipids to reach each other by Brownian motion in the triglyceride matrix and to attach to each other. This is shown by comparing the output conformation with the input conformation, were only minor changes can be observed [51].

With the presented validated system properties in addition to the studies where GAFF was applied and validated to predict properties of systems with similar molecular components, the use of GAFF for molecular dynamics simulations of chocolate seems to be justified and validated sufficiently. The sound validation together with the straightforward transferability to further molecules that could be of interest in chocolate research are the reasons that GAFF was chosen for the presented study. Again, it is stressed that the same setup can be extended to further studies, such as interaction of phospholipid with milk proteins, lactose, or cocoa proteins and other molecular components of cocoa particles as GAFF repeatedly showed its good transferability to a vast amount of different components.

4.2 Methods

4.2.1 Molecular model of chocolate

In order to answer scientific questions with molecular dynamics simulations, a representative molecular model of the system of interest has to be defined. When properties of a system such as chocolate, which is a complex mixture of a wide variety of different molecular components, are desired to be calculated, a molecular model has to be defined that is capable of capturing relevant system characteristics while remaining as simple as possible. In the case of this study, cocoa particles are not considered as they are less hydrophilic than sucrose particles and thus of minor importance for phospholipid interactions. As the interactions of phospholipids with sucrose are supposed to be calculated, a suitable representation of sucrose is required. During the manufacturing of chocolate, sucrose is added in a crystalline state. A recent study suggests that after the refining process the surfaces of the sucrose particles can be in a crystalline state or in an amorphous state and also in some kind of mixed state [93]. However, this matter is still under debate. In this study the interaction of phospholipids with crystalline sucrose is investigated. The crystal structure of sucrose was first reported by Beevers et al. [13] and further refined by Brown and Levy [18]. Campañá Cué et al. [23] gave detailed information of the relation of the macroscopic sucrose crystal surfaces to the molecular unit cell. The crystal coordinate file is extracted from [25] following de Graef and McHenry [34]. The sucrose crystal unit cell, which is shown in Figure 4.1a is used to build a sucrose crystal, which is shown in Figure 4.1b, for the simulations.

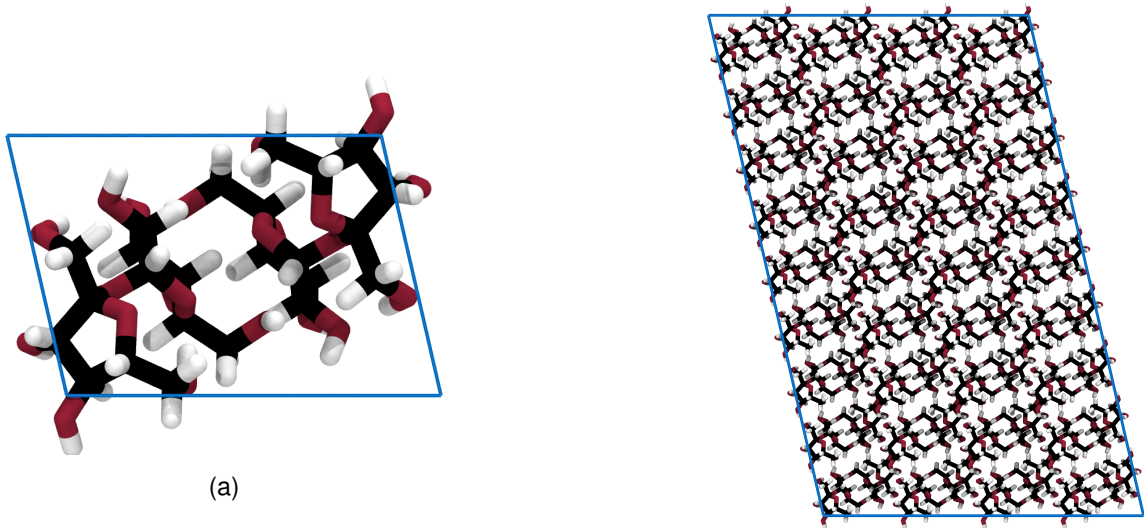

(a) (b)

Figure 4.1: Representation of the sucrose crystal unit cell (Figure 4.1a). Carbon atoms are shown in black, oxygen is shown in red, and hydrogen is shown in white. The presented color-code is used throughout this chapter. The sucrose crystal in Figure 4.1b is a replication of the unit cell in all spacial directions.

To represent cocoa butter in the molecular model, the three main molecular components are used. According to sample N of Foubert et al., the triglycerides POS (41.1 %), SOS (25.0 %), and POP (18.4 %) represent 84.5 % of the total mass of triglycerides. Given that triglycerides are the major part of cocoa butter and their chemical structure is the reason for many characteristic bulk-dependent properties of chocolate, as described in Section 2.1.1, this molecular representation is considered to be sufficient.

The interaction of six different phospholipids with sucrose are studied. The three most prominent head groups in vegetable lecithins are PC, PE, and PI [99, 136]. Each of the head groups is investigated in its most commonly occuring forms as phospholipids in soybean lecithin. The two main PC molecules are 1,2-dilinoleoyl-phosphatidylcholine (DLPC) and 1-palmitoyl-2-linoleoyl-phosphatidylcholine (PLPC). The two main PE molecules are 1,2-dilinoleoyl-phosphatidylethanolamine (DLPE) and 1-palmitoyl-2-linoleoyl-phosphatidylethanolamine (PLPE). Finally, the two main PI molecules are 1,2-dilinoleoyl-phosphatidylinositol (DLPI) and 1-stearoyl-2-linoleoyl-phosphatidylinositol (SLPI). In order to keep the simulations comparable 1-palmitoyl-2-linoleoyl-phosphatidylinositol (PLPI), the third most PI molecule, is investigated instead of SLPI. The DL molecules have two linolic fatty acids, which means each fatty acid has two unsaturated double bonds. The PL molecules have one plamitic and one linolic fatty acid, which means that they have one fatty acid with two unsaturated double bonds and one fatty acid that is saturated. The selection of these two molecules of each head group allows to investigate different aspects of phopholipid interaction with sucrose. On the one hand differences due to head groups can be investigated and on the other hand influences of different tail groups can be investigated. This setup represents the typical molecular diversity of vegetable soybean lecithin.

4.2.2 System building

When molecular mechanisms at interfaces are studied in molecular dynamics simulations, usually an infinite interface is built by using the concept of periodic boundary conditions. The simulation box is divided in two parts, where each one represents one of the two phases whose interface is of interest. An endless interface system of repeating cells is obtained by applying periodic boundary conditions. Before the building is explained, the final simulation box is shown in Figure 4.2 to enable the reader to follow the description more easily. In order to build the sucrose crystal, the sucrose crystal unit cell is replicated in all spacial directions, 4 times in x-direction, 9 times in y-direction, and 9 times in z-direction. This results in a sucrose crystal with an edge length of 7.8 nm in y-direction and 6.8 nm in z-direction, parallel to the interface of the final system, which is big enough to account for the minimum image convention and as small as possible to keep calculation times feasible. The biggest molecules of the final system, the phospholipids and triglycerides, have a length of about 4 nm, when they are as much stretched as possible. The short-range cut-off is 0.9 nm. The sum of the longest stretching plus two times the cut-off radius is smaller than the smallest box edge and thus the minimum image convention is fulfilled. The sucrose crystal has an edge length of 4.3 nm in x-direction, which is long enough to make sure that the later inserted lipid molecules at the interface have only short range interactions with sucrose molecules

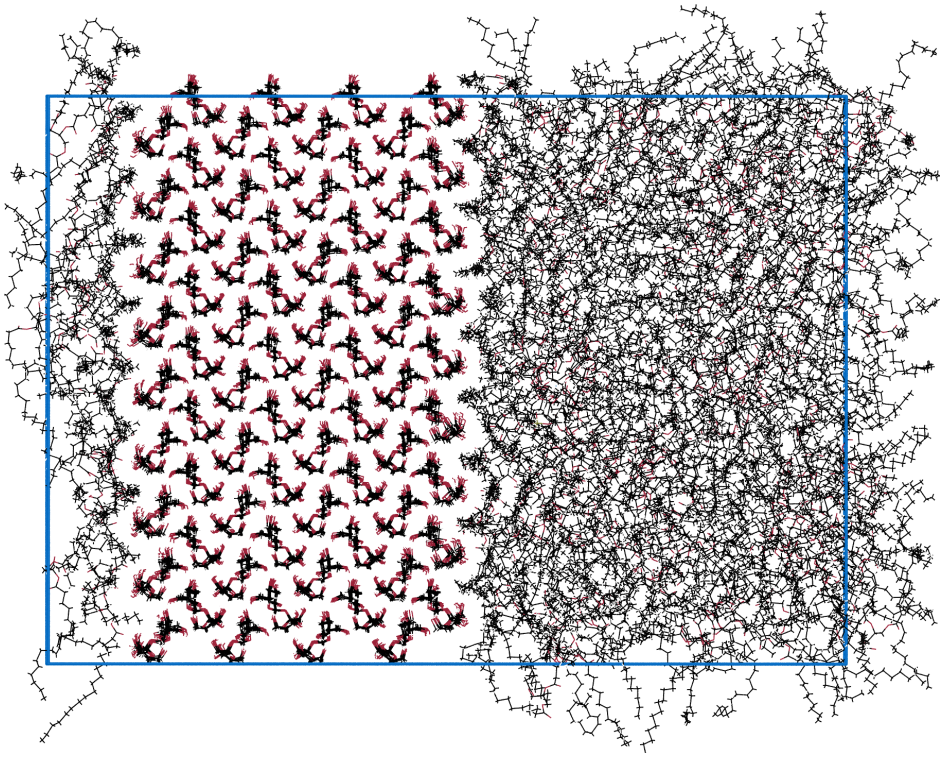

Figure 4.2: Example for the setup of the investigated systems of this study. The ordered structure is the sucrose crystal. Cocoa butter is on both sides of the sucrose crystal due to periodic boundary conditions. A single phosphpolipid is at the interface in the center of the figure and is hidden in the triglycerides.

and do not interact with the lipid molecules from the other side of the box through periodic boundary conditions. Subsequently, the simulation box is elongated in x-direction in order to have empty space, where the lipids can be inserted in the box. Next, in each box the specific single phospholipid is inserted and placed near the sucrose crystal surface. With that procedure it is ensured that the phospholipid molecule has the opportunity to adsorb at the crystal surface. Without placing it near the interface, simulation times are likely to be to short to allow the phospholipids to diffuse through the viscous cocoa butter matrix to the interface. Finally, cocoa butter triglycerides are randomly inserted into the rest of the box in the specific amount in order to give the desired triglyceride composition and in order to get a sufficient size of the simulation box, which is $11\,\mathrm{nm}$ in x-direction after equilibration. This is big enough to make sure that lipids only interact with one of the periodic sucrose crystal representations. To fulfill these requirements, 102 POS molecules, 60 SOS molecules, and 47 POP molecules are inserted into the box. For correct electrostatic charge treatment, when using Particle–Mesh–Ewald electrostatics, the system has to be charge neutral. An additionally positive Natrium ion is added in the PI systems to account for the negative net-charge of the PI head group. The described system represents the (100) sucrose crystal surface at the interface to liquid cocoa butter.

4.2.3 Equilibration and production run details

All simulations and parts of the analysis are performed with the Gromacs software Version 4.6.2 and 4.6.3 [133]. GAFF [143] is used for all simulations of this study. Molecular topologies are generated by using the tools ACPYPE [31] and Antechamber [141, 142]. AM1-BCC charges are calculated with the semi-empirical quantum chemistry method SQM [139], also with the help of ACPYPE and Antechamber. A $2\,\mathrm{fs}$ time step is used for integrating the equations of motion with help of the leap-frog algorithm [57]. Van der Waals interactions and short-range electrostatic interaction are calculated with a cut-off at $0.9\,\mathrm{nm}$. Long-range electrostatic interactions are calculated with the Particle-Mesh-Ewald method [33]. Temperature is controlled with the Berendsen thermostat in the equilibration and with the Nosè–Hoover thermostat during the production runs. Pressure is regulated with the Berendsen barostat during equilibration.

The following steps of the simulation procedure are performed for all six phospholipid systems. As a first step, an energy minimization is performed to make sure that the system is in a local energy minimum when the equilibration starts. Due to the randomized insertion of molecules during the system building, overlaps with very high potential energies can be present in the system. A steepest decent algorithm is used to get the system into a local energy minimum and is applied until the potential energy of the systems leveles out. The following equilibration procedure is performed to accomplish the following different objectives. The objectives are the generation of a system configuration that has typical conching temperature and pressure and minimization of the influence of the starting configuration of the phospholipid for comparable pull-code simulations. Therefore, three different equilibration steps are performed. At first, an isothermal-isobaric equilibration step is performed to get the system to the desired temperature of $80\,^{\circ}\mathrm{C}$, to allow the system to contract in x-direction, and to allow the phospholipid to adsorb on the sucrose crystal surface. A second equilibration step in the canonical ensemble is performed without the cocoa butter to allow the phospholipid to reach a energetically favorable configuration on the sucrose crystal. Without the cocoa butter it can move freely and explore a broader range of favorable configurations. Finally, a third isothermal-isobaric equilibration is performed until final temperature and pressure are reached. Subsequently, the final pull-code productions runs are performed in the canonical ensemble. The phospholipids are pulled from the sucrose crystal surface by applying a force to the center of mass of the phospholipids via a Hookean spring with a force constant of $5 \times 10^5\,\mathrm{kJ\,nm^{-2}\,mol^{-1}}$. The pull-code is applied with a constant velocity of $1 \times 10^{-4}\,\mathrm{nm\,ps^{-1}}$ in the canonical ensemble at $80\,^{\circ}\mathrm{C}$. Five different pull-code simulations with different starting configurations are performed for each phospholipid. All starting configurations are taken from the final isothermal-isobaric equilibration step, when the systems are already in equilibrium. The sucrose crystal is kept in its crystalline state by applying position restraints during all simulations. This procedure ensures that the sucrose crystal stays in a perfect crystalline state during all pull-code simulations and ensures that all phospholipids are adsorbed in a comparable spacial configuration at sucrose.

4.2.4 Analysis of the simulations

The pulling is performed with constant velocity, which allows to calculate the moved distance of the center of mass of the phospholipid. By integrating the applied pulling force over the moved distance, the required work can be calculated for the detachment of the phospholipid. The required detachment work results from the non-equilibrium pull-code molecular dynamics simulation and can be considered as an upper estimation of the equilibrium free energy difference between the transition start and end points [39].

$$\langle W \rangle \geq \Delta F \tag{4.1}$$

$\langle W \rangle$ is the average non-equilibrium work of different runs and F the Helmholtz free energy [65]. To differentiate between the head group detachment and tail group detachment the hydrogen bonds between the phospholipids and sucrose are monitored as shown in Figure 4.3. Hydrogen bonds are identified by a combination of two threshold values. First, the donor–acceptor distance hast to be $<0.35\,\mathrm{nm}$ and second, a hydrogen–donor–acceptor angle has to be $<30°$. Hydrogen bonds only start to break after

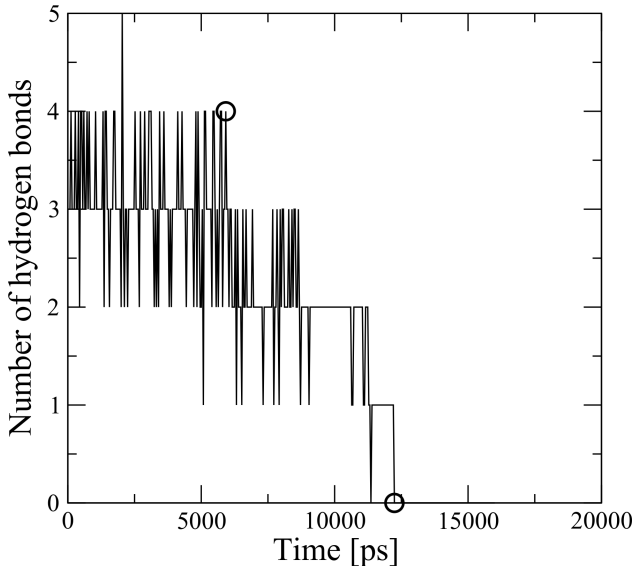

Figure 4.3: Number of hydrogen bonds between the phopholipid and the sucrose crystal over the simulation time. The markers (black circles) indicate the points that were taken as starting and end points of the head group detachment [70].

the hydrophobic tail groups are completely stretched into the cocoa butter in pulling direction, which explains that the number of hydrogen bonds decreases after a certain lag-time. The starting point of head group detachment is usually set to the point when the first hydrogen bond breaks permanently. In some simulations this cannot be taken as a distinct starting point due to rebuilding of hydrogen bonds during the detachment process. Thus, the distance between the centers of mass of the phospholipid head group and the sucrose crystal is analyzed as a further indicator of the head group detachment. This is shown in Figure 4.4. A strong indicator for head group detachment is the increase of the distance as

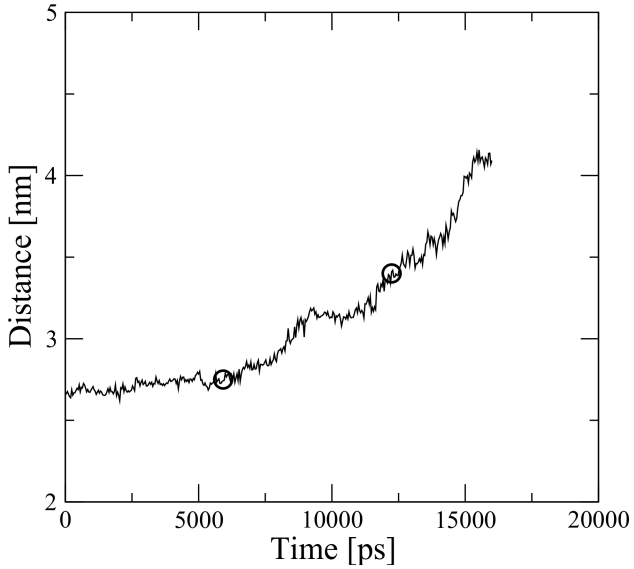

Figure 4.4: Distance between the centers of mass of the phospholipid head group and the sucrose crystal over the simulation time [70].

marked by the first circle in Figure 4.4. The end point of the head group detachment is clearly marked by the permanent breakage of the last hydrogen bond between the head group and the sucrose crystal in Figure 4.3. The specific head group detachment work can be calculated by transferring the starting and end markers for head group detachment to Figure 4.5. The work that is performed between the initial and final state can be calculated as the difference between the two markers on the ordinate in Figure 4.5. To access real free energy differences different approaches can be chosen. One direct possibility

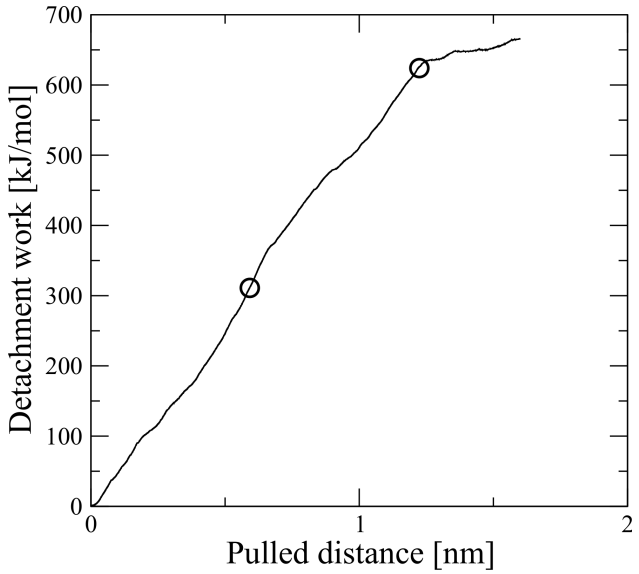

Figure 4.5: Detachment work over the pulled distance of the phospholipid [70].

with the present setup, would be to chose the pulling velocity so low that, despite the configurational

change, every configuration of the trajectory could be considered as an equilibrium structure. Unfortunately, this would result in unfeasible calculation times. Thus, the velocity is chosen as a trade off between keeping the structures possibly close to equilibrium and having acceptable calculation times for the six different systems and each five production runs. Further the spring can be considered as a buffer to allow the phospholipid to react to the applied force in a manner more comparable to equilibrium. A further possibility to obtain the free energy differences with the presented setup would be to apply Jarzynskis theorem, which allows to use multiple non-equilibrium calculations of detachment work to calculate the free energy differences [65]. Jarzynskis theorem is given by

$$\langle e^{-\beta W} \rangle = e^{-\beta \Delta F} \tag{4.2}$$

with W the non-equilibrium work and ΔF the free energy difference and $\beta = \frac{1}{k_B T}$. The non-equilibrium simulations of this thesis were considered to be evaluated with Jarzynskis theorem in order to obtain free energy differences, however, Jarzynski [66] showed that if the variance $var(W) \gg (k_B T)^2$, the calculated free energy difference will be dominated by the given trajectories and not yet be converged [39]. This is the case for the presented simulations and thus real free energy differences cannot be calculated.

4.3 Results and discussion

4.3.1 Different adsorption states

The phospholipids adsorb at the sucrose surface by attaching their hydrophilic head group to the hydrophilic sucrose surface. This is energetically the most favourable position for the phospholipid in the given system. Hydrophilic interactions in chocolate are maximized when the mobile hydrophilic head groups of phospholipids adsorb on the hydrophilic sucrose crystals. Only after all hydrophilic surfaces are covered by phospholipids, micelle formation of excess phospholipids would be the new optimal configuration. A highly idealized artificial system with only one phospholipid at the sucrose surface is investigated in this study, which allows to get very detailed specific insights. The adsorption is shown in Figure 4.6 by showing a mass density distribution of the different components along the x-axis of the simulation box. Figure 4.6 shows that the lecithin molecules adsorb at the interface between sucrose and cocoa butter and further shows the validity of the simulation setup as the density of sucrose and cocoa butter are represented accurately. Two different adsorption states of the phospholipid head groups are distinguished in this work. The (100) sucrose crystal surface has a specific structure of small hills and valleys, resulting in notches along the sucrose crystal surface, which can be seen in Figure 4.7. The phospholipid head groups are completely adsorbed within the notches of the sucrose crystal surface in four of the six examined systems, which is referred to as state A and shown in Figure 4.8a. PLPC and DLPC were found in a further state of adsorption where only a part of the phospholipid head groups is

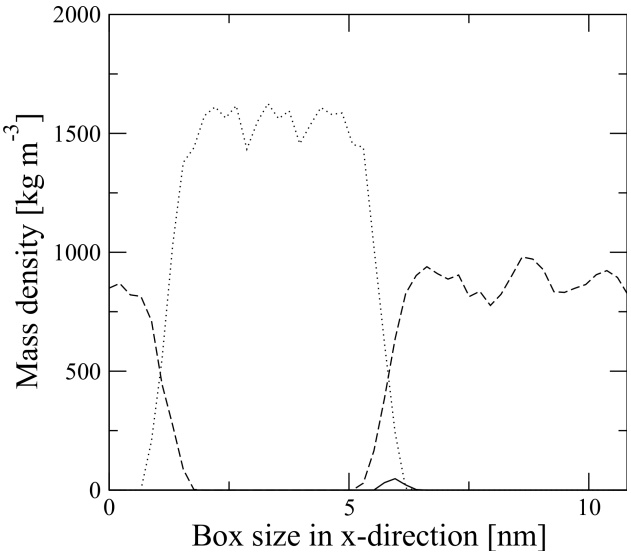

Figure 4.6: Mass density plot of sucrose (dotted line), DLPE (solid line), and cocoa butter (dashed line) along the x-axis [70].

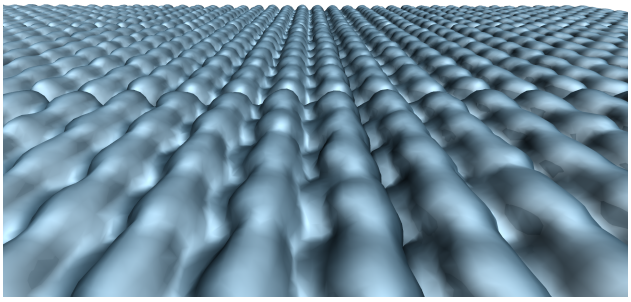

Figure 4.7: Surface representation of the (100) sucrose crystal surface, showing the notches in the molecular topography.

adsorbed in the notch and is referred to as state B and shown in Figure 4.8b. State B is identified after the first isothermal-isobaric equilibration step. After the additional canonical equilibration step the PLPC and DLPC system are also found in state A. Due to the maximized hydrophilic interaction of the head groups when they adsorb in state A, this is proposed to be the more favorable configuration. State B seems to be some kind of metastable state. The phospholipid has to move in the highly viscous cocoa butter to transit to state A, which does not necessarily happen in the short molecular dynamics time scales. Differences in the detachment work are shown and discussed in section 4.3.3. Figures 4.8a and 4.8b also show that the phospholipid tail groups are not stretched into the cocoa butter medium, which is commonly assumed for phospholipids monolayers at interfaces. The phospholipids adsorbed

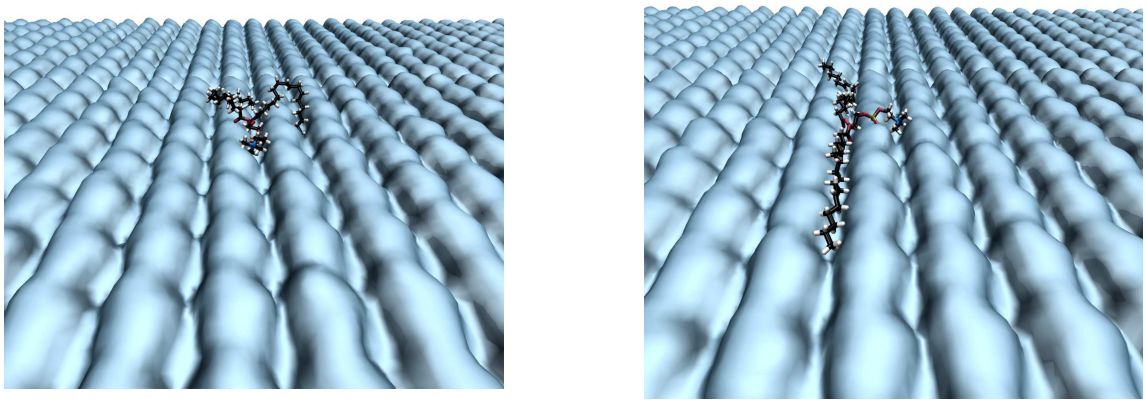

(a) (b)

Figure 4.8: Adsorption state A of the phospholipids is shown in Figure 4.8a. The head group is completely adsorbed in a notch of the molecular topography. Adsorption state B of the phospholipids is shown in Figure 4.8b. The head group is only partly adsorbed in a notch of the molecular topography. The phosphorus of the phospholipid is shown in light green and the nitrogen of the phospholipid is shown in dark blue. The presented color-code is used throughout this chapter. [70].

in this configuration during the equilibration procedure and did not change the configuration during the remaining equilibration time. This can be explained thermodynamically from two points of view, which lead to the same effects. First, molecular systems tend to minimize unfavorable interfaces. The fact that only one phospholipid is present in the investigated systems, means that the major part of the interface is a thermodynamically unfavorable interface between triglycerides and sucrose. It does not make a difference if the fatty acids of triglycerides are in contact to the hydrophilic sucrose surface or if the fatty acids of the phospholipids are in contact to the sucrose surface. Second, molecular systems tend to maximize attractive interactions. Johansson and Bergenstahl [68] argue that emulsifiers might lie flat on particle surfaces when present in low concentration because in this position all hydrophilic parts of the head group can interact with sucrose and not only the tip of the head groups. The presented lines of argumentation show that when only a single phospholipid is adsorbed at the sucrose surface, there is no energetic trigger for the phospholipids tails to stretch into the cocoa butter medium. When the interface is occupied by several phospholipids, the tail groups stretch into the cocoa butter as the head groups can further interact with each other, contributing to the adsorption energy [68]. Exactly this behavior is shown in Chapter 5, where several phospholipids at the sucrose–cocoa butter interface are simulated.

4.3.2 Detachment mechanisms of phospholipids

The detachment mechanism, which has earlier been shown by co-workers on the example of DLPC, gives detailed insights into the interactions of phospholipids and sucrose [51]. In this section, the predominant detachment mechanisms for the three different head groups as well as for the different

aliphatic chains are discussed in more detail. The molecular structures of the phospholipids are shown in Figures 2.4 and 2.5. Similarities and differences in the detachment mechanisms are highlighted in the following. An overall similar detachment mechanism could be observed for all six phospholipids. In a first step, the aliphatic chains, which are in direct contact to the sucrose surface as a result from the equilibration procedure, are detached from the sucrose surface. Both aliphatic chains are moved in the pulling directions until they are detached and stretched into the surrounding cocoa butter medium. This clearly shows that for all phospholipids the interactions of the head group with the sucrose surface are stronger than the interactions of the aliphatic tail groups with the sucrose surface. While the result itself was expected, it demonstrates that the pull code is suitable for investigating the interactions within the system. In a second step, the head groups are removed from the surface in pulling direction, which finally results in complete detachment from the sucrose surface. The detachment mechanism is shown in detail for DLPC in Figure 4.9, where further phenomena of the head group detachment can be seen. After the aliphatic chains are detached, the PC head group, which can be divided in three different

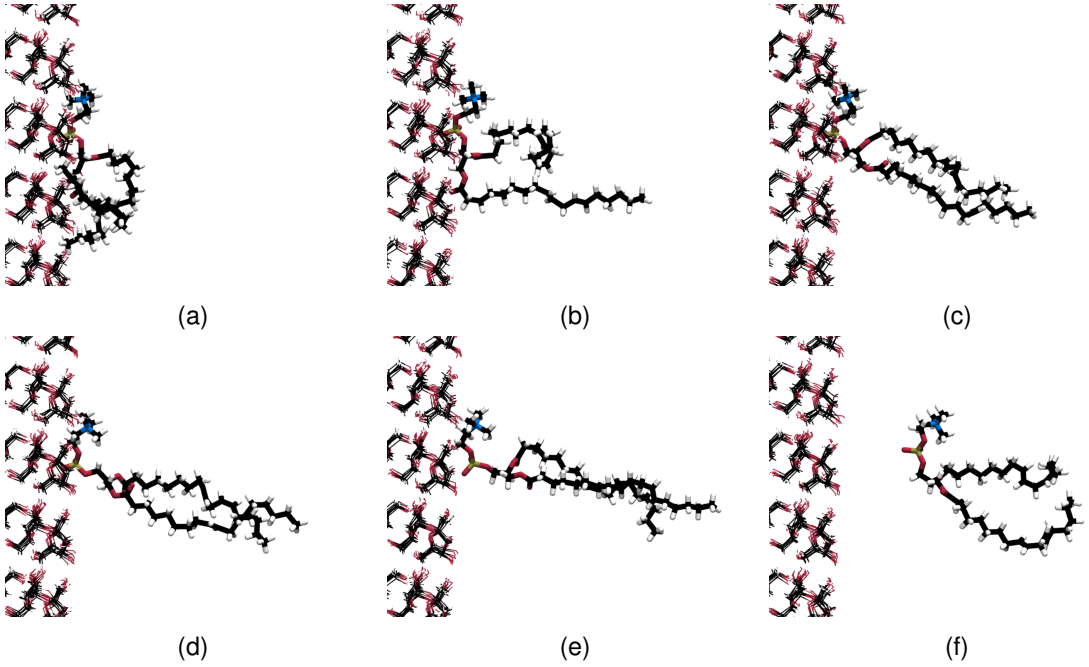

Figure 4.9: Detachment mechanism of DLPC.

hydrophilic parts, detaches. The three parts are the glycerol backbone, the phosphate group, and the choline group. By analyzing the detachment trajectories, it can be seen that the first part of the head group that starts to detach is the choline group. At a very early time point during the detachment simulations, it starts to move freely on the surface and is under the influence of thermal movement. It has a very limited range of movement, due to the covalent bonds to the still adsorbed phosphate group. The movement can be seen in the slightly different choline group positions by comparing Figures 4.9a, 4.9b, and 4.9c. This shows that the choline group exhibits weaker interaction with the sucrose surface than the other parts of the head group. This leads again to the conclusion that an adsorption state for

a single PC at the interface is more favorable in a flat position as the tip does not as strongly interact with sucrose as the other parts of the head group. The choline group is not able to form classical hydrogen bonds with other polar substances, which explains the lowest interaction with sucrose of the different head group parts and thus the easiest detachment. As a next step, the glycerol backbone starts to detach, where hydrogen bonds have to be broken. Since the oxygen atoms of the glycerol are separated by the hydrocarbon backbone of glycerol, it is a relatively large group, where parts of it strongly interact with sucrose and others do not. This makes it harder to detach than the choline group but still not as hard to detach as the phosphate group. Detachment of the glycerol group is shown in Figure 4.9c. The phosphate group finally is the last part of the hydrophilic head groups in the detachment process. It is a relativeley small group with strong electrostatic and van der Waals interactions and the possibility to build hydrogen bonds to sucrose.

PE detachment behaves in general similar to the detachment of PC. The only structural difference between PC and PE head groups is the ethanolamine instead of the choline group, which means that the hydrogens are connected to the nitrogen instead of methyl groups. The detachment process is the same, simply those two groups are exchanged. This means that the ethanolamine group has the lowest interaction with sucrose, followed by the glycerol group, and finally the phosphate group with the strongest interaction.

A fundamentally different detachment mechanism can be observed for PI head groups and is shown on the example of DLPI in Figure 4.10. PI head groups have a significant difference compared to PE and

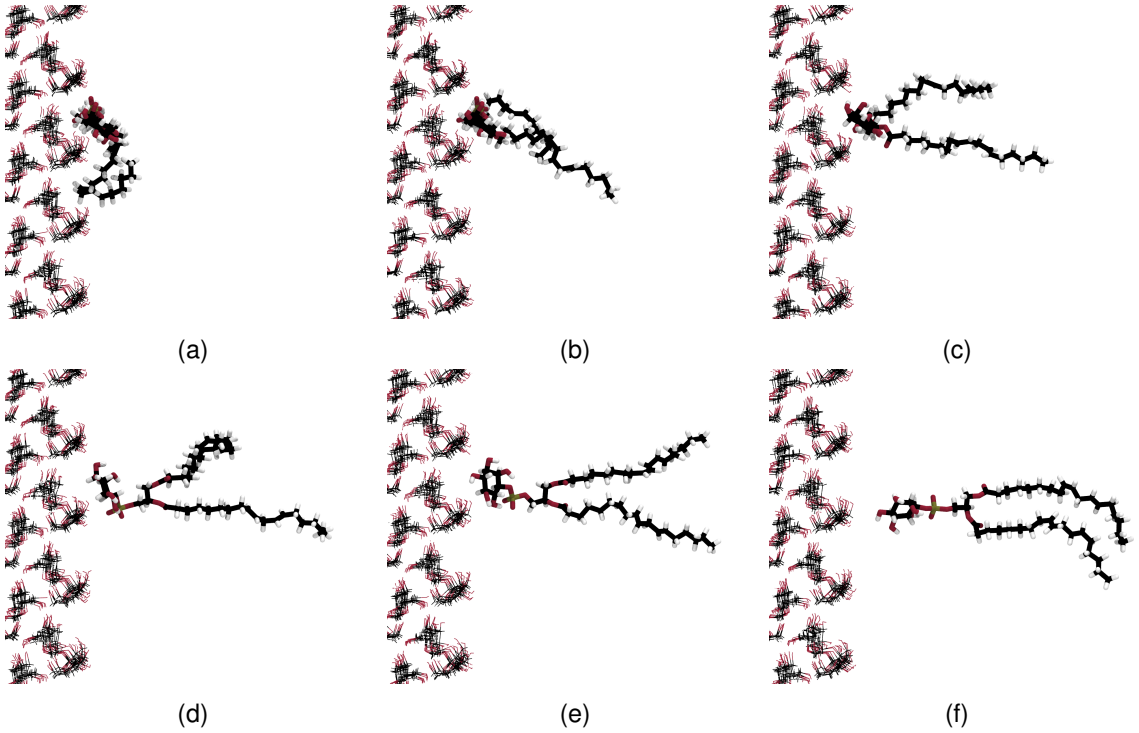

Figure 4.10: Detachment mechanism of DLPI.

PC molecules in their chemical structure. Instead of a nitrogen centered choline or ethanolamine group, an inositol group is at the tip of the head group. Inositol is a carboxylic sugar, very similar in its structure to the glucose ring in sucrose, which suggests a strong interaction. In the detachment of PI molecules the glycerol backbone starts to detach at first followed by the detachment of the phosphate group. This is shown in Figure 4.10b, 4.10c, and 4.10d. As last part finally, the inositol ring detaches, which can be seen in Figure 4.10e. The inositol ring forms several hydrogen bonds with the sucrose molecules due to its similar structure. All those hydrogen bonds have to be broken to detach the inositol ring from the sucrose surface. By analyzing the hydrogen bonds that are formed between the whole PI head group and the sucrose and the hydrogen bonds that are only formed between the inositol group and the sucrose, the described detachment mechanism can clearly be shown. In Figure 4.11a the hydrogens

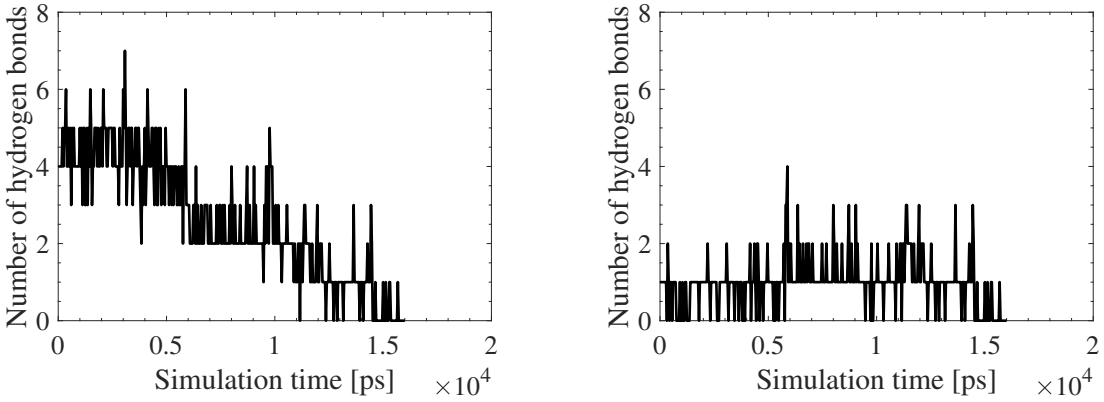

Figure 4.11: Hydrogen bonds of the complete DLPI head group with sucrose over simulation time are shown in Figure 4.11a. Hydrogen bonds of the inositol group of DLPI with sucrose over simulation time are shown in Figure 4.11b.

bonds with sucrose are shown for the total head group and in Figure 4.11b only for the inositol group. The figures are identical during the simulation time from 10 000 ps to 16 000 ps, which is the last part of the detachment process. This shows that the inositol head groups detaches at last and thus has the strongest interaction with sucrose. The intermediate increase of hydrogen bonds between the inositol group and the sucrose crystal is caused by thermal fluctuations and reorientation of the head group during the detachment process.

All six molecules have either one palmitic and one linolic fatty acid or two linolic fatty acids. The detachment of the fatty acids shows no mechanistic difference, which suggests similarly weak interactions with sucrose. After being pulled into the cocoa butter, the fatty acids of the phospholipids are in a hydrophobic and thus energetically favorable environment according to their own characteristics.

4.3.3 Detachment work of different head groups

Influence of different adsorption states on detachment work

Detachment work is calculated and compared for the different visually identified adsorption states A and B. Table 4.2 shows the detachment work for the DLPC and PLPE molecules that were found in adsorption state B and compares the detachment work to their state A detachment after the further canonical equilibration step. It is shown that the work that is required for the detachment from state B is less than for the detachment from state A.

Table 4.2: Mean value and standard deviation of detachment work for DLPC and PLPE in state A and B from the (100) sucrose crystal surface.

DLPC in state B		DLPC in state A	
Mean value	Standard dev.	Mean value	Standard dev.
$122.8\,\mathrm{kJ\,mol^{-1}}$	$18.4\,\mathrm{kJ\,mol^{-1}}$	$328.2\,\mathrm{kJ\,mol^{-1}}$	$27.8\,\mathrm{kJ\,mol^{-1}}$
PLPE in state B		PLPE in state A	
Mean value	Standard dev.	Mean value	Standard dev.
$80.0\,\mathrm{kJ\,mol^{-1}}$	$19.4\,\mathrm{kJ\,mol^{-1}}$	$140.4\,\mathrm{kJ\,mol^{-1}}$	$49.2\,\mathrm{kJ\,mol^{-1}}$

This confirms the hypothesis that the interactions of the head groups with sucrose are optimized when the head groups are adsorbed in the notches of the hydrophilic sucrose surface. Intermolecular interactions like van der Waals forces, electrostatic forces and hydrogen bonds are stronger in the notches. The reason for this can be seen in Equations 3.23 and 3.26, the Lennard-Jones-potential and the Coloumb potential, which describe the intermolecular interactions. They highly depend on the distance of the interacting atoms and can be maximized when they are in favorable spacial orientation to each other, which is more the case in the notches compared to the exposed hills of the crystal surface. Further, it is shown for PLPI that the detachment work also gets higher after the canonical equilibration without cocoa butter, although the head group is already adsorbed in the notch. This indicates that also within the positions in the notch, the unimpeded movement during the canonical equilibration allows to optimize the interactions further and is an important step to have comparable starting positions. The differences for PLPI are shown in Table 4.3.

Table 4.3: Mean value and standard deviation of detachment work for PLPI before and after the canonical equilibration from the (100) sucrose crystal surface.

PLPI before NVT equilibration		PLPI after NVT equilibration	
Mean value	Standard dev.	Mean value	Standard dev.
$302.6\,\mathrm{kJ\,mol^{-1}}$	$50.2\,\mathrm{kJ\,mol^{-1}}$	$424.4\,\mathrm{kJ\,mol^{-1}}$	$42.6\,\mathrm{kJ\,mol^{-1}}$

The results of the shown difference in detachment work that depend on the adsorption state, indicate that phospholipids in chocolate should tend to adsorb preferably in notches of sucrose crystal struc-

tures. This proposed behavior will be covered in a Section 5.3.2, where whole phospholipid layers in chocolate are investigated.

Detachment work for different phospholipid head groups

The different detachment work for the six investigates molecules in adsorptions state A are shown in Figure 4.12, sorted by the head groups. Again, all molecules had the possibility to move freely at the

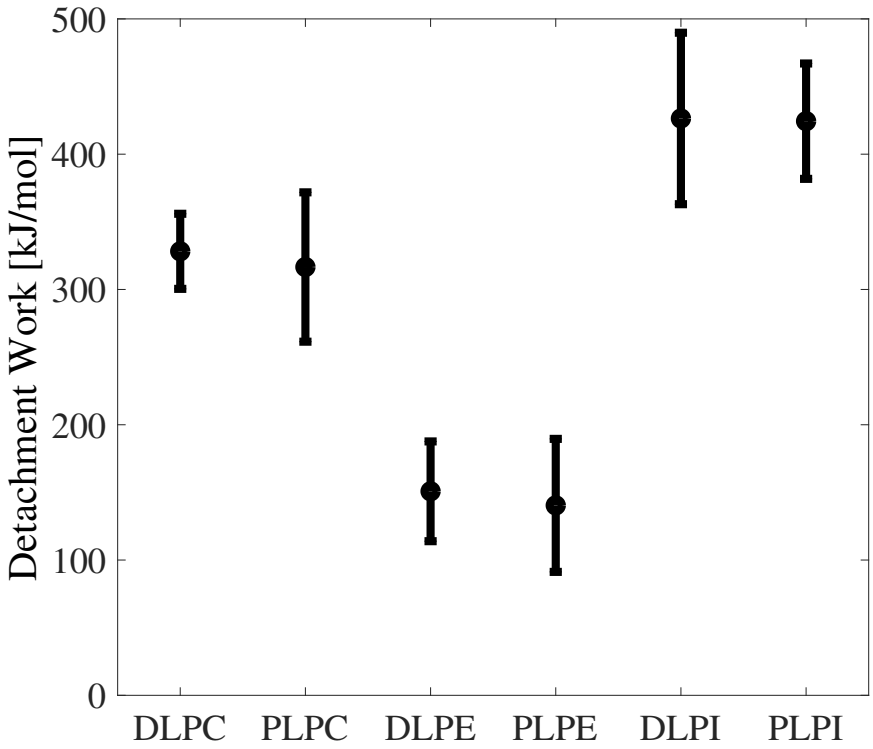

Figure 4.12: Detachment work of all six investiagted phospholipids in their adsorption state A. The error bars represent the standard deviation [70].

sucrose surface during a canonical equilibration step, which is shown to be an important step in order to have comparable starting configurations. PC, which is quantitatively the biggest part of phospholipids in vegetable lecithins and often assumed to play the most important role in reducing viscosity and yield stress in chocolate manufacturing, requires a higher detachment work than PE, which is quantitatively the second largest fraction. PI, which is the smallest fraction of investigated component in lecithins, is shown to require an even higher detachment work than PC. The number of hydrogen bonds between the hydrophilic head group and the sucrose surface is expected to play an important role. PI, which requires the highest detachment work, is found to build five to six hydrogen bonds. PC, which has the second strongest interaction, is found to build approximately three to five hydrogen bonds. PE, which has the weakest interaction, is found to build approximately two to three hydrogen bonds. The results are in good agreement with the detachment mechanism, where the interaction was already described.

PI, which has the possibility to interact with sucrose through additional hydrogen bonds compared to PC and PE, requires the strongest detachment work. While the detachment mechanisms of PC and PE are comparable and the choline group in PC showed similar behavior as the ethanolamine group in PE, the detachment work clearly shows differences. The choline group interacts stronger with sucrose than the ethanolamine group.

The magnitude of the standard deviation of the pull-code simulations, which is shown in Figure 4.12, is caused by several factors. At first, it has to be considered that the performed analysis of the pull code simulations itself is influenced by the definition of the starting point. Although the definition of the starting point of the head group detachment is based on tracking hydrogen bonds, the center of mass distance between head group and sucrose crystal, and visual inspection of the simulation trajectory, it is still subject to interpretation to a certain extent. Further, the presence of hydrogen bonds is simply defined by a combination of two threshold values. First, a donor–acceptor distance ($<0.35\,\mathrm{nm}$) and second, a hydrogen–donor–acceptor angle ($<30°$), which are prone to thermal fluctuation. Finally, the calculated detachment work depends on the phospholipid starting configuration, resulting from the final isothermal-isobaric equilibration step. Although the equilibration procedure was performed in order to minimize influences of the starting configuration, more elaborated techniques could be used. For example simulated annealing simulations could be performed to ensure to overcome local minima where the starting configuration might be stuck. Simulated annealing is based on a sequence of heating and cooling of the system. At high temperatures, the configuration can pass over energy barriers. As the temperature gets slowly decreased, the lower energy states become more probable in accordance with the Boltzmann distribution. Heating and cooling must be repeated multiple times to ensure the achievement of the global minimum statistically. However, this requires a lot additional simulation time and is beyond the scope of this work.

The calculated detachment work shows that the different phospholipids of soybean lecithin interact differently with sucrose. Nevertheless, this insight does not directly enhance the understanding of how phospholipids work in chocolate manufacturing. The results nevertheless suggest that PI molecules might have the strongest driving force to adsorb to sucrose surfaces. But still both other head groups also have a clear driving force to adsorb. A further aspect has to be considered when the results are transferred to a more realistic scenario. The adsorption should normally take place, when several phospholipids are at the interface. This means that for the adsorption energy, the interactions between the phospholipids at the interface have also to be taken into account. Eventually, this could lead to a different detachment work for the investigated molecules, when they are detached from lecithin-like phospholipid layers at sucrose crystals.

4.4 Conclusion

In this study, molecular dynamics simulations were performed to get insights into molecular interactions of phospholipids with sucrose during chocolate conching, which can hardly be gained by experiment. Molecular dynamics simulations were performed with atomistic resolution and gave dynamic insights into the system. Non-equilibrium molecular dynamics simulations were used to overcome a typical challenge of molecular dynamics simulations in food systems, which are often highly structured systems of diverse chemical complexity with high viscosity. Instead of directly accessing adsorption of lecithin molecules at sucrose surfaces in cocoa butter, the detachment process was investigated, by applying the so-called pull-code.

The most common phospholipids of vegetable lecithins, which are the main emulsifying agents, were investigated. PC, PE, and PI each with two different tail group combinations (DLPE, PLPC, DLPE, PLPE, DLPI, PLPI) were the subject of this study. The work that is required to detach the phospholipids from the (100) sucrose crystal surface in cocoa butter was calculated and thus the strength of interaction was quantified. PI head groups were shown to require the most detachment work, followed by PC, and finally PE with the lowest detachment work. The different tail groups were shown to have no notable impact on the head group detachment. The number of hydrogen bonds between the phospholipid and sucrose was shown to play a major role and to correlate with the detachment work. PI formed the most hydrogen bonds with the sucrose surface followed by PC, and finally by PE.

It was shown that the adsorption state of phospholipids on sucrose surfaces has an impact on the detachment work. Two different adsorption states were defined in this study, which are governed by the notches in the molecular topography of the sucrose crystal surface. State A corresponds to a complete adsorption of the polar head groups in a notch of the surface and state B to an adsorption were parts of the head group are not in the notch. Complete adsorption in the notch leads to stronger interaction with sucrose due to better spacial compatibility and thus to stronger detachment work.

The detachment mechanisms of the different head groups were investigated in detail. Similar behavior was observed for PC and PE head groups, where the phosphate group detached at last and thus had the strongest interaction with sucrose. Different behavior was observed for PI molecules, where the inositol group detached at last. The strong interaction of PI molecules with sucrose could be retraced to the similar chemical structure of the inositol group to the glucose monomer of sucrose and the resulting ability to form several hydrogen bond.

Chapter 5

Phospholipids structures surrounding sucrose particles

The aim of this study is to gain insights into phospholipid structures in chocolate for mechanistic explanations of rheological behavior. The major part of this chapter is based on the study by Kindlein et al. [71]. The well known increase of yield stress of chocolate by adding an excessive dose of lecithin is investigated [12, 35, 118, 135]. This phenomenon leads to the assumption that phospholipids show differences in their behavior in chocolate masses in higher concentration compared to lower concentration. Therefore, structures of lecithin-like phospholipid mixtures in different concentrations in chocolate are calculated.

To investigate the described problems, molecular systems have to be investigated that are able to capture the relevant phenomena. Compared to the systems that are investigated in Chapter 4, a part of the systems that are used here need to be designed differently. A single periodic interface system would not be feasible to investigate molecular structures of phospholipids surrounding sucrose particles at corners and edges, which could probably be of importance.

To overcome the problem of long computing times, due to the slow dynamics in cocoa butter and the big system size, coarse-grained molecular dynamics simulations are performed. The Martini FF [87, 88] is employed to simulate mixtures of phospholipids, sucrose, and cocoa butter, resembling again a chocolate-like system without considering cocoa particles and milk ingredients. Suitability of the Martini FF is discussed in Section 5.1 of this chapter. Phospholipids with the four most prominent hydrophilic head groups are considered for the representation of lecithin in this study. PC, PE, and PI are investigated accordingly to the study of last chapter, and additionally the PA head group is investigated, which is also quite common in vegetable lecithin [101]. Further, the influence of the degree of saturation of the phospholipid fatty acids on molecular structures is investigated.

The following specific investigations are performed in this study. Molecular structures of phospholipids

in cocoa butter are calculated for different phospholipid concentrations. Area per lipids in phospholipid monolayers, consisting of only one specific kind of phospholipid, at the sucrose–cocoa butter interface are compared. The composition of phospholipid monolayers at the sucrose–cocoa butter interface after adding a typical soybean lecithin-like phospholipid mixture is investigated. The structural behavior of excessive phospholipids that are not assembled in a monolayer around sucrose particles, is examined and the calculated structures are used to explain rheological phenomena and are related to experimental results from literature. Further, the concentration of phospholipids of one specific kind at the sucrose–cocoa butter interface, where phospholipids detach from the monolayer, is calculated.

5.1 Suitability of the Martini coarse-grained force field

The Martini FF was initially presented as a coarse-grained model for biomolecular simulations, which is parameterized in a systematic way by reproduction of partitioning free energies between non-polar and polar phases, the reproduction of free energy of vaporization as well as hydration, and interfacial tensions of different phases [87, 88]. Although the main focus of developing the lipid force field was primarily on lipid membrane simulations of biological cells, it can almost directly be used for the molecular components of this thesis. The phospholipids of vegetable lecithins used in food processing are more or less the same as in biological membranes. At least all building blocks that are required, such as the different hydrophilic head groups, the glycerol backbones, and the different saturated and unsaturated parts of the aliphatic chains, as well as the terminal ends of the aliphatic chains are available. Many membrane simulation studies have been conducted with the Martini FF and are in very good agreement with experimental data. In the initial force field development paper, bilayer properties, such as areas per lipids in bilayers, free energies of lipid desorption, and bilayer stress profiles were shown to be in good agreement with experimental data [88]. Several further studies have been conducted in which phospholipids were modeled with the Martini FF and are mentioned here exemplarily to show that the model is well established for phospholipid simulations [7, 32, 63, 95, 134, 149]. Triglycerides, which are built from the same building blocks as phospholipids, were also investigated with the Martini FF. Spherical high density lipoproteins, which contain triglycerides, were investigated [138] as well as low-density and high-density lipoproteins and lipid droplets [104], and lipid droplets containing oxidized triglycerides [94]. The high number of studies on triglycerides and phospholipids, employing the Martini FF, shows the validity of the model for these components. In addition to parameters for lipids, parameters for the carbohydrate sucrose are required for this work. These parameters are also readily available for the Martini FF, since it has been extended to carbohydrates [82]. The role of carbohydrates and glycolipids in biological membranes [82, 83], their behavior in aqueous solutions [82, 83, 95], as well as carbohydrates as ligands to enzymes [100] were studied. Additionally, a further relevant carbohydrate for food processing was studied with the Martini FF. Cellulose, which is often present in vegetable food raw materials and also in food products as fiber, was investigated in its crystalline state and was subject to

reparameterization to obtain the experimentally measured crystal structure [84]. Finally, proteins, the third class of energy-providing food components besides lipids and carbohydrates, are also present in the Martini FF and can be investigated in future studies with relation to food [98]. The presented number of studies shows that the Martini FF was used extensively for studying the different components of the here investigated systems. Although, they were studied in a different context, the molecular parameters can still be relied on. The simulations of this study are performed at atmospheric pressure and at moderate temperatures, which are within the range of the original model development. The presented literature review gives the model a solid validation and the force field will be applied without further validation. The results of this study will later be subject to a comparison to experimental findings, where several effects could be validated and no contradictions could be detected.

The interaction sites used in the Martini FF are based on a four-to-one mapping, which means that four heavy atoms are mapped to one coarse-grained bead on average, with molecular ring structures being the main exception, where only so much heavy atoms are mapped to one bead that the ring structure is preserved (mostly resulting in a two or three to one mapping). In order to keep the model as simple as possible and easily transferable, only four main interaction sites are defined. They are labeled: polar, non-polar (partly polar and partly apolar), apolar, and charged. Further, each main type has additional subtypes, giving in total 18 different beads. The subtypes are either defined by the possibility of forming hydrogen bonds (donor, acceptor, donor and acceptor, none) or by the degree of polarity in 5 steps from low polarity to a high polarity. An interaction matrix for Lennard-Jones interactions between the 18 different beads is given, defining 10 different levels of interactions. The well-depth ε of the Lennard-Jones potential rises from a weak interaction of $2.0\,\mathrm{kJ\,mol^{-1}}$ to a strong interaction of $5.6\,\mathrm{kJ\,mol^{-1}}$. σ, defining the interaction distance of the beads, is 0.47 nm for the all interactions except the weakest, where it is 0.62 nm.

5.2 Methods

5.2.1 Molecular model of chocolate

Similar to the study, shown in the last chapter, the investigated molecular components of this study are again sucrose, phospholipids to represent lecithin, and triglycerides to represent cocoa butter. Sucrose is again modeled in its crystalline state using the same crystal unit cell as in Chapter 4 [25, 34]. To perform coarse-grained simulations with crystalline sucrose, the all-atom unit cell is transformed to a coarse-grained unit cell. Therefore, the center of masses of the different sucrose atoms that are mapped together to one coarse-grained bead are calculated. The resulting coordinates are used for the coarse-grained sucrose beads. The procedure to get from the all-atom unit cell to the coarse-grained crystal is illustrated in Figure 5.1 It can be seen that the monomers of sucrose, which are glucose and fructose,

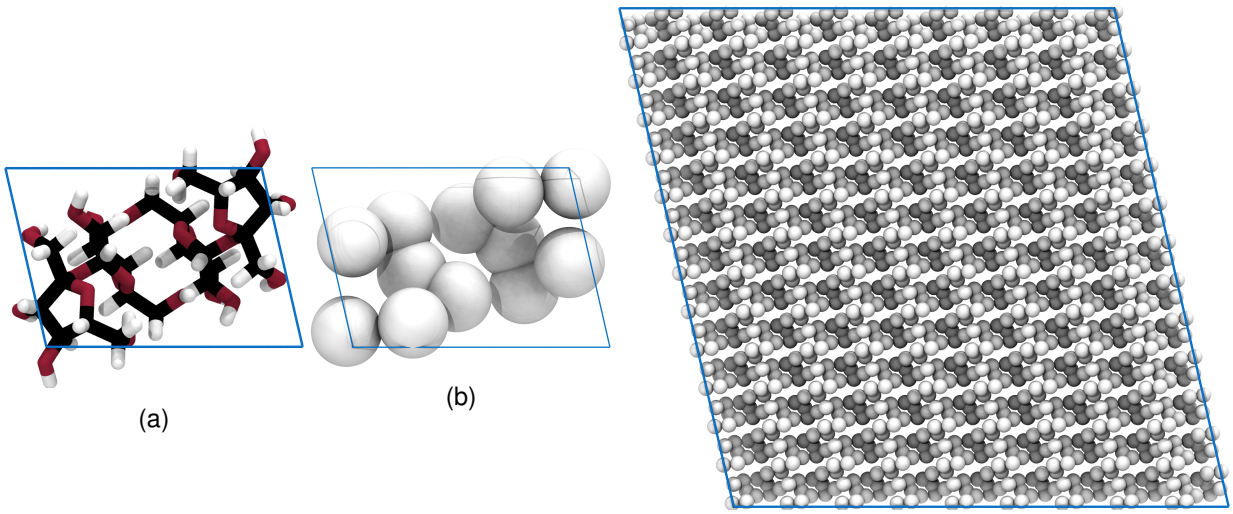

Figure 5.1: The all-atom sucrose crystal unit cell (Figure 5.1a) is used to calculate the coordinates for the coarse-grained sucrose crystal unit cell (Figure 5.1b). The crystalline sucrose particle is then a result of multiplying the coarse-grained unit cell along all spacial directions (Figure 5.1c). The white color for sucrose is used throughout this chapter.

each are represented by three coarse-grained beads in the Martini FF [82]. This results in 12 beads and represents the two sucrose molecules of the crystal unit cell as shown in Figure 5.1b.

Analogue to the study of the last chapter [70] cocoa butter is represented by its three main molecular components POS, SOS, and POP, which together are $84.5\,\mathrm{wt}\%$ of cocoa butter [47]. The coarse-grained representation of all three cocoa butter triglycerides is the same, only the chain beads are different in their mass due to the different chain lengths of palmitic and stearic acid. The coarse-grained structure is shown in Figure 5.2. The Martini FF representation of triglycerides consists of a central

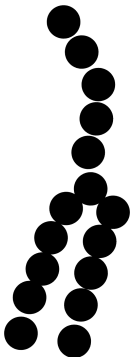

Figure 5.2: Coarse-grained representation of the three cocoa butter triglycerides in the Martini FF. All three triglycerides POS, SOS, and POP result in the same coarse-grained representation. The black color for triglycerides is used throughout this chapter.

bead, representing the glycerol backbone, which is connected to three further beads, which represent

the ester bonds to the aliphatic chains. The chains are then represented by beads according to their chain length and according to the degree of saturation. With the investigated triglycerides of this study, this results in a triglyceride that has two saturated chains and one unsaturated oleic chain, resulting in slightly different bond angles, as can be seen in the top aliphatic chain (oleic acid) in Figure 5.2.

The investigated phospholipids include again the three most prominent head groups PC, PE, and PI, and additionally the PA head group. They are investigated with each two linolic acid aliphatic chains, which gives the phospholipids DLPC, DLPE, DLPI, and DLPA. To pronounce differences of molecular structures in chocolate that are caused by the degree of saturation of the aliphatic chains, all head groups are additionally studied connected to two saturated stearic fatty acids, which have the same chain length as linolic acid. Thus, the further investigated phospholipids are DSPC, DSPE, DSPI, and DSPA. All eight investigated phospholipids of this study are shown in Figure 5.3.

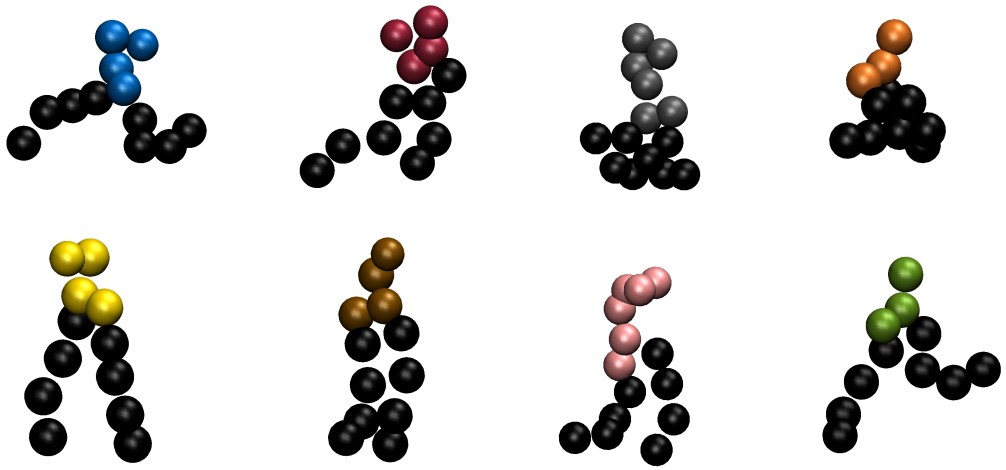

Figure 5.3: Coarse-grained representation of the investigated phospholipids of this study. Aliphatic chains are shown in black, the head groups are shown in different colors. Top from left to right DLPC (blue), DLPE (red), DLPI (gray), DLPA (orange) and bottom from left to right DSPC (yellow), DSPE (ochre), DSPI (pink), and DSPA (green). The presented color-code is used throughout this chapter.

5.2.2 System building

With the aim of this study to investigate molecular structures of phospholipids in chocolate, the challenge of defining a quantitatively representative molecular composition arises. This can be considered as a typical challenge for molecular modeling of complex food systems in general and is explained in the following. Phospholipids are added to chocolate during the conching process. Nevertheless, it cannot be assumed that the phospholipids are distributed evenly in the system. On the one hand this is caused by the hydrophilic–hydrophobic interfaces, where they are supposed to adsorb and probably the biggest part can be found there in the equilibrium state, and on the other hand, it is caused by the nature of the

stochastic mixing and the resulting distribution of the phospholipids in the system. It was shown that the phospholipid layers on sucrose particles in chocolate is very uneven. Ranging from no coverage at all up to a layer of 34 nm thickness. This layer consists of a mixture of triglycerides and phospholipids and the local content of the phases could not be analyzed further [92]. This circumstances make it quite challenging to define the molecular composition of the nano-scaled simulation system, since it is not possible to define one representative system. To account for that problem, five different simulation setups were investigated. This allows to investigate different limiting cases and likely scenarios of molecular composition in chocolate. An overview of the systems is given in Table 5.1 and Table 5.2 and the different setups are elucidated in the following.

Table 5.1: Overview of the different systems that include no periodic interface. The molar fraction χ of phospholipids in the surrounding lipids (without initial phospholipid monolayer) is given in $[\%]$. The table shows whether a central sucrose particle, an initial phospholipid monolayer at the sucrose crystal surface, and cocoa butter were present. Phospholipid refers to single phospholipids or soybean lecithin phospholipid mixtures.

System	χ [%]	Sucrose particle	Monolayer	Cocoa butter	Phospholipid
5.1a	1.06	no	no	yes	soybean
5.1b	5.04	no	no	yes	soybean
5.1c	17.53	no	no	yes	soybean
5.2a	100	yes	no	no	DLPC
5.2b	100	yes	no	no	DLPE
5.2c	100	yes	no	no	DLPI
5.2d	100	yes	no	no	DSPC
5.2e	100	yes	no	no	DSPE
5.2f	100	yes	no	no	DSPI
5.3a	0	yes	yes	yes	soybean
5.3b	3.45	yes	yes	yes	soybean
5.3c	28.72	yes	yes	yes	soybean
5.4	1.06	yes	no	yes	soybean

Table 5.2: Overview of the different systems that include a periodic interface. The different cells give the area per lipid of the monolayer. Either four or seven instances of each system 5.5a-f are investigated.

System 5.5a	System 5.5b	System 5.5c	System 5.5d	System 5.5e	System 5.5f
Investigated phospholipids					
DLPC	DLPE	DLPI	DSPC	DSPE	DSPI
Area per lipid [nm^2]					
0.5385	0.5385	0.5385	0.4039	0.4039	0.4039
0.5176	0.5176	0.5176	0.3920	0.3920	0.3920
0.5030	0.5030	0.5030	0.3835	0.3835	0.3835
0.4847	0.4847	0.4847	0.3728	0.3728	0.3728
0.4718	0.4718	0.4718			0.3627
0.4557	0.4557	0.4557			0.3507
0.4443	0.4443	0.4443			0.3417

To investigate structures and compositions of phospholipid micelles in cocoa butter without the influence of sucrose particles, three different systems are investigated, labeled as systems 5.1a-c (see Table 5.1). Therefore, a lecithin-like phospholipid mixture and a cocoa butter-like triglyceride mixture are randomly inserted in cubic simulation boxes and the total phospholipid concentration is varied.

Systems 5.2-5.4 are designed to investigate lipid structures surrounding a crystalline sucrose particle. Therefore, the sucrose crystal unit cell is replicated along its crystal axes for 9, 11, and 13 times, respectively. This gives a cuboidal sucrose particle, with edge lengths of about 9.5 nm with the angles of 90° and 102.94° according to the sucrose crystal unit cell. Subsequently, the resulting sucrose particle is centered in the simulation box and surrounded by a lipid phase. An example of the resulting setups is given in Figure 5.4

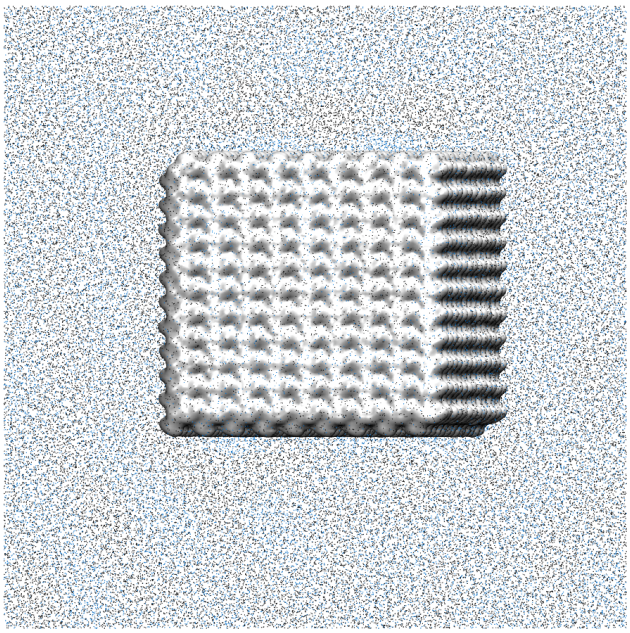

Figure 5.4: Setup of systems 5.2a-f, 5.3a-c, and 5.4 on the example of system 5.2a. A central sucrose particle is surrounded by lipids. The sucrose particle is shown in a surface representation. The lipids are shown as dots.

In systems 5.2a-f only phospholipids of one kind are inserted randomly, in order to investigate the resulting molecular structures in the vicinity of sucrose, when only phospholipids are present. This results in six different systems as only the head groups PC, PE, and PI are investigated here, each in the saturated and unsaturated version.

For the building of systems 5.3a-c a lecithin-like phospholipid mixture is added to the sucrose particle simulation box and equilibrated in a molecular dynamics run until a phospholipid layer adsorbs on the surface. The sucrose particle with the adsorbed monolayer of phospholipids is then extracted and again surrounded by only cocoa butter triglycerides (system 5.3a) or a mixture of cocoa butter triglycerides and phospholipids with different total phospholipid concentrations in the lipid phase (system 5.3b-c).

In the building of system 5.4, cocoa butter triglycerides and lecithin phospholipids are directly inserted randomly in the box around sucrose. In all simulations, the position of the sucrose molecules are fixed by applying an external force, so called position restraints. The phospholipid concentrations are chosen to account for a possibly broad range of scenarios that are either as realistic as possible or limiting cases and thus are a key feature of the presented study. These systems allow to get an idea of how phospholipid structures in chocolate look like. Systems 5.2a-f are some kind of a limiting case where only phospholipids are in the first few nanometers surrounding the sucrose particle. Systems 5.3a-c account for the effect that a complete phospholipid layer is at the sucrose surface and a further mixture of lipids is surrounding these structures. Since the formation of such a complete monolayer cannot be observed by straight forward molecular dynamics simulations, due to the limited calculation time, the described preparation of these structures is necessary. Nevertheless, this seems to be a realistic scenario as all adsorbed phospholipids in the simulation stay adsorbed during the whole simulation time, once they are adsorbed. System 5.4 represents the sucrose surfaces that have no phospholipids adsorbed, which are also found in chocolate [92].

An additional type of systems, similar to the periodic interfaces of Chapter 4, labeled system 5.5a-f, is investigated in this study and is shown in Figure 5.5. These systems are used to calculate the area

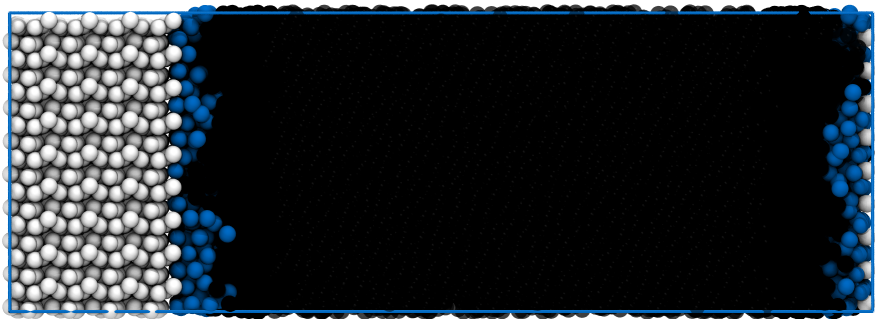

Figure 5.5: Exemplarily illustration of systems 5.5a-f, consisting of a periodic interface between a sucrose crystal and cococa butter with a phospholipid layer in between, on the example of system 5.5a.

per phospholipid at the sucrose surface where phospholipids start to detach. They consist of an infinite sucrose crystal slab, where on both sides a monolayer of phospholipids of a single kind is attached, with hydrophilic head groups adsorbed on the sucrose surface. On the other side of the phospholipid monolayers are cocoa butter triglycerides, resulting in systems with an infinite cocoa butter–sucrose interface with a phospholipid monolayer in between. The phospholipid monolayers are designed with different packing densities of the phospholipids, resulting in different areas per lipids. With that approach, the areas per lipid of phospholipids at the specific sucrose–triglyceride interface are investigated as phospholipids should only detach from that monolayer in the case the concentration is to high. The sucrose crystal is built by replicating the sucrose crystal unit cell for 4, 9, and 9 times in x-, y-, and z-direction, respectively. Afterwards, the box is elongated in x-direction to make room for the insertion of the phospholipid monolayer and the cocoa butter triglycerides. Phospholipid monolayers are generated with

the help of the *insane tool* of the Martini FF [144]. The *insane tool* generates phospholipid bilayers, where the type of phospholipid, the area of the bilayer, and the area per lipid can be defined. The area of the bilayer is chosen according to the sucrose–cocoa butter interface. The resulting bilayer is then separated in a way that two single phospholipid monolayers are obtained. The two monolayers are then used to build the interfaces of the systems 5.5a-f. Interfaces with different areas per lipid are investigated, in order to calculate the stable monolayer area per lipid for the different phospholipids at the specific interface. The different investigated phospholipid monolayers are shown in Table 5.2 for the different phospholipids. An additional system, which is labeled system 5.5g and is very similar to systems 5.5a-f, is built and only used in one simulation. Instead of the triglycerides it only contains DLPC molecules besides the sucrose crystal.

5.2.3 Equilibration and production run details

All simulations and parts of the analysis are performed with the Gromacs software package Version 5.1 [133]. Equations of motion are integrated with the leap-frog algorithm [57] with a time step of 10 fs. All non-bonded interactions are truncated with a cut-off of $1.1\,\mathrm{nm}$. The reaction field potential is used to calculate long-range electrostatics, as proposed by Marrink et al. [88]. The first step of all simulations is an energy minimization using the steepest decent algorithm until the potential energy leveled out. This delivers a starting configuration in a local energy minimum to avoid high potential energies during the integration of the equations of motion, which could result in a program crash. For systems 5.1-5.4 the following further simulation procedure is performed. A canonical equilibration is performed for $10\,\mathrm{ns}$ and subsequently, an isothermal-isobaric equilibration is performed for $100\,\mathrm{ns}$, in order to reach the desired temperature of $333\,\mathrm{K}$ and atmospheric pressure of $1\,\mathrm{bar}$. These can be considered as typical conching conditions. Temperature and pressure are controled using the Berendsen thermostat and the Berendsen barostat, respectively. The final production runs are performed in the canonical ensemble for $2\,\mathrm{to}\,3\,\mu\mathrm{s}$. The velocity-rescale thermostat is used for controlling temperature. For systems 5.5a-f the following further simulation procedure is performed. An isothermal-isobaric equilibration is performed for $5\,\mathrm{ns}$ to reach the desired temperature of $333\,\mathrm{K}$ and atmospheric pressure of $1\,\mathrm{bar}$. Temperature and pressure are controlled using the Berendsen thermostat and the Berendsen barostat, respectively. The final production runs are performed in the canonical ensemble for $200\,\mathrm{ns}$. The velocity-rescale thermostat is used for controlling temperature.

5.2.4 Analysis of the simulations

Adsorption of phospholipids on the sucrose particle is determined by evaluating a distance function, where all phospholipids are counted as adsorbed when the central bead of the polar head group is within a distance of $1.1\,\mathrm{nm}$ of the sucrose particle. This corresponds to the cut-off distance of the non-bonded interactions in the Martini FF and thus is a realistic distance wherein strong interactions are

present. The number of adsorbed molecules, determined with the described method, levels out during the productions runs and a steady state of adsorption is defined for the relevant systems of this study. Diffusion coefficients D of phospholipids are calculated using the Einstein relation

$$D = \lim_{t\to\infty} \frac{1}{6t} \langle \Delta \boldsymbol{r}(t)^2 \rangle, \tag{5.1}$$

where $\boldsymbol{r}$ is the coordinate vector of the molecules and t is the simulation time. The diffusion coefficient can be calculated by a linear regression of the mean square displacement $\langle \Delta \boldsymbol{r}(t)^2 \rangle$ over simulation time. Analysis of phospholipid structures and triglyceride structures are done by visual inspection. Phospholipid micelles were further characterized by analyzing the maximum number of phospholipids in one micelle, in other words the size of the largest micelle in the simulation system, and the average number of phospholipids per micelle. Phospholipids are counted as part of one cluster, when the central head group beads are at a maximum distance of $1\,\mathrm{nm}$, which is found to be an adequate value for micelles clusters. Detachment of phospholipids from the monolayers at interfaces of systems 5.5 are visually identified with help of the production run trajectories.

5.3 Results and discussion

5.3.1 Phospholipid micelles in cocoa butter

As amphiphilic molecules, phospholipids in solution are known to form micellar structures. The polarity of the solvent has a huge influence on the resulting structures. It defines whether the hydrophilic part or the hydrophobic part of phospholipids is oriented towards the bulk phase of the solvent. In this study cocoa butter can be considered as a hydrophobic solvent and thus determines that the phospholipid chain groups should be oriented towards the bulk solvent. To analyze the micellar structures of phospholipids in cocoa butter, systems 5.1a-c are investigated. Thus, the structures of the phospholipids are investigated for three different phospholipid concentrations at a typical conching temperature of $333\,\mathrm{K}$. The matter of concentration has to be considered very carefully as the resulting structures are influenced by the phospholipid concentration. Since local differences are likely, the concentration of phospholipids in real cocoa butter might not be constant over the system. The investigated range is suitable to give an idea of the different structures. It is shown in Figure 5.6a that at low concentrations of $1.06\,\mathrm{mol\%}$, mainly spherical micelles are present after a simulation time of $2\,\mu\mathrm{s}$. In Figure 5.6b at $5.04\,\mathrm{mol\%}$ more ellipsoidal micelles are present after $2\,\mu\mathrm{s}$. Whereas at a concentration of $17.53\,\%$ longer, wormlike micellar structures are present after $2\,\mu\mathrm{s}$, which is shown in Figure 5.6c. The presented structures are supported by the average and maximum cluster sizes, which are given as numbers of phospholipids in the clusters. It is shown that both the average and maximum cluster sizes are highest for the highest concentration of phospholipids, followed by the medium concentration, and finally the system with the lowest phospholipid concentration has the lowest average and maximum numbers. This is shown in

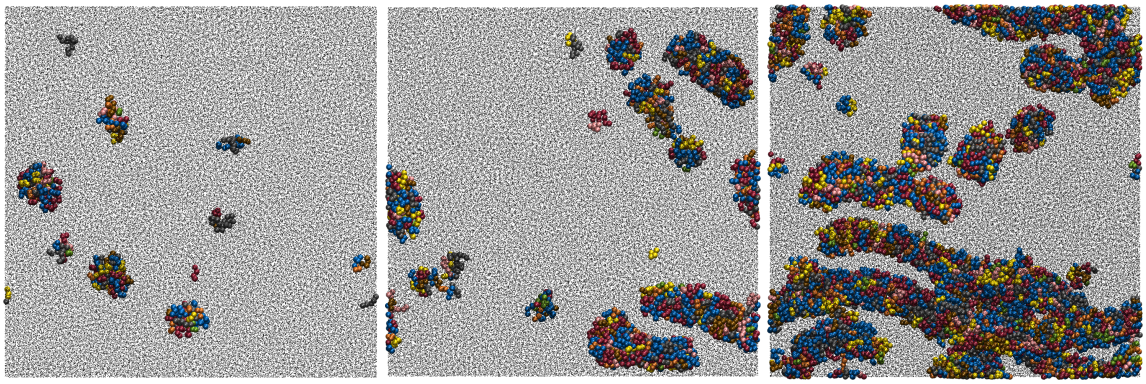

(a) (b) (c)

Figure 5.6: Micellar structures in system 5.1a (Figure 5.6a), system 5.1b (Figure 5.6b), and system 5.1c (Figure 5.6c) after 2 µs production run. Hydrophilic head groups are shown as spheres, while triglycerides and aliphatic chains of phospholipids are shown as dots.

Figure 5.7. The numbers seem to tend to their equilibrium value after 2 µs simulation time. For more detailed analysis, even longer simulations should be performed. Nevertheless, the relevant information for chocolate manufacturers can already be concluded from the presented data. Soybean lecithin-like phospholipid mixtures in cocoa butter triglycerides can form long-range structures of hydrophilic parts in the systems and thus lead to a network in the liquid chocolate mass.

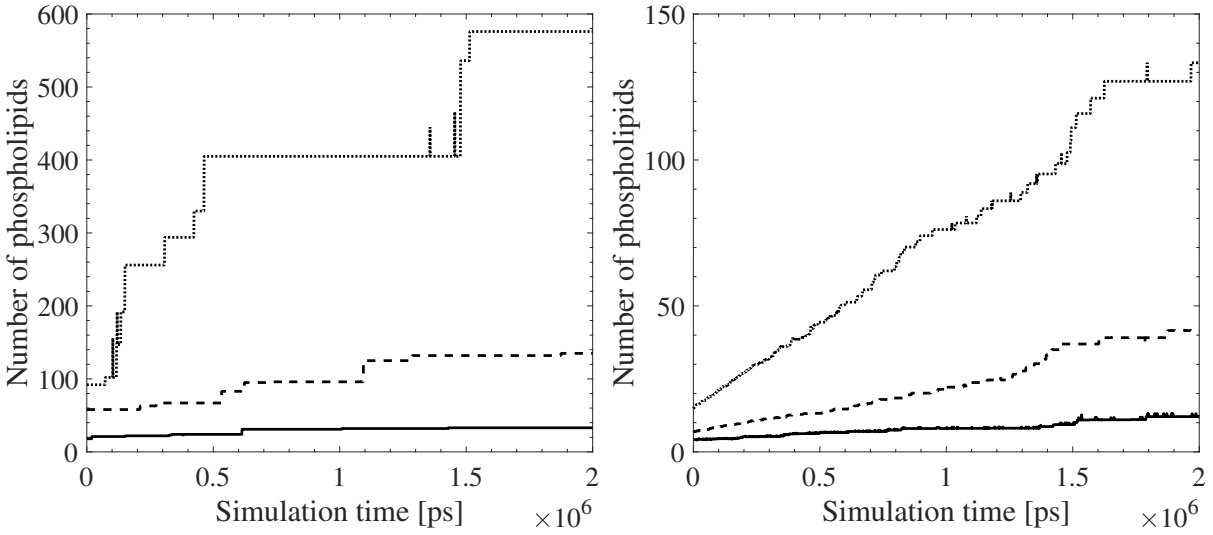

(a) Number of phospholipid molecules in the biggest micelles for systems 5.1a-c.

(b) Average number of phospholipid molecules in the micelles for systems 5.1a-c.

Figure 5.7: Characterization of the micelles for system 5.1a-c. System 5.1a is shown as solid line, system 5.1b is shown as dashed line, and system 5.1c is shown as dotted line.

5.3.2 Adsorption of head groups on crystalline sucrose

It is commonly agreed that phospholipids have to adsorb at hydrophilic–hydrophobic interfaces to lead to a positive influence on rheological properties in chocolate manufacturing. So far, no direct assessment of differences in the adsorption behavior for specific phospholipids has been reported. With the setup of systems 5.2a-f, it is possible to investigate the adsorption of pure phospholipids, which are only consisting of one kind of phospholipid molecule, on sucrose surfaces. Such a setup could hardly be investigated in experiments but with a simulation approach as shown in this study. The number of adsorbed molecules at the sucrose surface is investigated for the different head groups PC, PE, and PI and for the different degrees of saturation with either two two-fold unsaturated fatty acids or two saturated fatty acids. As already described, systems 5.2a-f only consist of a central sucrose particle and the specific randomly inserted phospholipids of one kind. During the equilibration simulations and the production runs the phospholipids adsorb with their head groups on the hydrophilic sucrose surfaces. The resulting numbers of adsorbed phospholipids are shown in Figure 5.8. Figure 5.8 shows that all

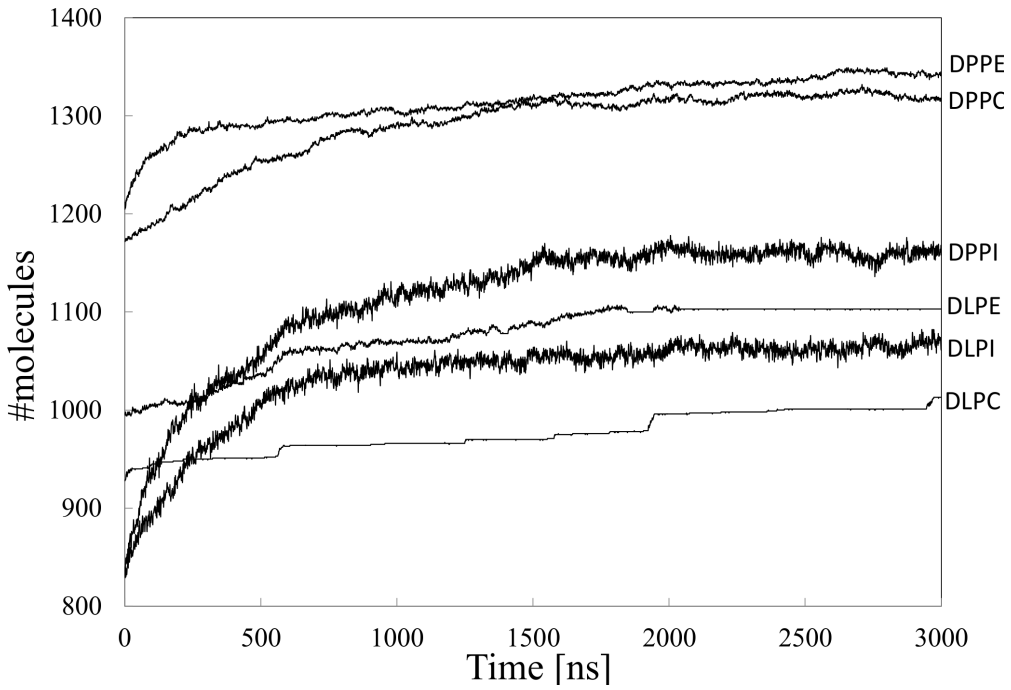

Figure 5.8: Numbers of adsorbed phospholipids at the sucrose particle during the production run.

phospholipids with the same head groups adsorb in a higher number in their saturated version. This means that unsaturated phospholipids have a higher area per lipid than their saturated counterparts. This behavior is also known from experimental studies of phospholipid membranes [74] as well as coarse-grained simulation studies of phospholipid membranes [144]. Phospholipid membranes are similar to the investigated systems of this study as they are also self-assembled phospholipid systems, where the different hydrophilic and hydrophobic parts form separate phases. The shown results suggest that the degree of saturation of the aliphatic chains has a higher impact on the area per lipid than the

phospholipid head group. Although it was shown in Chapter 4 that phospholipid head groups have a strong influence on the strength of interaction, the resulting number of adsorbed molecules is governed by the degree of saturation of the aliphatic chains, when the phospholipids are present in an excessive dose. This makes sence, since Chapter 4 clearly showed that all different head groups have a strong interaction with sucrose surfaces. Thus, all phospholipids should attach sooner or later. The total number of adsorbed molecules is then limited by the spacial requirements of the phospholipid tail groups. By analyzing the trajectories, it can further be seen that the phospholipids adsorb preferably in the notches of the sucrose crystal surface as the hydrophilic interaction is the strongest there.

5.3.3 Detachment from phospholipid layers

Systems 5.5a-f are used to investigate the detachment of phospholipids from sucrose–cocoa butter interfaces with an initially defined concentration of phospholipids. Table 5.3 shows the lowest concentration of phospholipids in the monolayers at the sucrose surface where detachment occurred on both interfaces. Detachment was defined by visual inspection, when phospholipids desorbed during the production runs from both monolayers. The results of the detachment calculations in Table 5.3 support

Table 5.3: Area per phospholipids where detachment occurred.

Detachment from both monolayers	Area per lipid [nm^2]
DLPC	0.4847
DLPE	0.4718
DLPI	0.4718
DSPC	0.3728
DSPE	0.3728
DSPI	0.3507

the results shown in Figure 5.8 that phospholipids with saturated stearic acid tails have a lower area per lipid and thus detach at higher concentrations than phospholipids with unsaturated linolic acid tails. The difference in the detachment concentration between DLPC, DLPE, and DLPI is too small to claim a difference on the basis of the shown simulations. For the saturated tails, a bigger difference is calculated. PI tends to detach at higher concentrations than PE and PC, which means that PI is more stable in monolayers with higher concentrations in the saturated case. The shown difference between the saturated and the unsaturated phospholipids should be caused by the different space requirements of the aliphatic chains. Unsaturated chains need a bigger area per lipid as they have kinks due to the double bonds. With this simulation setup and the setup from Section 5.3.2 it could be shown that saturated phospholpids have a lower area per lipid at the sucrose interface in two different plausible chocolate scenarios. First, when the sucrose particle is surrounded by phospholipids only, and second, when a monolayer of phospholipids is at the specific interface between cocoa butter and crystalline sucrose. In terms of phospholipid concentration-dependent behavior of chocolate, this could mean the following for

chocolate manufacturers: it should be experimentally tested if a higher amount of saturated phospholipids, could lead to the effect that a wider range of lecithin concentration still keeps the yield stress low. Saturated phospholipids can be packed more densely in the monolayer and thus yield stress inducing structures occur later, while positive effects are already present.

The detachment simulations can further be used to get insights into the detachment mechanism from layers and into resulting structures in chocolates with excessive phospholipid concentrations where the sucrose crystal is already covered with a phospholipid monolayer. The detachment of phospholipids from the monolayers is shown on the example of DLPC for the systems with an area per lipid of $0.4557\,\mathrm{nm}^2$ in the monolayer in Figure 5.9. Figure 5.9a shows a snapshot from the beginning of

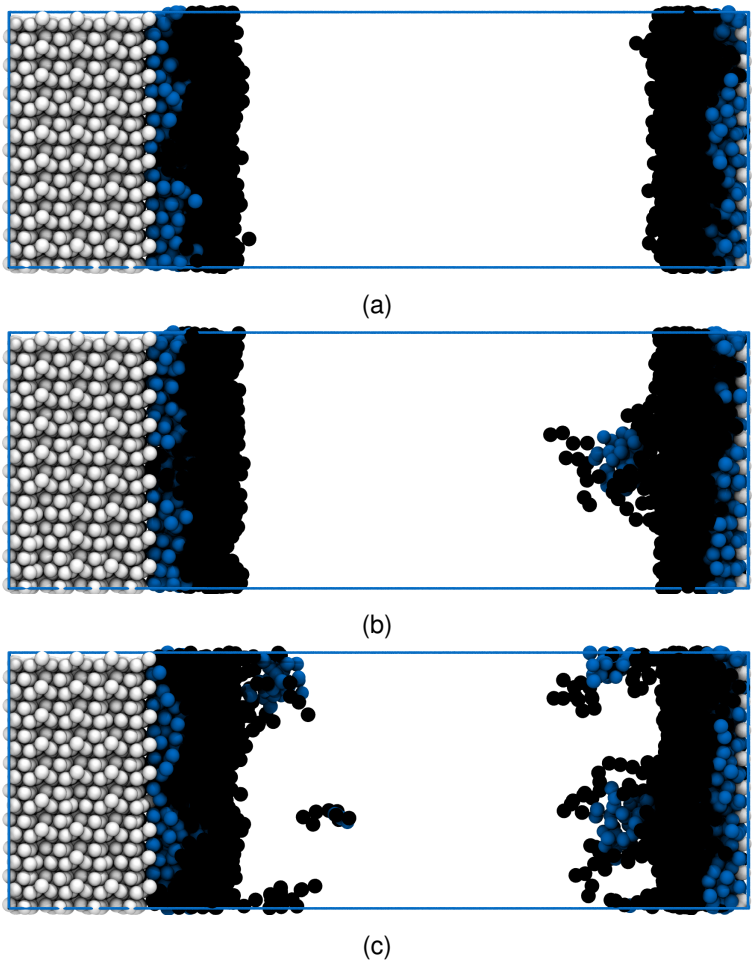

Figure 5.9: Detachment of phospholipids from phospholipid monolayers at the sucrose surface–cocoa butter interface. Three different snapshots from the production run are shown in chronological order in Figures 5.9a , 5.9b, 5.9c for DLPC. Cocoa butter is omitted for sake of clarity.

the production run, where the sucrose crystal is shown on the left side of the simulation box. To the right side of the sucrose crystal the phospholipid monolayer is shown and on the far right side of the simulation box the other monolayer is shown, which actually is to the left side of the sucrose crystal

due to periodic boundary conditions. In order to see the phospholipids clearly, cocoa butter, which is in between the two phospholipid monolayers, is not shown in Figure 5.9. The movement of the phospholipids through the monolayer away from the sucrose crystal takes time, due to the stochastic nature of the detachment process. Thus, no complete detachment is visible in the beginning of the production run. Nevertheless, as few disturbances in the monolayer can already be spotted in Figure 5.9a, for example on the top right side of the simulation box, where a few tail group beads are close to the sucrose crystal in the hydrophilic head group layer. Figure 5.9b shows the system with a first detached group of phospholipids from the monolayer on the right side of the simulation box. The phospholipids form a micelle in the cocoa butter medium. This indicates that direct formation of a secondary layer is not favorable through interaction of the phospholipids with each other. The monolayer on the left side of the simulation box is also showing that detachment processes start as similar disturbances in the monolayer can be spotted. Figure 5.9c shows the state were several phospholipids have detached and moved into the cocoa butter medium. According to their amphiphilic nature, they start directly to form micellar structures with the hydrophilic head groups in the center. This shows again that formation of secondary layers seems not to be favorable compared to the formation of micellar structures, although this has been hypothesized in chocolate literature [12, 68].

Similar observations as for the shown example of DLPC have been made for the DLPI and DLPE systems of the same concentration. Either the detachment leads to single phospholipids diffusing in the vicinity of the monolayer until they form micellar structures with other detached phospholipids or detachment in already formed micellar structures is observed. This is shown in Figure 5.10. Higher concentrations of phospholipids in the monolayer, lead to a detachment of more phospholipids from the sucrose surface. This results in different micellar structures that will be described in more detail in Section 5.3.5. Rodlike micellar structures occur, which is shown in Figure 5.11.

5.3.4 Diffusion coefficients of phospholipids

Diffusion coefficients that are calculated from coarse-grained simulations only give qualitative values. By representing several atoms in one coarse-grained bead and the resulting loss of degrees of freedom, the potential energy surface is more smooth, leading to reduced friction and thus to an increased mobility. Nevertheless, the diffusion coefficients obtained here give qualitative information about the kinetic behavior of phospholipids in the investigated systems. Table 5.4 shows that all saturated phospholipids have lower diffusion coefficients than their unsaturated counterparts in systems 5.2a-f. As already shown in Figure 5.8, the saturated phospholipids adsorb in higher numbers on the sucrose particle, resulting in a more dense packing of the phospholipid layer on the sucrose particle, which is proposed as the reason for the lower mobility. Additionally, systems 5.3a and 5.1c were used to calculate the differences in mobility of phospholipids that are assembled in micelles and in monolayers at the interface of a sucrose particle and cocoa butter. The diffusion coefficient of the phospholipids in the monolayer (system 5.3a) is $0.0017 \times 10^{-9}\,\mathrm{m^2\,s^{-1}}$. Compared to the diffusion coefficients of the

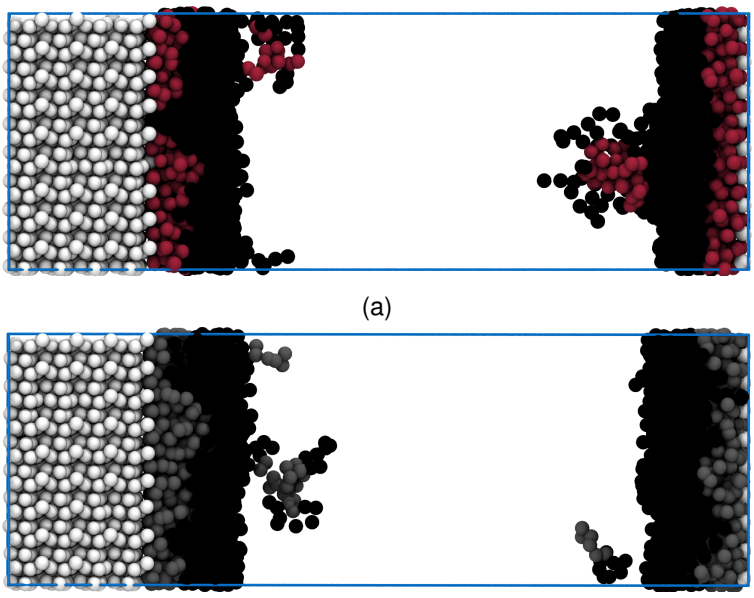

(a)

(b)

Figure 5.10: Detachment of phospholipids from phospholipid monolayers at the sucrose surface–cocoa butter interface is shown for single snapshots during the prodution run of DLPE (5.10a) and DLPI (5.10b). Cocoa butter is omitted for sake of clarity.

Table 5.4: Diffusion coefficients of phospholipids in systems 5.2a-f.

Phospholipid	Diffusion coefficient [$m^2 s^{-1}$]
DLPC	0.0215×10^{-9}
DSPC	0.0193×10^{-9}
DLPE	0.0149×10^{-9}
DSPE	0.0117×10^{-9}
DLPI	0.0081×10^{-9}
DSPI	0.0072×10^{-9}

phospholipids in cocoa butter (system 5.1c), which is $0.0101 \times 10^{-9}\,m^2 s^{-1}$, it can be seen that the phospholipids are immobilized at the particle surface.

5.3.5 Phospholipid structures surrounding sucrose particles

Phospholipids adsorb at hydrophilic–hydrophobic interfaces in food systems. As already mentioned, Middendorf et al. [92] showed that there is a very uneven lipid layer surrounding sucrose particles in chocolate. The layer thickness ranges from no coverage at all up to 34 nm. This layer consists of phospholipids and triglycerides, but the exact molecular structures and the distribution of phospholipids within the layer are unknown. To investigate these structures, systems 5.2a-f are analyzed as a first step. Differences in structures between different phospholipids can be investigated because these

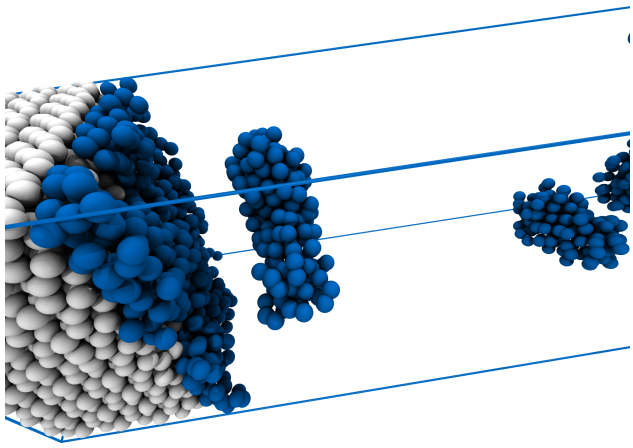

Figure 5.11: Formation of rodlike structures from detached DLPC molecules in cocoa butter. Cocoa butter and aliphatic chains are omitted for sake of clarity.

systems only contain phospholipids of one kind. Additionally, systems 5.2a-f allow to investigate the self-assembling structures of pure phospholipids surrounding sucrose particles, which is considered as a limiting case as it makes the assumption that the nearest neighbors of sucrose particles in chocolate are only phospholipids and no triglycerides. The resulting structure is exemplarily shown in Figure 5.12 for DLPC. For sake of better visualization, the polar head group beads are represented as spheres, while all other phospholipid beads are represented as dots and the sucrose particle is represented by its surface. It is shown that the sucrose particle is mainly covered by phospholipid head groups, as already shown in Section 5.3.2, which is claimed to be the main molecular phenomenon behind the viscosity and yield stress reducing effects of phospholipids in chocolate. Furthermore, Figure 5.12 shows the formation of wormlike phospholipid micelles. They form a wormlike hydrophilic network that surrounds the phospholipid covered sucrose particle. The formation of wormlike structures of phospholipids has been reported in the literature in several systems [43]. A cross section of a periodical representation of the simulation box of DLPC shows that the phospholipids assemble in a reverse hexagonal structure as shown in Figure 5.13. The hexagonal structures can also be found in the periodic interface system 5.5g. Analogous to the system 5.2a-f, at the direct interface a phospholipid monolayer is formed and beyond that layer a typical lyotropic liquid crystalline structure emerges. This is shown in Figure 5.14. DSPI assembles in a lamellar structure, which is a further known structure for self-assembled phospholipids. These so-called lyotropic liquid crystalline mesophases have been reported in various pure lipid systems, indicating that the first monolayer at the sucrose surface does not lead to a long-range order in the surrounding phospholipid phase. The accuracy of the calculated phases is not discussed in detail here as experimental measurements for completely pure phospholipids might not be possible and thus could not be found in literature. One of the most investigated lecithin system is Epikuron 200, which consists of phosphatidylcholine with a purity of 95% [6]. The tail groups are a mixture of different chain lengths and degrees of saturation and thus it is not directly comparable to the system of this study. Angelico et al. [6] found a lamellar phase for pure Epikuron 200. Again,

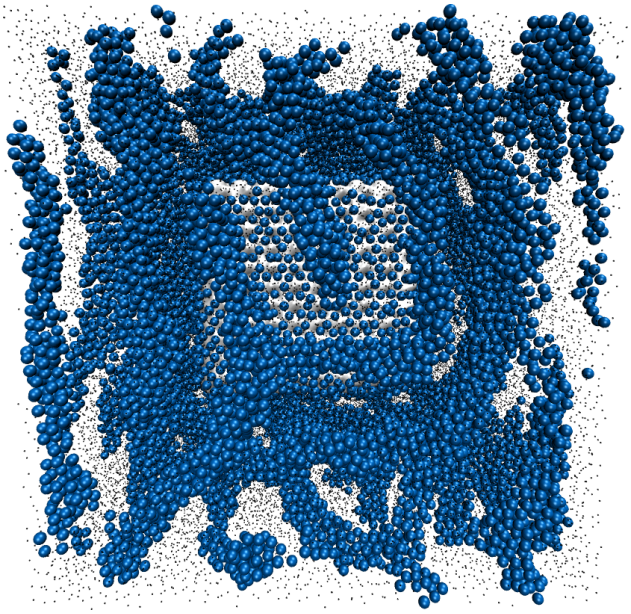

Figure 5.12: Sucrose is in the center of the box and visualized with a surface representation. Hydrophilic head groups of DLPC are shown as spheres, aliphatic chains are shown as dots.

the important result from the simulation with respect to chocolate is that after a first monolayer, the phospholipids seem to be more prone to structuring effects of pure phospholipid systems, than to structuring due to the presence of the sucrose particles.

By inspection of the first phospholipid layer on the sucrose particle it can be observed that the head groups can build hydrophilic bridges between sucrose particles and hydrophilic head groups of the surrounding phospholipids. These bridges arise only on edges and corners of the sucrose particle and are observed for PI head groups mostly. DSPC and DSPE each form one hydrophilic bridge, while DLPC and DLPE form none. This is shown in Figure 5.15, where DLPC does not form bridges to the head groups of the surrounding phospholipids but DLPI does. The strong tendency of PI to form hydrophilic bridges can be explained by the larger head groups that occupy more space than the other investigated head groups (compare Figure 2.4) and thus can not be completely shielded by their aliphatic chains. Because of that they come into contact with surrounding hydrophilic head groups that are not part of the monolayer. The tendency of PC and PE systems to form hydrophilic bridges only with saturated chains can be explained by the fact that the saturated chains occupy less space and thus cannot completely shield the hydrophilic head groups of the monolayer from the surrounding head groups at edges and corners of the sucrose particle.

As already mentioned, in systems 5.3a-c the sucrose particle is at first simulated in a soybean lecithin phospholipid mixture to make sure that it is covered with phospholipids. This is achieved after several hours of chocolate conching in the manufacturing process. The resulting monolayer in the simulation contains 1124 phospholipids, where the proportions of the eight different phospholipids are comparable

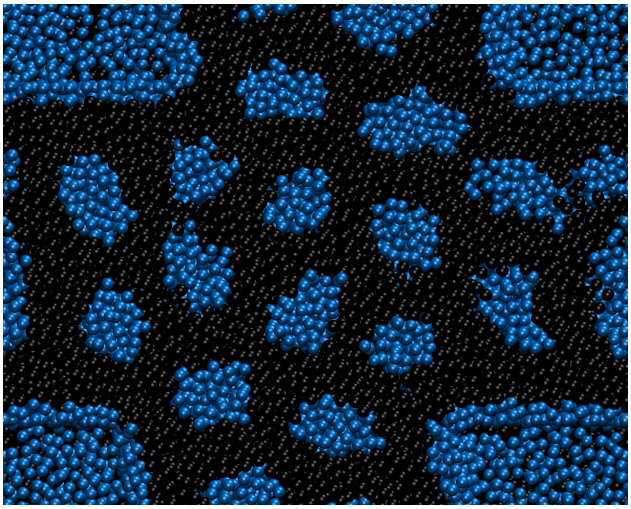

Figure 5.13: Cross section of the periodic representation of the simulation box of system 5.2a (DLPC) reveals the formation of a reverse hexagonal structure.

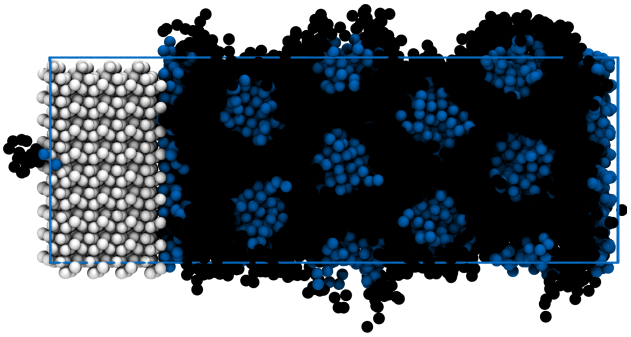

Figure 5.14: The periodic interface system 5.5g of DLPC at the sucrose interface also reveals the formation of a reverse hexagonal structure.

to the initially added composition. The numbers of adsorbed molecules are given in brackets: DLPC (323), DLPE (257), DLPI (145), DLPA (120), DSPC (112), DSPE (75), DSPI (57), and DSPA (35). This shows that all phospholipid components of soybean lecithin adsorb in a homogeneously mixed layer at the sucrose particle surface without preferential adsorption of specific phospholipid fractions. The phospholipids are evenly distributed in the monolayer and no phase separation of unsaturated and saturated phospholipids or phase separation of phospholipids with different head groups can be observed. This is shown in Figure 5.16. After transferring the sucrose particle with the phospholipid monolayer into cocoa butter (resulting in system 5.3a) and a cocoa butter–phospholipids mixture (resulting in system 5.3b–c), the number of phospholipids in the monolayer is constant or increases over the simulation time. This shows that phospholipids are at a very stable position at the interface between cocoa butter and sucrose particles.

System 5.3b shows that phospholipids that are not part of the monolayer at the sucrose particle form spherical micelles at low concentration in cocoa butter triglycerides. This is shown in Figure 5.17.

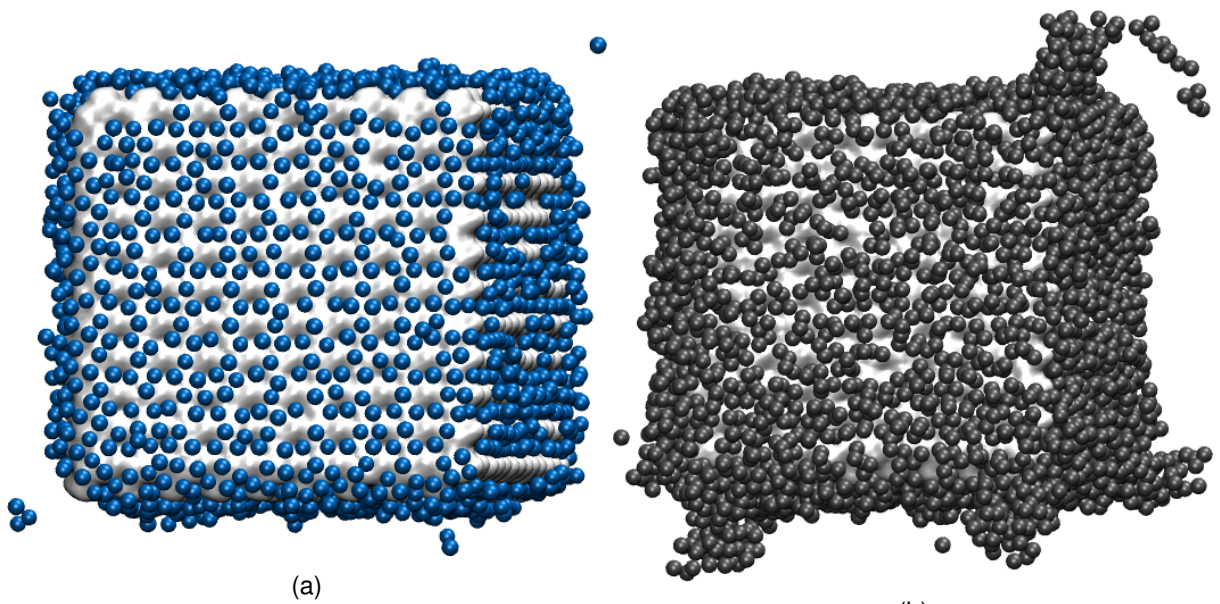

(a) (b)

Figure 5.15: Sucrose particle (surface representation) with hydrophilic phospholipid head groups (spheres) in direct vicinity. DLPC (Figure 5.15a) without bridges and DLPI (Figure 5.15b) with multiple bridges to the surrounding hydrophilic parts.

There is no direct contact between the hydrophilic parts of the monolayer at the particle surface and the surrounding head groups of the micelles. Actual second layers, attaching to the first monolayer, which have been discussed in the literature [2], are not observed in this study. This is also supported by energetic reasoning. It should not be energetically favorable for phospholipids to form a second layer in the specific systems. There is no driving force for the aliphatic chains of phospholipids to assemble specifically on the aliphatic chains of the phospholipids of the monolayer surrounding the sucrose particle as the interaction potentials are the same as with the aliphatic chains of the cocoa butter triglycerides. Additionally, a second layer would also mean that the hydrophilic head groups of this second layer would be exposed to the surrounding hydrophobic phase. System 5.3c, where the phospholipid concentration is higher than in 3b, shows phospholipid structures in cocoa butter similar to those observed in system 5.1c. Less spherical and more wormlike micelles can be found. This is shown in Figure 5.18, where a cross section through the center of the simulation box is shown.

In system 5.4, a sucrose particle surrounded by cocoa butter triglycerides and a soybean-like phospholipid mixture is investigated. System 5.4 represents the phospholipid concentration as it is present in the resulting lipid layer of $34\,\mathrm{nm}$ thickness surrounding sucrose particles after conching in experiment [92]. In system 5.4, only 17 phospholipids were observed to adsorb on the sucrose particle. All other phospholipids are assembled in spherical micelles at the end of the production run. Nevertheless, all phospholipids that adsorbed on the sucrose particle did not desorb during the complete production run. Thus, longer simulations should lead to a higher number of adsorbed phospholipids. Compared with the chocolate conching process during manufacturing, where hours of steering are necessary until phos-

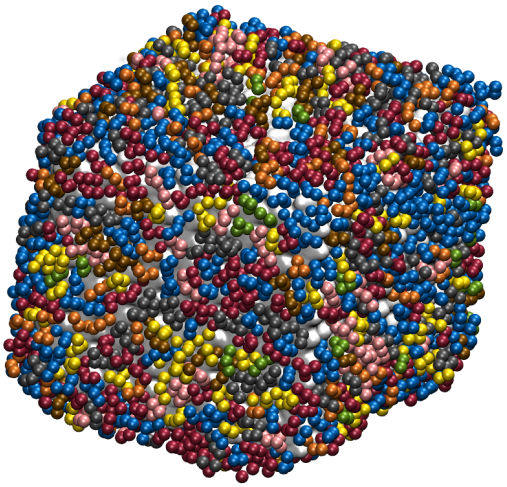

Figure 5.16: Snapshot of system 5.3a. Distribution of different phospholipid head groups in the monolayer at the sucrose–cocoa butter interface. Sucrose is shown in a surface representation. Phospholipid head groups are shown as spheres.

pholipids adsorption is in equilibrium, it seem obvious that after microseconds of molecular dynamics simulation the phospholipids do not cover the sucrose surface sufficiently. In addition, this simulation supports the findings of Middendorf et al. [92] where not all parts of the sucrose particles are covered with phospholipid layers. Phospholipids assemble in stable micelles in cocoa butter and have to come into close contact with the sucrose particle to cover the interface.

5.3.6 Impact of structures on chocolate rheology

A major drawback in using lecithins in chocolate manufacturing as emulsifiers is the fact that an excessive dose results in an increased yield stress of the liquid chocolate after it decreased at a lower concentration. The viscosity of the chocolate mass instead stays low despite further addition of lecithin. Quantitative values of these effects are given in studies from the literature [12, 118]. So far, formation of phospholipid double layers or some kind of unspecified micelle formation have been hypothesized to explain the stated rheological behavior. The molecular structures presented here, such as the wormlike micelles shown in system 5.1c, the lamellar and the reverse hexagonal structures obtained for systems 5.2a-f, and the possibility of forming hydrophilic bridges between sucrose particles, can lead to three-dimensional hydrophilic networks in chocolate, given that the phospholipid concentration is locally high enough. This network has to be broken in order to induce flow of the chocolate mass and thus can result in an increased yield stress. As it was shown that hydrophilic bridges are only present at corners and edges of the sucrose particle, it might also be possible that the sucrose particle shape can have an

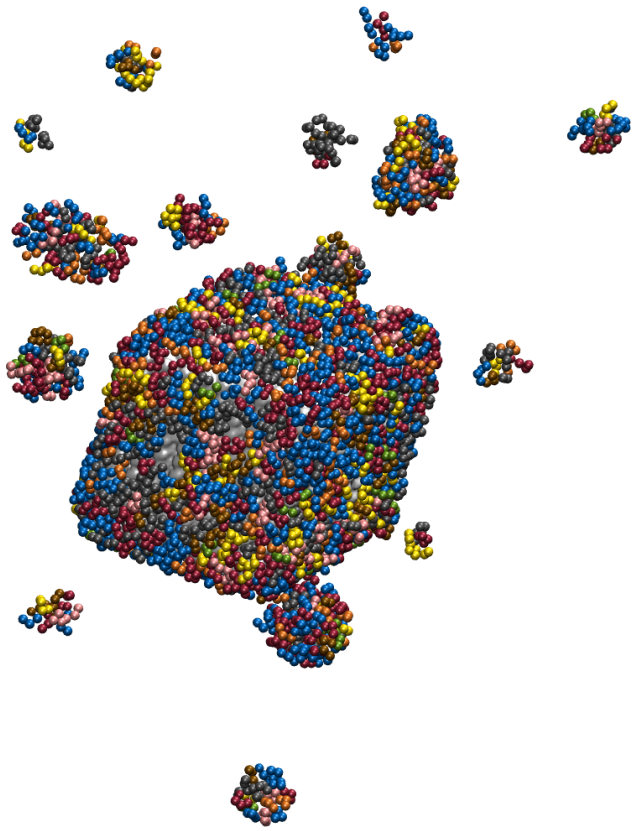

Figure 5.17: Snapshot of system 5.3b. Sucrose particle with a monolayer of phospholipids and surrounding phospholipid micelles. Only the sucrose particle (surface representation) and the phospholipid head groups are shown (spheres).

impact on the rheological properties of chocolate. Further, as PI was shown to form more hydrophilic bridges than other phospholipids, a reduction of PI might help to minimize the increase in yield stress with increasing phospholipid concentration. This result is strongly supported by findings from the literature, where it was shown that PI-enriched lecithins have the strongest yield stress increasing effect at higher concentrations in chocolate [135]. It is further supported by the findings of Arnold et al. [9]. They found the yield stress increasing effect with concentration for soybean lecithin but not for DPPC, DPPE, and DPPA. The only major head group that was not investigated individually in this study was PI. Arnold et al. [9] also state that the different behavior between the soybean been phospholipid mixture and the investigated fractions might be due to that missing component.

The given structural insights and derived effects on rheological properties of chocolate give impulses for experimental studies and can help to improve the control of chocolate rheology during manufacturing. To a certain extent, the described phenomena can be tested experimentally. Rheological measurements of model chocolates such as sucrose particles in cocoa butter with addition of single phospholipid fractions would be recommended as a first direct experimental approach to test the described phenomena. Other experimental measurements that could give insights on the molecular structures within the

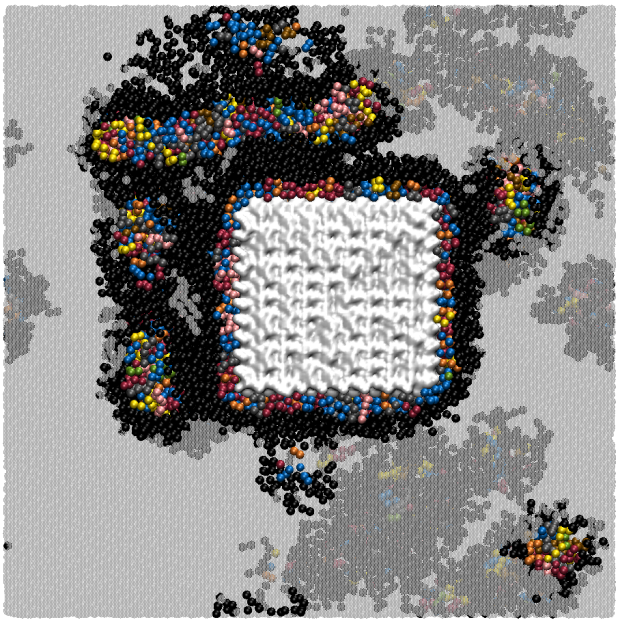

Figure 5.18: Snapshot of system 5.3c. Sucrose particle (surface representation) with a monolayer of phospholipids (spheres) and surrounding phospholipids micelles. Cocoa butter is shown in transparent gray.

suggested model chocolate such as atomic force microscopy, small-angle X-ray diffraction, and nuclear magnetic resonance techniques might be helpful to check the suggested mechanistic explanations of rheological behavior.

5.4 Conclusion

The presented study gave detailed insights into molecular structures of phospholipids in chocolate. Before this study, there was no substantial understanding of the molecular mechanisms induced by overdosage of lecithin and their potential effect on rheological properties of chocolate. The micellar structures of a soybean lecithin-like phospholipid mixture in cocoa butter were calculated and it could be shown that micellar structures with a long-range order are a possible scenario.

Adsorption simulations showed that the soybean lecithin phospholipids with saturated aliphatic chains tend to adsorb at sucrose particle surfaces in a higher number and thus have a lower area per lipid than their unsaturated counterparts. This could be shown for DLPC, DLPE, DLPI, DSPC, DSPE, and DSPI. The same trend could be shown for the phospholipids at the specific sucrose–cocoa butter interface in detachment simulations, where assembled phospholipid monolayers were attached to a sucrose–cocoa butter interface. Phospholipids detached depending on the stability of the monolayer at the given

concentration. It could be shown that saturated phospholipids desorb at a higher interface concentration than the unsaturated phospholipids and thus the saturated ones occupy a lower area per lipid.

Diffusion coefficients of pure phospholipids surrounding sucrose were shown to have a lower diffusion coefficient than in cocoa butter. The saturated ones have a lower diffusion coefficient, according to their lower area per lipid.

Several structural features that give possible explanations for known rheological phenomena in chocolate could be shown. In the limiting case, which assumes that pure phospholipids are in the vicinity of sucrose in chocolate, it could be shown that only a monolayer of phospholipids is attached to the sucrose surface. All further phospholipids tend to form structures that are not influenced by the sucrose but are known lyotropic liquid crystalline phases, which are typical for phospholipids. The highly structured systems have a long-range order and can build structures in the system that could influence the rheology. Especially observed hydrophilic bridges between sucrose particles and the hydrophilic parts of the phospholipids are proposed to explain increasing yield stress at high lecithin concentrations. Hydrophilic bridges were observed at corners and edges of the crystals indicating that the crystal shape could also influence rheological behavior in combination with excessive lecithin dosage.

Chapter 6

Cocoa butter structures and immobilization on sucrose crystal surfaces

One of the discussed effects of lecithin in chocolate is its ability to adsorb on particle surfaces and thus make surface immobilized cocoa butter available as continuous matrix. Centrifuge experiments of sucrose particles in liquid cocoa butter show that the cocoa butter can only be separated from the sucrose particles to a certain degree and that up to $0.33\,\mathrm{g\,m^{-2}}$ cocoa butter per sucrose surface are immobilized [92]. That amount contains cocoa butter immobilized at surfaces and in aggregate voids. In the presented study, surface immobilization of cocoa butter is investigated, by analyzing molecular interactions between a perfect crystalline sucrose surface and the surrounding cocoa butter matrix. Entrapment of immobilized fat in aggregate voids cannot be examined with this setup. However, the assumption that phospholipids enhance flow behavior of chocolate by attaching to the hydrophilic surfaces and allowing the immobilized cocoa butter to detach and be available as bulk matrix where the particles flow in can be examined with the presented setup. Phospholipids are not part of the investigated system. By calculating cocoa butter immobilization at sucrose surfaces without phospholipids at the interface, the extent of the negative effect on flow behavior through the immobilization can be estimated. New insights to the question if cocoa butter immobilization is a physico-chemical phenomenon based on its electrostatic and van der Waals interactions with crystalline sucrose or if other phenomena are responsible for cocoa butter immobilization can be given. Detailed insights, as presented in this study, are hardly accessible by experimental procedures and thus this study is a further example of the usage of molecular simulations in food process engineering.

Cocoa butter immobilization is investigated on an infinite interface of a sucrose crystal and liquid cocoa butter by performing all-atom molecular dynamics simulations. Due to the periodic boundary conditions, the systems include the (010) and $(0\bar{1}0)$ crystal surfaces of sucrose. Due to the refining process during

chocolate production a wide variety of different sucrose crystal surfaces and even amorphous surfaces is expected to be present. The selected surfaces are chosen as examples. Diffusion coefficients of liquid triglycerides are calculated for pure cocoa butter and at the crystalline sucrose interface. Further the behavior of single triglycerides directly at the interface to sucrose and in bulk is tracked in detail. Additionally, radial distribution functions of cocoa butter triglycerides are calculated, in order to get a detailed understanding of molecular structures in liquid cocoa butter.

6.1 Methods

6.1.1 Molecular model of chocolate

For this study both GAFF, which was used for the study in Chapter 4, and the Martini FF, which was used for the study in Chapter 5, are employed. Arguments on the validity of the models have been presented in the last two chapters and are thus omitted here. The molecular representation of the chocolate is similar to the studies before. Sucrose is modeled in its crystalline state and cocoa butter is represented by its three main molecular components POS, SOS, and POP. The only major difference is that in this study phospholipids do not have to be considered, in order to investigate cocoa butter immobilization at the sucrose surface.

6.1.2 System building

The molecular systems that are investigated in this study, are either pure liquid cocoa butter bulk phases or, similar to the study in Chapter 4, infinite interfaces between sucrose and cocoa butter. Those systems are used to investigate cocoa butter immobilization as well as structuring effects in liquid triglycerides. In the pure cocoa butter system 204 POS molecules, 120 SOS molecules, and 94 POP molecules are inserted randomly for the investigation of pure triglyceride bulk properties. The pure cocoa butter systems are built in an all-atom version and a coarse-grained version, in order to get additional validation on the suitability of the coarse-grained Martini FF for calculation of triglycerides structures. For cocoa butter immobilization, only the all-atom GAFF simulations are used because dynamic properties are of interest and the time scale of the Martini FF has no direct physical meaning. The all-atom version of the pure triglyceride system is labeled system 6.1a and the coarse-grained version is labeled system 6.1b in this chapter.

In order to build the sucrose crystal of the interface systems, the sucrose crystal unit cell is replicated in all spacial direction, 8 times in x-direction, 5 times in y-direction, and 10 times in z-direction. This results in a sucrose crystal with an edge length of $8.7\,\mathrm{nm}$ in x-direction and $7.6\,\mathrm{nm}$ in z-direction, which represents the size of the investigated interface. The biggest molecules of the investigated systems

are the triglycerides, which have a length of about 4 nm when they are stretched to the maximum. The short-range cut-off is $0.9\,\mathrm{nm}$. The sum of the longest stretching and two times the cut-off is smaller than the smallest box edge and thus the minimum image convention is fulfilled. Further, with this setup, the box is as small as possible to keep calculation times feasible. The sucrose crystal has an edge length of $4.4\,\mathrm{nm}$ in y-direction, which is long enough to ensure that the molecules at the interface have only short range interactions with sucrose molecules and do not interact with the triglycerides on the other side of the sucrose crystal, which are there due to the periodic boundary conditions. After building the crystalline structure, the box is elongated in y-direction and triglycerides are inserted in cocoa butter-like composition. Two cocoa butter layers with different thicknesses at the sucrose surface are investigated, in order get an idea of how far the immobilization effect reaches into the cocoa butter phases. For the thinner layer, 102 POS molecules, 60 SOS molecules, and 47 POP molecules are randomly inserted into the box. The resulting system is labeled system 6.2a within this chapter. For the thicker layer, 204 POS molecules, 120 SOS molecules, and 94 POP molecules are inserted into the box. The resulting system is labeled system 6.2b within this chapter. An overview of the investigated systems of this study is given in Table 6.1.

Table 6.1: Overview of the different simulation systems in this study. The table shows whether a central sucrose crystal is present or if a pure triglyceride system is investigated. The number of triglycerides in the systems 6.2a and 6.2b gives information about the layer thickness.

System	Sucrose crystal	Number of triglycerides	Resolution
6.1a	no	418	all-atom
6.1b	no	418	coarse-grained
6.2a	yes	209	all-atom
6.2b	yes	418	all-atom

6.1.3 Equilibration and production run details

All simulations of this study and their analysis are performed with the Gromacs software Version 5.1.1 [133]. GAFF [143] is used for the all-atom simulations of this study. A $2\,\mathrm{fs}$ time step is used for integrating the equations of motion with help of the leap-frog algorithm [57]. Van der Waals interactions and short-range electrostatic interaction are calculated with a cut-off at $0.9\,\mathrm{nm}$. Long-range electrostatic interactions are calculated with the Particle–Mesh–Ewald Method [33]. Temperature is regulated with the Berendsen thermostat in the equilibration runs and with the velocity rescale thermostat during the production runs. Pressure was regulated with the Berendsen barostat during equilibration and the Parrinello–Rahman barostat during production runs. The following simulation procedure is performed for the different all-atom systems. Energy minimization is performed, using the steepest decent algorithm until the potential energy levels out. Afterwards two equilibration steps are performed. At first, equilibration in the canonical ensemble is performed to get the system to the desired temperature of $80\,^{\circ}\mathrm{C}$ and to allow the randomly inserted triglycerides to form clusters. Secondly, equilibration in the

isothermal-isobaric ensemble is performed until the atmospheric pressure and constant system density are reached. Subsequently the productions runs are performed in the isothermal-isobaric ensemble for 500 ns. The sucrose crystal, if present, is kept in its crystalline state by applying position restraints to the sucrose molecules during all simulations.

The Martini FF is used for the coarse-grained simulations of this study. Equations of motion are integrated with the leap-frog algorithm with a time step of 10 fs. All non-bonded interactions are truncated with a cut-off of 1.1 nm. The reaction field method is used to calculate long-range electrostatics. Energy minimization is performed, using the steepest decent algorithm until the potential energy levels out. At first, equilibration in the canonical ensemble is performed to get the system to the desired temperature of 80 °C and to allow the randomly inserted triglycerides to form clusters. Second, equilibration in the isothermal-isobaric ensemble is performed until the atmospheric pressure and constant system density are reached. For equilibration the Berendsen thermostat and barostat are used for controlling temperature and pressure. The final production runs are performed in the isothermal-isobaric ensemble for 2 µs. The velocity-rescale thermostat is used for controlling temperature, the Parrinello–Rahman barostat is used for controlling pressure in the production runs.

6.1.4 Analysis of the simulations

Diffusion coefficients of the cocoa butter triglycerides are calculated with help of the Einstein relation similar to Chapter 5.2.4. As diffusion at a periodic interface is investigated, lateral two-dimensional diffusion is investigated, to account for the effect of restricted diffusion in direction of the sucrose crystal. The Einstein relation has to be adjusted accordingly and is given as

$$D = \lim_{t\to\infty} \frac{1}{4t} \langle \Delta \boldsymbol{r}(t)^2 \rangle \tag{6.1}$$

in the two dimensional case.

The normalized radial distribution functions are calculated as

$$g(r) = \frac{dN}{dr} \frac{1}{4\pi\rho_0 r^2}, \tag{6.2}$$

with the number of particles N, the average particle number density ρ_0, and the radial distance r. Radial distribution functions are calculated for different molecular beads and centers of mass. More details are given directly in the results section below.

6.2 Results and discussion

6.2.1 Structures in liquid cocoa butter

Before the interactions of triglycerides with sucrose are investigated, a further investigation of pure triglycerides is performed. If the triglyceride behavior at the interface differs from that in bulk, it is a result of the interaction with sucrose as the presence of sucrose is the only difference between the two setups. Although triglycerides form a macroscopically very homogeneous phase, some structuring effects have already been investigated. It is shown by molecular dynamics simulations that during the crystallization process, the glycerol backbones start to attach to each other and build more and more layered structures [108]. Aggregation of glycerol backbones is also shown for liquid triglycerides in molecular dynamics simulations [129]. These structuring effects are caused by the molecular structure of triglycerides. As already described in Section 2.1.1, triglycerides consist of fatty acids, which are bonded to a glycerol backbone via ester bonds. The glycerol backbone, and especially the ester bonds are more polar than the aliphatic chains, leading to polar interactions, which induces microscopical structuring effects, as shown in the mentioned studies. In Figure 6.1, the radial distribution functions of the central glycerol beads of the different triglycerides are given for system 6.1a (Figure 6.1a) and 6.1b (Figure6.1b). The plots clearly show that interaction of glycerol backbones is favorable in cocoa butter. It shows a value higher than one for the first interaction site at a distance of about $0.5\,\mathrm{nm}$. This indicates the above average likelihood for glycerol backbones to have another central glycerol bead as a neighbor atom. The second smaller peak at about $1\,\mathrm{nm}$ distance is also slightly higher than one and indicates the above average likelihood of a neighbor at this distance, giving hints at an aggregation of glycerol backbones. After that, the radial distribution functions level out against one, which is a typical behavior for liquids. Comparable results of structuring of triglycerides are present for both molecular models. The similar structuring results are a further sign of validity of the coarse-grained force field in investigations of liquid triglyceride structures. The only difference is the height of the peaks, which is probably due to the different natures of both models. While for system 6.1a the radial distribution function is calculated for the central carbon atom of the glycerol backbone, for system 6.1b the radial distribution function is calculated for the whole glycerol group as it is a single bead in the coarse-grained representation. Thus, the coarse-grained model is not able to account for structural variability within the glycerol backbone. Nevertheless, it cannot be stated if one or the other force field might underestimate or overestimate the glycerol backbone structuring because no experimental data for comparison could be found.

The radial distribution function for the interface system 6.2a also looks similar compared to the plot for the pure triglyceride systems and is given in Figure 6.2. Overall, the plot is shifted toward higher values as a sucrose crystal is present in this system and thus the number density of the central glycerol backbone carbons gets lower. Nevertheless, qualitatively the same first two peaks can be observed, before the radial distribution function is descending. This indicates that the overall structure of triglycerides in

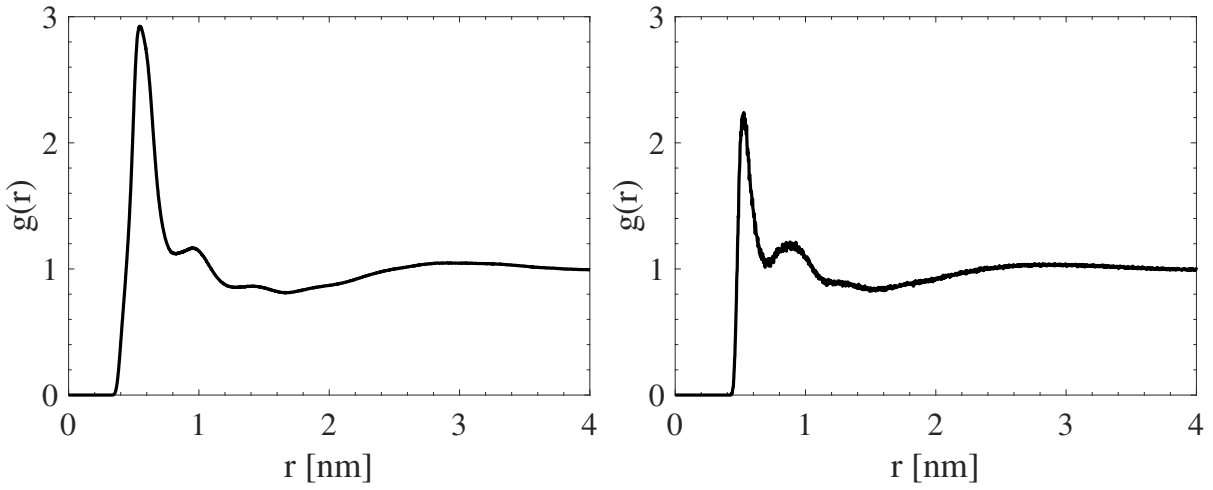

(a) Radial distribution function for the interaction of central carbon atom of the glycerol backbone of the triglycerides POS, SOS, and POP for system 6.1a.

(b) Radial distribution functions for the interaction of the glycerol backbone bead of the triglycerides POS, SOS, and POP for system 6.1b.

Figure 6.1: Comparison of radial distribution functions for the system 6.1a (all-atom) and 6.1b (coarse-grained).

the sucrose vicinity is not changed compared to its bulk properties. Due to ongoing structuring effects in the system, which will be discussed in the following section, changes of the presented radial distribution function are possible.

System 6.2a is shown exemplarily in order to visualize the glycerol backbone structuring in cocoa butter in Figure 6.3. The three dimensional clustering of glycerol backbones is clearly visible. As a consequence of backbone clustering, there are also clearly visible parts in the lipid structure that only consist of aliphatic chains. Thus, the presented structure is favorable in terms of maximizing the polar interaction between the glycerol backbones as well as maximizing van der Waals interactions between the aliphatic chains, leading to a parallel orientation of the aliphatic chains in some parts of the systems 6.1a, 6.2a, and 6.2b during the simulation. Whether or not this effects might be to strong pronounced for the simulation temperature of 80 °C and might represent starting crystallization, cannot be evaluated in the presented work because no experimental data is available for comparison.

6.2.2 Adsorption of cocoa butter at the sucrose interface

In order to get a more comprehensive understanding of the phenomena directly at the triglyceride–sucrose interfaces, the system trajectories were investigated more closely. Following the hypothesis that cocoa butter is immobilized at sucrose interfaces based on non-bonded molecular interactions, it seems natural that certain parts of the triglycerides interact stronger with sucrose than others. The natural assumption in this case is that the polar glycerol backbones are more prone to sucrose inter-

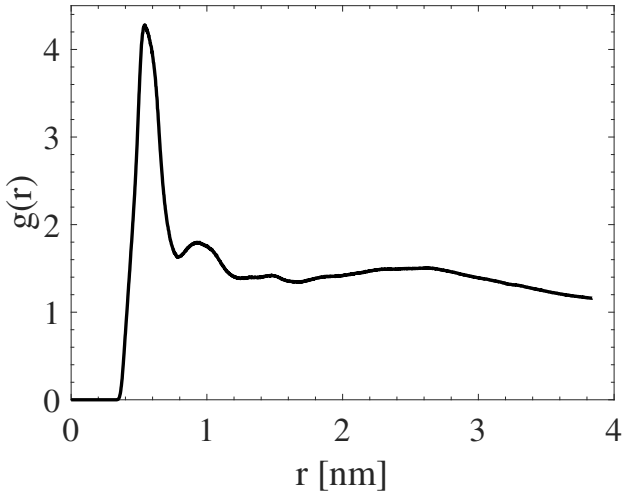

Figure 6.2: Radial distribution function for the central glycerol backbone carbon atom of POS, SOS, and POP in system 6.2a.

actions than the aliphatic chains. The number density of triglyceride backbones along the y-axis of the simulation box is shown to increase on the surfaces over the simulation time of 500 ns. This indicates that adsorption of backbones at the interface takes place during the simulation time. This is shown by number density plot of ester groups along the y-axis of system 6.2b in Figure 6.4. An increase in the number density of ester groups directly at the sucrose interface (at about 4 to 5 nm and at about 14 to 15 nm) can be noted. Further the maxima and minima get more pronounced over the simulation time, which has to be interpreted as ongoing structuring effects. Due to the high viscous nature of the system and the resulting slow dynamics the systems might not be in equilibrium after 500 ns simulation time. The orientation of triglyceride backbones towards the sucrose surface seems to be in progress. To get further understanding of the immobilization at the interface, diffusion coefficients are calculated and trajectories of single triglycerides at the interface are analyzed and are presented in the following section.

6.2.3 Immobilization of cocoa butter on sucrose crystal surfaces

Diffusion coefficients of pure cocoa butter and cocoa butter at a sucrose interface are compared. In order to account for the effect that the motion of cocoa butter molecules in y-direction is prohibited in the systems 6.2a and 6.2b directly at the sucrose interface, two dimensional diffusion coefficients, so-called lateral diffusion coefficients, are calculated. Thus, molecular motion perpendicular to the sucrose crystal surface has not been taken into account in these values. Diffusion coefficients are calculated for the simulation time between 100 and 400 ns. The lateral self diffusion coefficient for system 6.1a is $0.0016 \times 10^{-9}\,\mathrm{m^2\,s^{-1}}$, for system 6.2a is $0.0005 \times 10^{-9}\,\mathrm{m^2\,s^{-1}}$, and for system 6.2b is $0.0011 \times 10^{-9}\,\mathrm{m^2\,s^{-1}}$. By comparing system 6.1a with system 6.2a the biggest difference can be seen.

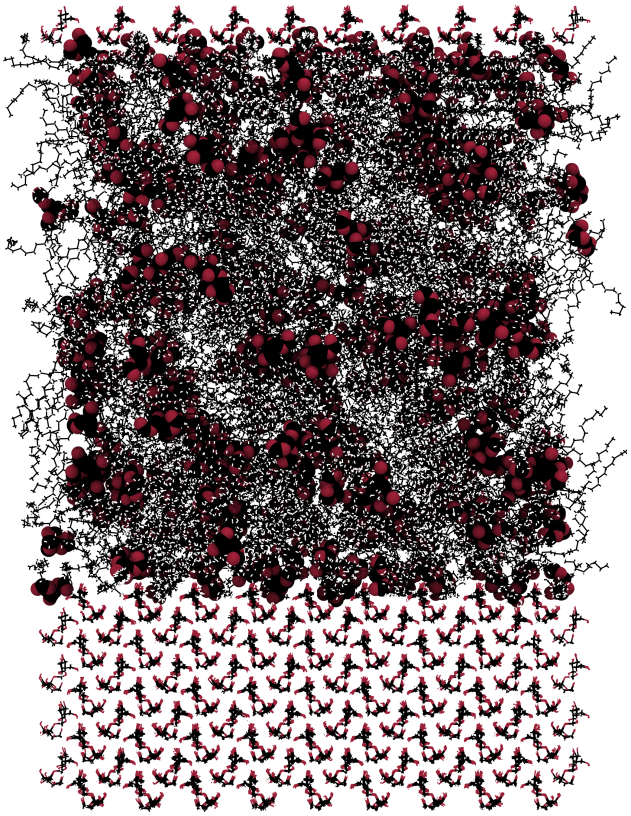

Figure 6.3: Glycerol backbones are shown as red and black spheres, all other atoms are shown in a line representations. Carbons are shown in black, oxygens are shown in red, and hydrogens are shown in white. The presented color-code is used throughout this chapter.

This indicates that the fat in the relatively small slab between sucrose crystals is slower in its lateral motion compared to pure bulk triglycerides. System 6.2b has a diffusion coefficient in between the values of systems 6.1a and 6.2a, indicating that the triglyceride slab in this case is big enough to be already more governed by triglyceride bulk behavior.

For a comparison of the absolute values of the diffusion coefficients two experimental studies were found. Callaghan and Jolley [21] measured the diffusion coefficient of triolein at 70 °C, which was found to be $0.049 \times 10^{-9}\,\mathrm{m^2\,s^{-1}}$. Ladd-Parada et al. [75] measured the diffusion coefficient of cocoa butter at 70 °C, which was found to be $0.038 \times 10^{-9}\,\mathrm{m^2\,s^{-1}}$. The experimental values are about one order of magnitude higher than the calculated values, indicating that the mobility of triglycerides is underestimated by the used force field. With this underestimation of diffusion coefficients, it seems likely that the structuring effects that are presented in Section 6.2.1 might be overestimated where GAFF is employed. Several aspects that have to be considered in the interpretation of the deviation between simulation and experiment are discussed in the following. As a first aspect, it has to be considered that experimental measurements of diffusion coefficients have strong deviations itself. It is shown in literature that values of diffusion coefficients of phospholipid membranes can differ widely, depending on the measurement

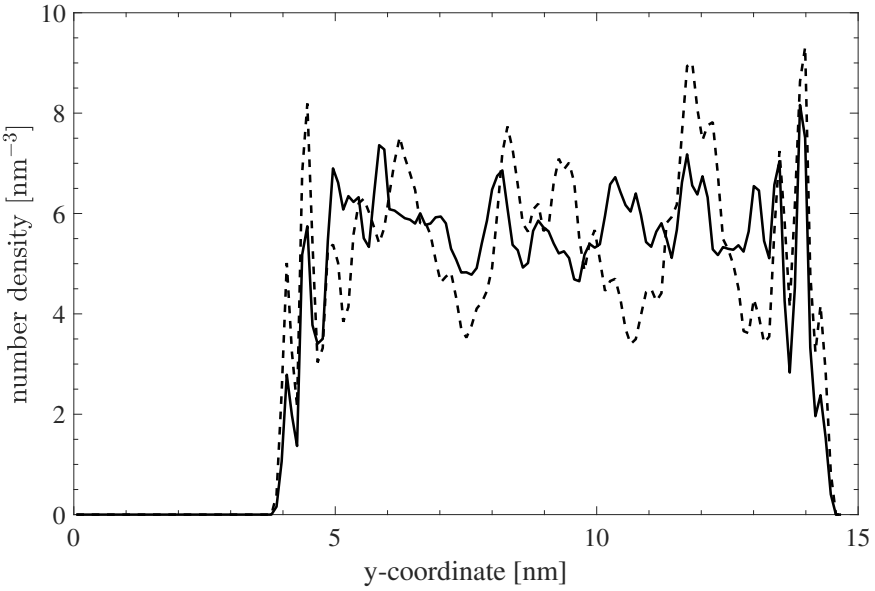

Figure 6.4: The number density of the polar ester groups along the y-axis of the simulation box is shown. The solid line represents the number density during the first 10 ns of the simulation, the dashed line represents the number density between 490 and 500 ns.

technique and even within the same measurement techniques. Deviations of up to one order of magnitude are reported [109, 110]. Due to lack of experimental data, it cannot be stated that measurements of diffusion coefficients for vegetable fats, such as cocoa butter, are similarly prone to error but still should be considered. A second aspect is that despite diffusion coefficients of pure solvents, such as benzene, cyclohexane, and ethanol, that were calculated with GAFF were also underestimated in the range of one order of magnitude, it was shown that relative comparisons are still valid for some properties [140]. The temperature dependence of calculated diffusion coefficients was shown to give good correlations. Underestimation of diffusion coefficients in the range of one order of magnitude with molecular dynamics simulations has also been shown for ionic liquids, although density was predicted within 2 % deviation [132]. Tsuzuki et al. [132] also showed that relative effects, such as the influence on molecular weight on diffusion coefficients, accurately follows the experimental trend. Although it has been shown that comparison of relative values is valid for some characteristics, despite deviation of absolute values, this cannot be stated for the cocoa butter immobilization because no experimental validation could be given so far. A third aspect that might explain a part of the deviation from the experimental value is that not all parts of cocoa butter are considered in the molecular representation of this study. Especially mono- and diglycerides, which have a lower molecular mass and thus higher diffusion coefficients, are not part of the setup. It remains a non-trivial task to find force fields that are suitable for several characteristics of molecular complex system, such as chocolate. The presented method can be used with improved force fields in the future and can then help to get a quantitative understanding of cocoa butter immobilization.

In order to evaluate the differences of cocoa butter immobilization over the distance to the sucrose surface, trajectories of single triglycerides of system 6.2b were analyzed. On the one hand two triglycerides at the sucrose interface, with their glycerol backbones adsorbed at the crystal were randomly picked, and on the other hand two triglycerides in the fat bulk of systems 6.2b were randomly picked. After showing that the overall lateral diffusion is smaller for the interface systems, this investigation allows to get further insights into the differences within the cocoa butter layer at the interface. Two figures are presented to show the difference in mobility of directly adsorbed and non-adsorbed triglyceride backbones of system 6.2b. Figure 6.5 shows the trajectories for four different tryglyceride backbones. Two of them are adsorbed and two of them are in the bulk of the fat phase of systems 6.2b. All positions

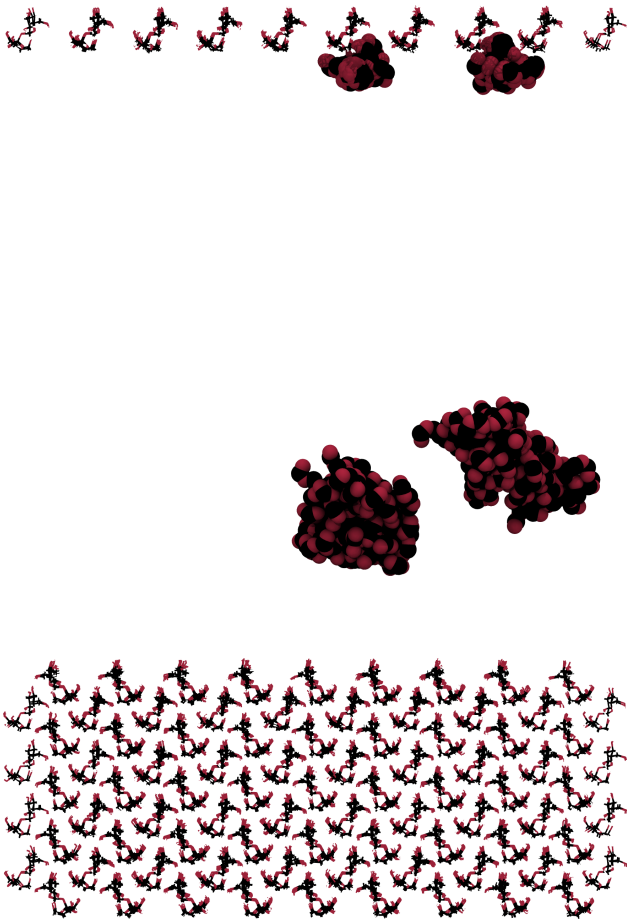

Figure 6.5: Glycerol backbones of exemplarily selected triglycerides are shown as red and black spheres and atoms of sucrose are shown in a line representation, while all other atoms are omitted for sake of clarity. All position of the selected glycerol backbones during the production run are shown in this plot.

of the glycerol backbones for 500 ns are shown here in one plot to give an impression of the molecular trajectories of glycerol backbones in different adsorption states of the system. Additionally, the center of mass motion of the ester groups of the backbones for the two triglycerides on the left of Figure 6.5 are given in Figure 6.6.

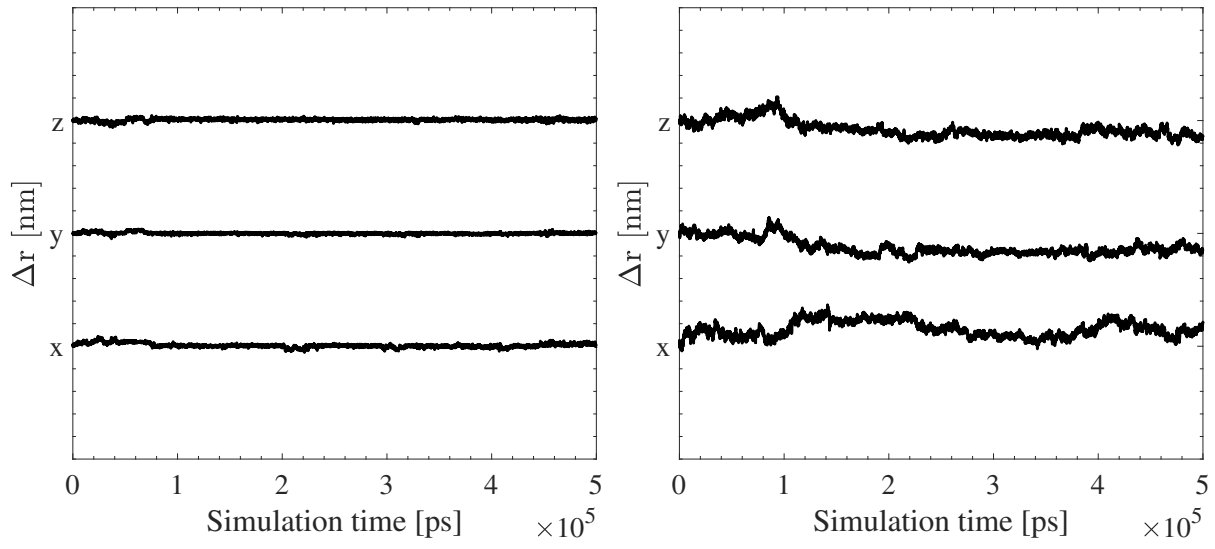

Figure 6.6: Comparison of center of mass motion of ester groups in the glycerol backbone in all spacial directions. On the left, an adsorbed molecule at the sucrose surface is shown, on the right, a non-adsorbed backbone is shown.

It is clearly shown that the mobility of the glycerol backbones at the interface is strongly inhibited. Motion in y-direction would mean that the glycerol backbone would intrude into the sucrose crystal or that desorption would occur. Both phenomena are not observed, as is shown in Figure 6.6a. Motion in z- and x-direction would represent lateral diffusion at the sucrose interface. Motion along the x-axis (from left to right in Figure 6.5) is not observed in the analyzed system 6.2b, as is shown in Figure 6.6a. As the position in the notch seems to be favorable, leaving this position in lateral diffusion is supposed to be accompanied by overcoming an energy barrier as the glycerol backbone would have to leave the notch-like structure of the sucrose surface. Motion along the z-axis (into the drawing plane of Figure 6.5) would mean diffusion along the notch. This motion is also inhibited, as is shown in Figure 6.6a over the course of the 500 ns simulation time and therefore, the molecular interactions between sucrose and the triglycerides seem to be quite strong. The glycerol backbones in the triglyceride bulk phase are significantly more mobile than the adsorbed ones, which is shown in Figure 6.6b, where the x, y, and z value are not constant for the non-adsorbed glycerol backbones. The molecular trajectories of Figure 6.5 show cloud-like structures for the glycerol backbones, indicating typical random walk movement for the non-adsorbed backbones. The bigger the cloud-like structures are, the higher is the mobility.

The presented results indicate that the phenomenon of cocoa butter immobilization in chocolate manufacturing can – to a certain degree – be explained by molecular interactions of sucrose and cocoa butter triglycerides. Triglycerides that are oriented to the sucrose crystal with their glycerol backbone directly at the sucrose interface are shown to be immobilized. Orientation of glycerol backbones towards the sucrose interface seems to be a slow phenomenon, which seems plausible according to the high viscosity of system. This orientation has already been investigated in a system similar to chocolate, as already

mentioned in the literature review. Claesson et al. [29] performed measurements of the forces acting between mica surfaces in a triolein medium with an interferometric surface force apparatus. From the force distance curves they could conclude that triglycerides are oriented with their glycerol backbones towards the hydrophilic mica surfaces, which is the same type of triglyceride orientation that was found here. From the presented increasing number of adsorbed triglyceride molecules during the nanosecond scale molecular dynamics simulations and the experimental measurement by Claesson et al. [29], it can be concluded that in fact immobilized triglycerides are present at perfect sucrose crystal surfaces. Hints at formation of multiple equally strongly immobilized cocoa butter layers are neither given by the molecular dynamics simulations of this study nor by the force distance curves of Claesson et al. [29]. The simulations show that the immobilization decreases rapidly with the distance of the triglycerides from the sucrose surface by comparing the lateral diffusion in pure triglyceride bulk to the lateral diffusion at sucrose surfaces with different triglyceride layer thicknesses. The immobilization of triglycerides at the sucrose surface gives more detailed insight into the big impact of lecithin on chocolate rheology. In the scenario that lecithin would form a monolayer at the surface, the otherwise immobilized triglycerides would be available as liquid matrix after lecithin addition. The presented results of cocoa butter immobilization can be used in rheological models like the fluid immobilization model of Windhab [148]. As a first step it is suggested to consider a monolayer of triglycerides as an additional part of the surface immobilized solid volume fraction Φ_{sif} in equation 2.8.

A few further implications of the results presented in this section are discussed in the following. Given the case that triglycerides would eventually adsorb in a monolayer surrounding sucrose, they would in fact have much the same effect as phospholipids. By adsorbing with the hydorphilic head group (in the case of phospholipids) or with the glycerol backbone (in the case of triglycerides) the sucrose surface would be rendered lipophilic by the hydrophobic tail groups, which are directed towards the fat bulk. Nevertheless, it is well established that phospholipids have a much stronger effect on rheology than triglycerides. This indicates that the phospholipid layer has to be either, more homogeneous, stable, or dense in rendering the particles lipophilic. Further, the cocoa butter immobilization at the surface should be stronger when no phospholipids are present, which is indicated by the flow properties. This means that the phospholipid layer at the sucrose particle, must build some kind of smooth interface, in a way that surrounding triglycerides are less immobilized than when a layer of triglycerides is at the interface. This could be accessed in more detail when the systems 6.2a and 6.2b are simulated with a phospholipid layer in between the phases and lateral diffusion coefficients would be evaluated.

6.3 Conclusion

In the presented study the phenomenon of cocoa butter immobilization in chocolate was investigated by performing molecular dynamics simulations. Additionally, molecular structures in pure cocoa butter triglycerides and at sucrose interfaces were calculated. Structures that were calculated with the Martini

FF were compared to structures that were calculated with GAFF. It was shown that the glycerol backbones of triglycerides tend to form aggregates, which was already observed in molecular dynamics simulations of liquid triglycerides in the literature [129]. Both the Martini FF and GAFF deliver comparable results for the structures in pure cocoa butter triglycerides. Similar aggregates of triglycerides were shown in vicinity to a sucrose particle surface.

Lateral diffusion of triglycerides is smaller at sucrose surfaces than in bulk. The closer the triglycerides are to the sucrose surface, the lower the lateral diffusion seems to get. Triglycerides that are directly adsorbed at the sucrose surface were shown to be strongly immobilized. No random walk motion was observed for adsorbed triglycerides but was observed for triglycerides farther away from the sucrose surface. It has to be noted though that calculated values of the diffusion coefficients for cocoa butter were found to be about one order of magnitude lower than experimental values and more simulations with more suitable force fields are suggested for the future.

It was shown that triglycerides adsorb with their glycerol backbone on the sucrose surface. An increase in adsorbed glycerol backbones at the sucrose interface was observed over 500 ns simulation time, indicating ongoing fat immobilization.

Chapter 7

Conclusion and Outlook

7.1 Conclusion

In the introduction of the presented thesis two main goals were stated. The first goal was to deliver understanding of specific molecular phenomena, interactions, and mechanisms that govern the rheology of chocolate by employing molecular dynamics simulations. The three following specific questions were raised in the introduction and the given answers are summarized in this chapter:

- Do different phospholipids interact more or less strong with sucrose crystals?
- Can concentration-dependent molecular phospholipid structures at the sucrose–cocoa butter interface explain rheological behavior of chocolate?
- Is cocoa butter immobilization at sucrose crystal surfaces based on molecular interactions?

The second goal was to promote the usage of molecular dynamics simulations in investigations of complex food systems in order to gain food process engineering relevant insights, to discuss the method's restrictions and to show possible solutions. This section gives a conclusion of the results of this thesis, by summarizing the answers to the three stated questions and by summarizing the challenges and possibilities of molecular dynamics simulations usage in food process engineering.

7.1.1 Interaction of phospholipid head groups with sucrose crystals

As lecithins are mixtures of different phospholipids and varying compositions of these phospholipids are common due to environmental influences as well as lecithin of different vegetable sources are used in chocolate manufacturing, it is of interest if the different lecithin fractions interact differently with sucrose. To shed light on this question, which is hardly accessible experimentally, non-equilibrium molecular

dynamics simulations were performed. Single phospholipids at the specific sucrose–cocoa butter interface were pulled away from the sucrose surface. Thereby it could be shown that different phospholipid head groups require different detachment work. PI head groups require the strongest detachment work, followed by PC, and finally PE head groups. Detachment was shown to be proportional to the number of hydrogen bonds between head groups and sucrose. The aliphatic chains of the phospholipids have no impact on detachment work. It was shown that different adsorption states of phospholipids at the sucrose interface lead to more or less detachment work and that a specific equilibration procedure has to be performed to obtain comparable starting configurations in the viscous cocoa butter matrix. By analyzing the detachment mechanisms, interactions between the different phospholipid head groups and sucrose were examined on a detailed level and it could be shown that different parts of the head groups interact differently strong with sucrose.

7.1.2 Phospholipid structures surrounding sucrose particles

After evaluating interactions of single phospholipids with sucrose crystals in chocolate, phospholipid structures were investigated in order to explain rheological behavior and gain a more detailed system understanding, which could eventually be used in tailoring of emulsifiers and adaption to changed raw materials. To overcome the problem of slow dynamics in the system chocolate, coarse-grained molecular dynamics were performed. As a first step, it could be shown that soybean lecithin-like phospholipid mixtures tend to build long-range molecular structures such as wormlike micelles in the triglyceride-based solvent cocoa butter. This behavior is stronger pronounced at high lecithin concentrations. As a second step, molecular structures of pure phospholipid systems surrounding a sucrose particle were calculated. The scenario of pure phospholipids surrounding a sucrose crystal can be assumed as a limiting scenario in chocolate as detailed molecular composition in the nanometer vicinity of sucrose is hardly accessible. It was shown that all investigated phospholipids build a monolayer adsorbing at the sucrose surface. The area per lipid was shown to depend mainly on the degree of saturation of the aliphatic chains as unsaturated chains require more space than saturated ones, what is also known for biological membranes. The structures beyond the first monolayer were shown to be more connected to structures of pure phospholipid phases than to be influenced by the presence of the sucrose particle. It was shown that hydrophilic bridges can be formed between sucrose particles and the surrounding hydrophilic parts of the system, which is considered as an explanation for the well known phenomenon of increased yield stress at excessive doses of lecithin. No hints at formation of a second layer could be found, instead phospholipid structures beyond the first layer resemble lyotropic crystalline phases.

7.1.3 Cocoa butter structures and immobilization on sucrose crystal surfaces

Cocoa butter immobilization at sucrose surfaces, which is commonly assumed to be one of the mechanisms that makes liquid chocolate a viscous fluid and is overcome by lecithin addition, was investigated.

Structures of liquid fat were investigated and details of molecular interactions were given in form of radial distribution functions. The tendency of triglycerides to form a aggregates, where the glycerol backbones attach to each other, were confirmed for the specific cocoa butter triglyceride mixture. It was shown that triglycerides adsorb very stable with their glycerol backbones at the sucrose surface and are strongly immobilized. Diffusion coefficients of cocoa butter layers at sucrose crystals were shown to be lower for thin layers and are more closely to the triglyceride bulk diffusion coefficients for thicker layers, which indicates that only triglycerides directly at the sucrose crystals are strongly immobilized. It has to be noted though that the calculated values of the diffusion coefficients for cocoa butter were found to be about one order of magnitude lower than experimental values.

7.1.4 Molecular simulations in food process engineering

As already stated in the literature review, food process engineers have been using mathematical modeling tools for quite a long time on the continuum level, in order to model phenomena such as heat transfer or mass transfer. Mathematical modeling and simulations of processes on the micro- or nanoscale, however, have only scarcely been done in food process engineering. This thesis gives examples of questions that can be answered with the help of molecular simulation tools in a food process engineering context. With chocolate, this is shown on the example of a food, which is a complex mixture of different components. In this thesis the crystalline solid sucrose, the liquid triglyceride phase during conching, and the emulsifier lecithin, which is a mixture of different phospholipids, were considered for the representation of chocolate. The application of a non-equilibrium methods was shown, in order to access certain specific interactions in the system. Further, two methods that can be used to overcome the slow dynamics of the typically viscous food system were demonstrated and their theory was explained. The presented methods were the so-called implicit solvation molecular dynamics, which was briefly introduced and first results were shown, and coarse-grained molecular dynamics, which were shown in detail as a major part of the presented results are based on this method. The usage of such a calculation time enhancing method is inevitable with current computational resources, when self assembly of molecular structures in complex food systems is investigated. Further, in the study of complex food systems the meaning of the starting configuration for the molecular systems is emphasized. Depending on the research question, the food should be represented in a starting configuration that is as representative as possible for the food system in the equilibrium state. Self assembly of the desired state is usually not feasible, due to restrictions of computational resources.

7.2 Outlook

7.2.1 From classical to structure related rheological models

As final part of the presented thesis an outlook is given on three exemplary but important aspects that need to be elaborated in more detail in order to further promote the presented results. A future task for the continuation of the presented thesis would be to close the gap between commonly used rheological models and the results that can be gained by molecular dynamics simulations. The molecular insights that were achieved in the studies of Chapters 5, 4, and 6 were interpreted in a way to explain rheological behavior of chocolate. Ideally, the molecular structures would be quantified and could be used as input for rheological models in a multiscale modeling approach. The established rheological models that are mainly used in chocolate rheology, the Casson, Bingham, and Hershel-Bulkley models, which were presented in Chapter 2.3, are simple empirical models, which give a mathematical relation between the viscosity, shear stress, and shear rate. The models are not able to represent relevant structural changes on the molecular scale of chocolate as no structural parameters are present in the equations.

The fluid immobilization model by Windhab [148] has the shear rate-dependent effective solid volume fraction as a model parameter, which includes surface immobilized fluids. This parameter is related to the results from Chapter 6, where cocoa butter immobilization is calculated from molecular dynamics simulations and thus in this case a multiscale framework is at hand. Further, particle aggregates, which could arise due to formed hydrophilic bridges between particles, could be included in this model. Additionally a structure-dependent yield stress would have to be introduced here. Unfortunately, the fluid immobilization model is not well established in chocolate research and industry, probably due to the difficulties of measuring the shear rate-dependent solid volume fraction for different chocolate recipes.

To use the results of Chapter 5 as input for rheological models, an even more elaborate rheological model would be required. The model would be required to include the structural lecithin concentration-dependent features, which were shown in this thesis, and would further be required to describe the rheological behavior that is caused by these structures. Flow behavior of systems that contain wormlike micellar structures have been investigated in other fields of research, and were shown to be non-trivial. Self-assembled surfactant structures can have a wide variety of microstructures with a wide range of different properties [24]. In contrast to polymer wormlike structures, surfactant worms are formed reversibly, and often refered to as living polymer, where breakage and reformation lead to a length distribution of the micelles [113]. Those systems further have a nonlinear rheological behavior with viscoelastic properties that are tunable over orders of magnitude. Experimental investigations have further unraveled that wormlike micellar solutions show the phenomenon of shear banding behavior, where the flow profile across a shear cell has different macroscopic bands with different viscosities [44]. It is not suggested that chocolate might show the same flow behavior as wormlike micellar solutions, but

the dimensions of different aspects that have to be considered when structural properties are included, is intended to be shown.

Closing the gap between rheological models that can be used for the description of flow behavior of complex fluids, such as chocolate, and molecular simulations is a complex tasks. The view presented here is merely that of a non-expert and probably a huge oversimplification. Probably this task has to be considered in a more nuanced way than it was done here.

7.2.2 The influence of water on rheology

Another future task for the continuation of the presented thesis, would be to investigate the influence of water on molecular structures. Water has a crucial effect on the rheology of chocolate, which was already discussed in Section 2.1.2. As first simulation, similar to system 5.4, is presented with additional water molecules. It gives first insights on the mechanisms that water induces in chocolate and how they might further have an impact on rheology, based on the distribution of water in the chocolate model and the shown results of Chapter 5. Figure 7.1 shows that water is mainly located in the hydrophilic parts of chocolate. The water adsorbs at the central sucrose crystal as water and sucrose have strong hy-

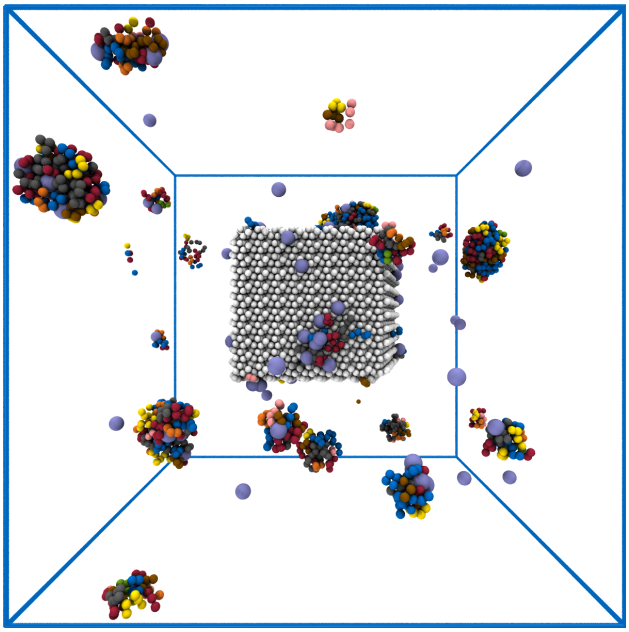

Figure 7.1: Snapshot of a simulation of water in chocolate. Water is shown as big green spheres, the head groups of the phospholipids are shown as small spheres. Cocoa butter and the aliphatic chains of the phospholipids are not shown.

drophilic interactions. Further, water is present in the hydrophilic cores of phospholipid micelles. Only a few water molecules are solved in the cocoa butter matrix. Two different rheological effects are supported by these finding. First, solvation of the sucrose crystal surfaces, which causes them to be more

sticky and to interact more strongly as proposed in literature [12] is supported by the presence of the water molecules on the sucrose surface in this simulation. Solvation and an increasing stickiness itself cannot be shown by the presented simulations as the sucrose crystal is fixed with position restraints. Second, addition of water to mixtures of phospholipids and non-polar solvents enhances the building of wormlike micellar structures [121]. This is supported by the presence of the water molecules in the hydrophilic micelles in this simulation. Strong wormlike hydrophilic structures would lead to stronger hydrophilic networks, supposedly also between the sucrose crystals and other hydrophilic parts, and increase the yield stress. In future molecular dynamic simulations, the water and lecithin concentrations could be varied, to get a an understanding of critical concentrations and the resulting self-assembled structures.

7.2.3 Cocoa particles in molecular dynamics simulations

The last presented future task for the continuation of this thesis, would be to investigate the parts of chocolate that were neglected here. A main challenge would be to model the parts that are not simply composed of chemically well-defined pure substances, such as cocoa particles. In the author's view, the best approach would be to analyze the chemical composition and their exact structure experimentally and subsequently, the different components should be simulated independently. Several simulations would be necessary for cocoa particles. The interactions between a representative protein fraction of cocoa particles and lecithins had to be calculated. Physico-chemical properties of proteins are highly diverse and range from hydrophilic to hydrophobic, often within a single molecule, leading - already for proteins - to a high number of necessary simulations. Further carbohydrate parts of cocoa particles, such as cellulose, would have to be considered. As cellulose is a food fiber, it might not be the major carbohydrate present in cocoa particles. Nevertheless, it was investigated as a first approach to cocoa particles in this thesis. Similar simulations to those of Chapter 5 were performed. Already during implementing the Martini FF representation of cellulose, the high similarity to the molecular representation of sucrose became obvious. As expected, similar results to those of Chapter 5, which were gained for sucrose, were observed and due to redundancy not further presented in this thesis.

After conclusion of the results and an exemplary outlook on future tasks, I hope that the reader could be convinced by the presented thesis and sees it as an important, even if only a small, step towards unraveling the secrets that are still hidden inside chocolate.

Bibliography

[1] J.-M. Aeschlimann and S. T. Beckett. International inter-laboratory trials to determine the factors affecting the measurement of chocolate viscosity. *Journal of Texture Studies*, 31(5):541–576, 2000. doi: 10.1111/j.1745-4603.2000.tb01019.x.

[2] E. O. Afoakwa, A. Paterson, and M. Fowler. Factors influencing rheological and textural qualities in chocolate - a review. *Trends in Food Science & Technology*, 18(6):290–298, 2007. doi: 10.1016/j.tifs.2007.02.002.

[3] E. O. Afoakwa, A. Paterson, and M. Fowler. Effects of particle size distribution and composition on rheological properties of dark chocolate. *European Food Reserach and Technology*, 226(6): 1259–1268, 2008. doi: 10.1007/s00217-007-0652-6.

[4] E. O. Afoakwa, A. Paterson, M. Fowler, and J. Vieira. Comparison of rheological models for determining dark chocolate viscosity. *International Journal of Food Science & Technology*, 44(1): 162–167, 2009. doi: 10.1111/j.1365-2621.2008.01710.x.

[5] M. P. Allen and D. J. Tildesley. *Computer simulation of liquids: second edition*. Oxford University Press, 2017. ISBN 9780192524706.

[6] R. Angelico, A. Ceglie, U. Olsson, and G. Palazzo. Phase diagram and phase properties of the system lecithin–water–cyclohexane. *Langmuir*, 16(5):2124–2132, 2000. doi: 10.1021/la9909190.

[7] C. Arnarez, J. J. Uusitalo, M. F. Masman, H. I. Ingólfsson, D. H. de Jong, M. N. Melo, X. Periole, A. H. d. Vries, and S. J. Marrink. Dry martini, a coarse-grained force field for lipid membrane simulations with implicit solvent. *Journal of Chemical Theory and Computation*, 11(1):260–275, 2015. doi: 10.1021/ct500477k.

[8] G. Arnold. *Wirkungsbeziehungen von Lecithinen und Phospholipiden in ölbasierten Systemen*. Disseratation, Technische Universität Dresden, 2014.

[9] G. Arnold, E. Schade, Y. Schneider, J. Friedrichs, F. Babick, C. Werner, and H. Rohm. Influence of individual phospholipids on the physical properties of oil-based suspensions. *Journal of the American Oil Chemists' Society*, 91(1):71–77, 2014. doi: 10.1007/s11746-013-2361-6.

[10] D. Bashford and D. A. Case. Generalized born models of macromolecular solvation effects. *Annual Review of Physical Chemistry*, 51:129–152, 2000. doi: 10.1146/annurev.physchem.51.1.129.

[11] C. I. Bayly, P. Cieplak, W. D. Cornell, and P. A. Kollman. A well-behaved electrostatic potential based method using charge restraints for deriving atomic charges - the resp model. *Journal of Physical Chemistry*, 97(40):10269–10280, 1993. doi: 10.1021/j100142a004.

[12] S. T. Beckett. *Industrial chocolate manufacture and use: fourth edition*. John Wiley & Sons, 2009.

[13] C. A. Beevers, T. R. R. McDonald, J. H. Robertson, and F. Stern. The crystal structure of sucrose. *Acta Crystallographica*, 5(5):689–690, 1952. doi: 10.1107/S0365110X52001908.

[14] H. J. C. Berendsen, J. P. M. Postma, W. F. van Gunsteren, A. DiNola, and J. R. Haak. Molecular dynamics with coupling to an external bath. *The Journal of Chemical Physics*, 81(8):3684–3690, 1984. doi: 10.1063/1.448118.

[15] G. Betz, A. Aeppli, N. Menshutina, and H. Leuenberger. In vivo comparison of various liposome formulations for cosmetic application. *International Journal of Pharmaceutics*, 296(1-2):44–54, 2005. doi: 10.1016/j.ijpharm.2005.02.032.

[16] M. Bodennec, Q. Guo, and D. Rousseau. Molecular and microstructural characterization of lecithin-based oleogels made with vegetable oil. *RSC Advances*, 6(53):47373–47381, 2016. doi: 10.1039/C6RA04324K.

[17] A. Brasiello, S. Crescitelli, and G. Milano. Development of a coarse-grained model for simulations of tridecanoin liquid-solid phase transitions. *Physical Chemistry Chemical Physics*, 13(37): 16618–16628, 2011. doi: 10.1039/C1CP20604D.

[18] G. M. Brown and H. A. Levy. Further refinement of structure of sucrose based on neutron-diffraction data. *Acta Crystallographica Section B - Structural Science*, 29(4):790–797, 1973. doi: 10.1107/S0567740873003353.

[19] B. L. Bush, C. I. Bayly, and T. A. Halgren. Consensus bond-charge increments fitted to electrostatic potential or field of many compounds: Application to MMFF94 training set. *Journal of Computational Chemistry*, 20(14):1495–1516, 1999. doi: 10.1002/(SICI)1096-987X(19991115)20:14<1495::AID-JCC3>3.0.CO;2-3.

[20] G. Bussi, D. Donadio, and M. Parrinello. Canonical sampling through velocity rescaling. *The Journal of Chemical Physics*, 126(1):014101, 2007. doi: 10.1063/1.2408420.

[21] P. T. Callaghan and K. W. Jolley. Translational motion in the liquid phases of tristearin, triolein and trilinolein. *Chemistry and Physics of Lipids*, 27(1):49–56, 1980. doi: 10.1016/0009-3084(80)90047-X.

[22] B. Calvignac, E. Rodier, J.-J. Letourneau, P. M. Almeida dos Santos, and J. Fages. Cocoa butter saturated with supercritical carbon dioxide: Measurements and modelling of solubility, volumetric expansion, density and viscosity. *International Journal of Chemical Reactor Engineering*, 8(1), 2010. doi: 10.2202/1542-6580.2191.

[23] C. Campañá Cué, A. R. Ruiz Salvador, S. Aguilera Morales, F. L. Falcon Rodriguez, and P. Pérez González. Raffinose–sucrose crystal interaction modelling. *Journal of Crystal Growth*, 231(1-2): 280–289, 2001. doi: 10.1016/S0022-0248(01)01489-0.

[24] M. E. Cates and Candau S. J. Statics and dynamics of worm-like surfactant micelles. *Journal of Physics: Condensed Matter*, 2(33):6869, 1990. doi: 10.1088/0953-8984/2/33/001.

[25] ccp14. Sucrose crystal unit cell: Last accessed on 12.07.2018, 2018. URL `www.ccp14.ac.uk/ccp/ccp14/ftp-mirror/platon-spek/pub/special/sucrose.cif`.

[26] J. Chevalley. Rheology of chocolate. *Journal of Texture Studies*, 6(2):177–196, 1975. doi: 10.1111/j.1745-4603.1975.tb01247.x.

[27] P. Cieplak, W. D. Cornell, C. I. Bayly, and P. A. Kollman. Application of the multimolecule and multiconformational resp methodology to biopolymers - charge derivation for dna, rna, and proteins. *Journal of Computational Chemistry*, 16(11):1357–1377, 1995. doi: 10.1002/jcc.540161106.

[28] P. A. Cirkel and G. J. M. Koper. Characterization of lecithin cylindrical micelles in dilute solution. *Langmuir*, 14(25):7095–7103, 1998. doi: 10.1021/la971326x.

[29] P. M. Claesson, A. Dedinaite, B. Bergenståhl, B. Campbell, and H. Christenson. Interactions between hydrophilic mica surfaces in triolein: Triolein surface orientation, solvation forces, and capillary condensation. *Langmuir*, 13(6):1682–1688, 1997. doi: 10.1021/la960975q.

[30] W. D. Cornell, P. Cieplak, C. I. Bayly, I. R. Gould, K. M. Merz, D. M. Ferguson, D. C. Spellmeyer, T. Fox, J. W. Caldwell, and P. A. Kollman. A 2nd generation force-field for the simulation of proteins, nucleic-acids, and organic-molecules. *Journal of the American Chemical Society*, 117 (19):5179–5197, 1995. doi: 10.1021/ja00124a002.

[31] A. W. S. da Silva and W. F. Vranken. Acpype-antechamber python parser interface. *BMC research notes*, 5(1):367, 2012. doi: 10.1186/1756-0500-5-367.

[32] M. D. Daily, B. N. Olsen, P. H. Schlesinger, D. S. Ory, and N. A. Baker. Improved coarse-grained modeling of cholesterol-containing lipid bilayers. *Journal of Chemical Theory and Computation*, 10(5):2137–2150, 2014. doi: 10.1021/ct401028g.

[33] T. T. Darden, D. York, and L. Pedersen. Particle mesh ewald - an n log(n)method for ewald sums in large systems. *Journal of Chemical Physics*, 98(12):10089–10092, 1993. doi: 10.1063/1.464397.

[34] M. de Graef and M. E. McHenry. *Structure of materials: An introduction to crystallography, diffraction and symmetry*. Cambridge University Press, 2012.

[35] V. de Graef, F. Depypere, M. Minnaert, and K. Dewettinck. Chocolate yield stress as measured by oscillatory rheology. *Food Research International*, 44(9):2660–2665, 2011. doi: 10.1016/j.foodres.2011.05.009.

[36] S. M. Deckers, T. Venken, M. Khalesi, K. Gebruers, G. Baggerman, Y. Lorgouilloux, Z. Shokribousjein, V. Ilberg, C. Schönberger, J. Titze, H. Verachtert, C. Michiels, H. Neven, J. Delcour, J. Martens, G. Derdelinckx, and M. de Maeyer. Combined modeling and biophysical characterisation of CO2 interaction with class II hydrophobins: New insight into the mechanism underpinning primary gushing. *Journal of the American Society of Brewing Chemists*, 70(4):249–256, 2012. doi: 10.1094/ASBCJ-2012-0905-01.

[37] A. Dedinaite, P. M. Claesson, B. Campbell, and H. Mays. Interactions between modified mica surfaces in triglyceride media. *Langmuir*, 14(19):5546–5554, 1998. doi: 10.1021/la980237x.

[38] M. Delbianco, A. Kononov, A. Poveda, Y. Yu, T. Diercks, J. Jiménez-Barbero, and P. H. Seeberger. Well-defined oligo- and polysaccharides as ideal probes for structural studies. *Journal of the American Chemical Society*, 140(16):5421–5426, 2018. doi: 10.1021/jacs.8b00254.

[39] C. Dellago and G. Hummer. Computing equilibrium free energies using non-equilibrium molecular dynamics. *Entropy*, 16(1):41–61, 2014. doi: 10.3390/e16010041.

[40] C. J. Dickson, L. Rosso, R. M. Betz, R. C. Walker, and I. R. Gould. GAFFlipid: a general amber force field for the accurate molecular dynamics simulation of phospholipid. *Soft Matter*, 8(37): 9617, 2012. doi: 10.1039/c2sm26007g.

[41] T.-A. L. Do, J. M. Hargreaves, B. Wolf, J. Hort, and J. R. Mitchell. Impact of particle size distribution on rheological and textural properties of chocolate models with reduced fat content. *Journal of Food Science*, 72(9):E541–52, 2007. doi: 10.1111/j.1750-3841.2007.00572.x.

[42] Doree Sitkoff, Kim A. Sharp, and and Barry Honig. Accurate calculation of hydration free energies using macroscopic solvent models. *The Journal of Physical Chemistry*, 98:1978–1988, 1994. doi: 10.1021/j100058a043.

[43] C. A. Dreiss. Wormlike micelles: Where do we stand? recent developments, linear rheology and scattering techniques. *Soft Matter*, 3(8):956–970, 2007. doi: 10.1039/B705775J.

[44] S. M. Fielding. Shear banding in soft glassy materials. *Reports on progress in physics. Physical Society (Great Britain)*, 77(10):102601, 2014. doi: 10.1088/0034-4885/77/10/102601.

[45] B. L. Foley, M. B. Tessier, and R. J. Woods. Carbohydrate force fields. *Wiley Interdisciplinary Reviews: Computational Molecular Science*, 2(4):652–697, 2012. doi: 10.1002/wcms.89.

[46] W.-K. Fong, R. Negrini, J. J. Vallooran, R. Mezzenga, and B. J. Boydbilay. Responsive self-assembled nanostructured lipid systems for drug delivery and diagnostics. *Journal of Colloid and Interface Science*, 484:320–339, 2016. doi: 10.1016/j.jcis.2016.08.077.

[47] I. Foubert, P. Vanrolleghem, O. Thas, and K. Dewettinck. Influence of chemical composition on the isothermal cocoa butter crystallization. *Journal of Food Science*, 69(9):E478–E487, 2004. doi: 10.1111/j.1365-2621.2004.tb09933.x.

[48] D. Frenkel and B. Smit. *Understanding molecular simulation*. Academic Press, 2002.

[49] C. A. Godoy, M. Valiente, R. Pons, and G. Montalvo. Effect of fatty acids on self-assembly of soybean lecithin systems. *Colloids and Surfaces B: Biointerfaces*, 131:21–28, 2015. doi: 10.1016/j.colsurfb.2015.03.065.

[50] M. Greiner, A. M. Reilly, and H. Briesen. Temperature- and pressure-dependent densities, self-diffusion coefficients, and phase behavior of monoacid saturated triacylglycerides: Toward molecular-level insights into processing. *Journal of Agricultural and Food Chemistry*, 60(20): 5243–5249, 2012. doi: 10.1021/jf3004898.

[51] M. Greiner, B. Sonnleitner, M. Mailaender, and H. Briesen. Modeling complex and multi-component food systems in molecular dynamics simulations on the example of chocolate conching. *Food & Function*, 5(2):235–242, 2014. doi: 10.1039/c3fo60355e.

[52] M. Griebel, S. Knapek, G. Zumbusch, and A. Caglar. *Numerische Simulation in der Moleküldynamik: Numerik, Algorithmen, Parallelisierung, Anwendungen*. Springer-Lehrbuch. SPRINGER, Berlin and Heidelberg, 2004. ISBN 9783540418566. doi: 10.1007/978-3-642-18779-7.

[53] A. Hall, J. Repakova, and I. Vattulainen. Modeling of the triglyceride-rich core in lipoprotein particles. *Journal of Physical Chemistry B*, 112(44):13772–13782, 2008. doi: 10.1021/jp803950w.

[54] G. D. Hawkins, C. J. Cramer, and D. G. Truhlar. Parametrized models of aqueous free energies of solvation based on pairwise descreening of solute atomic charges from a dielectric medium. *Journal of Physical Chemistry*, 100(51):19824–19839, 1996. doi: 10.1021/jp961710n.

[55] W. J. Hehre, R. Ditchfield, and J. A. Pople. Self-consistent molecular orbital methods. XII. further extensions of gaussian-type basis sets for use in molecular orbital studies of organic molecules. *The Journal of Chemical Physics*, 56(5):2257–2261, 1972. doi: 10.1063/1.1677527.

[56] Q. T. Ho, J. Carmeliet, A. K. Datta, T. Defraeye, M. A. Delele, E. Herremans, L. Opara, H. Ramon, E. Tijskens, R. van der Sman, P. van Liedekerke, P. Verboven, and B. M. Nicolai. Multiscale modeling in food engineering. *Journal of Food Engineering*, 114(3):279–291, 2013. doi: 10.1016/j.jfoodeng.2012.08.019.

[57] R. Hockney, S. Goel, and J. Eastwood. Quiet high-resolution computer models of a plasma. *Journal of Computational Physics*, 14(2):148–158, 1974. doi: 10.1016/0021-9991(74)90010-2.

[58] H. Hoffmann, W. Mauch, and W. Untze. *Zucker und Zuckerwaren*. Behr, Hamburg, second edition, 2002. ISBN 3860229370.

[59] W. G. Hoover. Canonical dynamics: Equilibrium phase-space distributions. *Physical Review A*, 31(3):1695–1697, 1985. doi: 10.1103/PhysRevA.31.1695.

[60] M. F. Horstemeyer and D. Raabe. *Integrated computational materials engineering (ICME) for metals: Using multiscale modeling to invigorate engineering design with science*. Wiley, 2012. ISBN 9781118342657.

[61] J. M. Hoskin and P. S. Dimick. Observations of chocolate during conching by scanning electron-microscopy and viscometry. *Journal of Food Science*, 45(6):1541–1545, 1980. doi: 10.1111/j.1365-2621.1980.tb07558.x.

[62] W. Humphrey, A. Dalke, and K. Schulten. Vmd: Visual molecular dynamics. *Journal of Molecular Graphics*, 14(1):33 – 38, 1996. doi: 10.1016/0263-7855(96)00018-5.

[63] H. I. Ingólfsson, C. A. Lopez, J. J. Uusitalo, D. H. de Jong, S. M. Gopal, X. Periole, and S. J. Marrink. The power of coarse graining in biomolecular simulations. *Wiley Interdisciplinary Reviews: Computational Molecular Science*, 4(3):225–248, 2014. doi: 10.1002/wcms.1169.

[64] A. Jakalian, B. L. Bush, D. B. Jack, and C. I. Bayly. Fast, efficient generation of high-quality atomic charges. AM1-BCC model: I. method. *Journal of Computational Chemistry*, 21(2):132, 2000. doi: 10.1002/(SICI)1096-987X(20000130)21:2<132::AID-JCC5>3.3.CO;2-G.

[65] C. Jarzynski. Nonequilibrium equality for free energy differences. *Physical Review Letters*, 78 (14):2690–2693, 1997. doi: 10.1103/PhysRevLett.78.2690.

[66] C. Jarzynski. Rare events and the convergence of exponentially averaged work values. *Physical review. E, Statistical, nonlinear, and soft matter physics*, 73(4 Pt 2):046105, 2006. doi: 10.1103/PhysRevE.73.046105.

[67] J. Jin, Q. Jin, X. Wang, and C. C. Akoh. Improving heat and fat bloom stabilities of “dark chocolates” by addition of mango kernel fat-based chocolate fats. *Journal of Food Engineering*, 246: 33–41, 2019. doi: 10.1016/j.jfoodeng.2018.10.027.

[68] D. Johansson and B. Bergenstahl. The influence of food emulsifiers on fat and sugar dispersions in oils. 1. adsorption, sedimentation. *Journal of the American Oil Chemists' Society*, 69(8):705–717, 1992. doi: 10.1007/BF02635905.

[69] J. Kennedy and H. Heymann. Projective mapping and descriptive analysis of milk and dark chocolates. *Journal of Sensory Studies*, 24(2):220–233, 2009. doi: 10.1111/j.1745-459X.2008.00204.x.

[70] M. Kindlein, M. Greiner, E. Elts, and H. Briesen. Interactions between phospholipid head groups and a sucrose crystal surface at the cocoa butter interface. *Journal of Physics D: Applied Physics*, 48(38):384002, 2015. doi: 10.1088/0022-3727/48/38/384002 https://iopscience.iop.org/article/10.1088/0022-3727/48/38/384002 © IOP Publishing. Reproduced with permission. All rights reserved.

[71] M. Kindlein, E. Elts, and H. Briesen. Phospholipids in chocolate: Structural insights and mechanistic explanations of rheological behavior by coarse-grained molecular dynamics simulations. *Journal of Food Engineering*, 228:118–127, 2018. doi: 10.1016/j.jfoodeng.2018.02.014.

[72] I. Kralova and J. Sjöblom. Surfactants used in food industry: A review. *Journal of Dispersion Science and Technology*, 30(9):1363–1383, 2009. doi: 10.1080/01932690902735561.

[73] I. M. Krieger and T. J. Dougherty. A mechanism for non–newtonian flow in suspensions of rigid spheres. *Transactions of the Society of Rheology*, 3(1):137–152, 1959. doi: 10.1122/1.548848.

[74] N. Kučerka, M.-P. Nieh, and J. Katsaras. Fluid phase lipid areas and bilayer thicknesses of commonly used phosphatidylcholines as a function of temperature. *Biochimica et Biophysica Acta (BBA) - Biomembranes*, 1808(11):2761–2771, 2011. doi: 10.1016/j.bbamem.2011.07.022.

[75] M. Ladd-Parada, M. J. Povey, J. Vieira, and M. E. Ries. Fast field cycling nmr relaxometry studies of molten and cooled cocoa butter. *Molecular Physics*, 4(2):1–8, 2019. doi: 10.1080/00268976.2018.1508784.

[76] G. Lelong, W. S. Howells, J. W. Brady, C. Talon, D. L. Price, and M.-L. Saboungi. Translational and rotational dynamics of monosaccharide solutions. *Journal of Physical Chemistry B*, 113(39): 13079–13085, 2009. doi: 10.1021/jp905001q.

[77] R. M. Levy, L. Y. Zhang, E. Gallicchio, and A. K. Felts. On the nonpolar hydration free energy of proteins: Surface area and continuum solvent models for the solute-solvent interaction energy. *Journal of the American Chemical Society*, 125(31):9523–9530, 2003. doi: 10.1021/ja029833a.

[78] H. J. Limbach and K. Kremer. Multi-scale modelling of polymers: Perspectives for food materials. *Trends in Food Science & Technology*, 17(5):215–219, 2006. doi: 10.1016/j.tifs.2005.11.001.

[79] H. J. Limbach and J. Ubbink. Structure and dynamics of maltooligomer-water solutions and glasses. *Soft Matter*, 4(9):1887–1898, 2008. doi: 10.1039/b719471d.

[80] M. Lipp and E. Anklam. Review of cocoa butter and alternative fats for use in chocolate – part a. compositional data. *Food Chemistry*, 62(1):73–97, 1998. doi: 10.1016/S0308-8146(97)00160-X.

[81] I. Loncarevic, B. Pajin, J. Petrovic, D. Zaric, M. Sakac, A. Torbica, D. M. Lloyd, and R. Omorjan. The impact of sunflower and rapeseed lecithin on the rheological properties of spreadable cocoa cream. *Journal of Food Engineering*, 171:67–77, 2016. doi: 10.1016/j.jfoodeng.2015.10.001.

[82] C. A. López, A. J. Rzepiela, A. H. d. Vries, L. Dijkhuizen, P. H. Hanenberger, and S. J. Marrink. Martini coarse-grained force field: Extension to carbohydrates. *Journal of Chemical Theory and Computation*, 5(12):3195–3210, 2009. doi: 10.1021/ct900313w.

[83] C. A. López, Z. Sovova, F. J. van Eerden, A. H. d. Vries, and S. J. Marrink. Martini force field parameters for glycolipids. *Journal of Chemical Theory and Computation*, 9(3):1694–1708, 2013. doi: 10.1021/ct3009655.

[84] C. A. López, G. Bellesia, A. Redondo, P. Langan, S. P. S. Chundawat, B. E. Dale, S. J. Marrink, and S. Gnanakaran. Martini coarse-grained model for crystalline cellulose microfibers. *The Journal of Physical Chemistry B*, 119(2):465–473, 2015. doi: 10.1021/jp5105938.

[85] A. G. Marangoni. Organogels: An alternative edible oil-structuring method. *Journal of the American Oil Chemists' Society*, 89(5):749–780, 2012. doi: 10.1007/s11746-012-2049-3.

[86] A. Markina, V. Ivanov, P. Komarov, A. Khokhlov, and S. H. Tung. Self-assembly of micelles in organic solutions of lecithin and bile salt: Mesoscale computer simulation. *Chemical Physics Letters*, 664:16–22, 2016. doi: 10.1016/j.cplett.2016.09.078.

[87] S. J. Marrink and D. P. Tieleman. Perspective on the martini model. *Chem Soc Rev*, 42(16): 6801–6822, 2013. doi: 10.1039/C3CS60093A.

[88] S. J. Marrink, H. J. Risselada, S. Yefimov, D. P. Tieleman, and A. H. d. Vries. The martini force field: Coarse grained model for biomolecular simulations. *The Journal of Physical Chemistry B*, 111(27):7812–7824, 2007. doi: 10.1021/jp071097f.

[89] A. Matheson, G. Dalkas, R. Mears, S. R. Euston, and P. S. Clegg. Stable emulsions of droplets in a solid edible organogel matrix. *Soft Matter*, 14(11):2044–2051, 2018. doi: 10.1039/c8sm00169c.

[90] D. D. Mellor, T. Sathyapalan, E. S. Kilpatrick, S. Beckett, and S. L. Atkin. High-cocoa polyphenol-rich chocolate improves hdl cholesterol in type 2 diabetes patients. *Diabetic Medicine*, 27(11): 1318–1321, 2010. doi: 10.1111/j.1464-5491.2010.03108.x.

[91] D. Middendorf, A. Juadjur, U. Bindrich, and P. Mischnick. AFM approach to study the function of PGPR's emulsifying properties in cocoa butter based suspensions. *Food Structure*, 4:16–26, 2015. doi: 10.1016/j.foostr.2014.11.003.

[92] D. Middendorf, U. Bindrich, P. Mischnick, A. Juadjur, K. Franke, and V. Heinz. Atomic force microscopy study on the effect of different lecithins in cocoa-butter based suspensions. *Col-*

loids and Surfaces A: Physicochemical and Engineering Aspects, 499:60–68, 2016. doi: 10.1016/j.colsurfa.2016.03.057.

[93] D. Middendorf, U. Bindrich, P. Mischnick, K. Franke, and V. Heinz. AFM-based local thermal analysis is a suitable tool to characterize the impact of different grinding techniques on sucrose surface properties. *Journal of Food Engineering*, 235:50–58, 2018. doi: 10.1016/j.jfoodeng.2018.04.021.

[94] D. Mohammadyani, V. A. Tyurin, M. O'Brien, Y. Sadovsky, D. I. Gabrilovich, J. Klein-Seetharaman, and V. E. Kagan. Molecular speciation and dynamics of oxidized triacylglycerols in lipid droplets: Mass spectrometry and coarse-grained simulations. *Free Radical Biology and Medicine*, 76: 53–60, 2014. doi: 10.1016/j.freeradbiomed.2014.07.042.

[95] G. Moiset, C. A. López, R. Bartelds, L. Syga, E. Rijpkema, A. Cukkemane, M. Baldus, B. Poolman, and S. J. Marrink. Disaccharides impact the lateral organization of lipid membranes. *Journal of the American Chemical Society*, 136(46):16167–16175, 2014. doi: 10.1021/ja505476c.

[96] V. Molinero and W. A. Goddard. Microscopic mechanism of water diffusion in glucose glasses. *Physical Review Letters*, 95(4), 2005. doi: 10.1103/PhysRevLett.95.045701.

[97] F. A. Momany and J. L. Willett. Molecular dynamics calculations on amylose fragments. I. glass transition temperatures of maltodecaose at 1, 5, 10, and 15.8% hydration. *Biopolymers*, 63(2): 99–110, 2002. doi: 10.1002/bip.10014.

[98] L. Monticelli, S. K. Kandasamy, X. Periole, R. G. Larson, D. P. Tieleman, and S.-J. Marrink. The martini coarse-grained force field: Extension to proteins. *Journal of Chemical Theory and Computation*, 4(5):819–834, 2008. doi: 10.1021/ct700324x.

[99] K. S. Mukhamedova and A. I. Glushenkova. Molecular composition of soybean phospholipids. *Chemistry of Natural Compounds*, 33(6):693–694, 1997.

[100] T. Negami, K. Shimizu, and T. Terada. Coarse-grained molecular dynamics simulations of protein–ligand binding. *Journal of Computational Chemistry*, 35(25):1835–1845, 2014. doi: 10.1002/jcc.23693.

[101] M. T. Nguyen, D. van de Walle, C. Petit, B. Beheydt, F. Depypere, and K. Dewettinck. Mapping the chemical variability of vegetable lecithins. *Journal of the American Oil Chemists' Society*, 91 (7):1093–1101, 2014. doi: 10.1007/s11746-014-2455-9.

[102] Y. Nishizuka. Intracellular signaling by hydrolysis of phospholipids and activation of protein kinase c. *Science*, 258(5082):607–614, 1992. doi: 10.1126/science.1411571.

[103] S. Nosé. A molecular dynamics method for simulations in the canonical ensemble. *Molecular Physics*, 52(2):255–268, 1984. doi: 10.1080/00268978400101201.

[104] O. H. S. Ollila, A. Lamberg, M. Lehtivaara, A. Koivuniemi, and I. Vattulainen. Interfacial tension and surface pressure of high density lipoprotein, lowâ density lipoprotein, and related lipid droplets. *Biophysical Journal*, 103(6):1236–1244, 2012. doi: 10.1016/j.bpj.2012.08.023.

[105] A. Onufriev, D. Bashford, and D. A. Case. Exploring protein native states and large-scale conformational changes with a modified generalized born model. *Proteins - Structure Function and Bioinformatics*, 55(2):383–394, 2004. doi: 10.1002/prot.20033.

[106] M. Parrinello and A. Rahman. Polymorphic transitions in single crystals: A new molecular dynamics method. *Journal of Applied Physics*, 52(12):7182–7190, 1981. doi: 10.1063/1.328693.

[107] D. A. Pink and M. S. G. Razul. Computer simulation techniques for food science and engineering: Simulating atomic scale and coarse-grained models. *Food Structure*, 1(1):71–90, 2014. doi: 10.1016/j.foostr.2013.11.005.

[108] A. Pizzirusso, A. Brasiello, A. de Nicola, A. G. Marangoni, and G. Milano. Coarse-grained modelling of triglyceride crystallisation: A molecular insight into tripalmitin tristearin binary mixtures by molecular dynamics simulations. *Journal of Physics D: Applied Physics*, 48(49):494004, 2015. doi: 10.1088/0022-3727/48/49/494004.

[109] D. Poger and A. E. Mark. Lipid bilayers: The effect of force field on ordering and dynamics. *Journal of Chemical Theory and Computation*, 8(11):4807–4817, 2012. doi: 10.1021/ct300675z.

[110] D. Poger, B. Caron, and A. E. Mark. Validating lipid force fields against experimental data: Progress, challenges and perspectives. *Biochimica et Biophysica Acta*, 1858(7):1556–1565, 2016. doi: 10.1016/j.bbamem.2016.01.029.

[111] D. Qiu, P. S. Shenkin, F. P. Hollinger, and W. C. Still. The GB/SA continuum model for solvation. a fast analytical method for the calculation of approximate born radii. *Journal of Physical Chemistry A*, 101(16):3005–3014, 1997. doi: 10.1021/jp961992r.

[112] M. S. G. Razul, C. J. MacDougall, C. B. Hanna, A. G. Marangoni, F. Peyronel, E. Papp-Szabo, and D. A. Pink. Oil binding capacities of triacylglycerol crystalline nanoplatelets: Nanoscale models of tristearin solids in liquid triolein. *Food & Function*, 5(10):2501–2508, 2014. doi: 10.1039/c3fo60654f.

[113] S. A. Rogers, M. A. Calabrese, and N. J. Wagner. Rheology of branched wormlike micelles. *Current Opinion in Colloid & Interface Science*, 19(6):530–535, 2014. doi: 10.1016/j.cocis.2014.10.006.

[114] P. Rousset, P. Sellappan, and P. Daoud. Effect of emulsifiers on surface properties of sucrose by inverse gas chromatography. *Journal of Chromatography A*, 969(1-2):97–101, 2002. doi: 10.1016/S0021-9673(02)00370-9.

[115] B. Roux and T. Simonson. Implicit solvent models. *Biophysical Chemistry*, 78(1-2):1–20, 1999. doi: 10.1016/S0301-4622(98)00226-9.

[116] M. G. Saunders and G. A. Voth. Coarse-graining methods for computational biology. *Annual review of biophysics*, 42:73–93, 2013. doi: 10.1146/annurev-biophys-083012-130348.

[117] M. Schaefer, C. Bartels, and M. Karplus. Solution conformations and thermodynamics of structured peptides: Molecular dynamics simulation with an implicit solvation model. *Journal of Molecular Biology*, 284(3):835–848, 1998. doi: 10.1006/jmbi.1998.2172.

[118] B. Schantz and H. Rohm. Influence of lecithin-PGPR blends on the rheological properties of chocolate. *LWT - Food Science and Technology*, 38(1):41–45, 2005. doi: 10.1016/j.lwt.2004.03.014.

[119] C. Servais, H. Ranc, and I. D. Roberts. Determination of chocolate viscosity. *Journal of Texture Studies*, 34:467–497, 2003. doi: 10.1111/j.1745-4603.2003.tb01077.x.

[120] Y. A. Shchipunov. Lecithin organogel: A micellar system with unique properties. *Colloids and Surfaces A: Physicochemical and Engineering Aspects*, 183:541–554, 2001. doi: 10.1016/S0927-7757(01)00511-8.

[121] Y. A. Shchipunov and E. V. Shumilina. Lecithin bridging by hydrogen bonds in the organogel. *Materials Science and Engineering: C*, 3(1):43–50, 1995. doi: 10.1016/0928-4931(95)00102-6.

[122] T. W. Sirk, E. F. Brown, A. K. Sum, and M. Friedman. Molecular dynamics study on the biophysical interactions of seven green tea catechins with lipid bilayers of cell membranes. *Journal of Agricultural and Food Chemistry*, 56(17):7750–7758, 2008. doi: 10.1021/jf8013298.

[123] I. C. J. Soeters. Das physikalische Verhalten und die chemischen Zusammensetzung von Schokolade, Kakaobutter und einigen Kakaobutter-Austauschfetten. *Fette, Seifen, Anstrichmittel*, 72(8), 1970. doi: 10.1002/lipi.19700720817.

[124] A. Sokmen and G. Gunes. Influence of some bulk sweeteners on rheological properties of chocolate. *LWT - Food Science and Technology*, 39(10):1053–1058, 2006. doi: 10.1016/j.lwt.2006.03.002.

[125] J. J. P. Stewart. Mopac 6 manual, 1990.

[126] W. C. Still, A. Tempczyk, R. C. Hawley, and T. Hendrickson. Seminanalytical treatment of solvation for molecular mechanics and dynamics. *Journal of the American Chemical Society*, 112(16): 6127–6129, 1990. doi: 10.1021/ja00172a038.

[127] T. A. Stortz and A. G. Marangoni. Heat resistant chocolate. *Trends in Food Science & Technology*, 22(5):201–214, 2011. doi: 10.1016/j.tifs.2011.02.001.

[128] T. A. Stortz, D. C. de Moura, T. Laredo, and A. G. Marangoni. Molecular interactions of ethylcellulose with sucrose particles. *RSC Advances*, 4(98):55048–55061, 2014. doi: 10.1039/c4ra12010h.

[129] A. K. Sum, M. J. Biddy, J. J. de Pablo, and M. J. Tupy. Predictive molecular model for the thermodynamic and transport properties of triacylglycerols. *Journal of Physical Chemistry B*, 107(51):14443–14451, 2003. doi: 10.1021/jp035906g.

[130] S. Tanizaki and M. Feig. A generalized born formalism for heterogeneous dielectric environments: Application to the implicit modeling of biological membranes. *Journal of Chemical Physics*, 122 (12), 2005. doi: 10.1063/1.1865992.

[131] M. Torres-Moreno, E. Torrescasana, J. Salas-Salvado, and C. Blanch. Nutritional composition and fatty acids profile in cocoa beans and chocolates with different geographical origin and processing conditions. *Food Chemistry*, 166:125–132, 2015. doi: 10.1016/j.foodchem.2014.05.141.

[132] S. Tsuzuki, W. Shinoda, H. Saito, M. Mikami, H. Tokuda, and M. Watanabe. Molecular dynamics simulations of ionic liquids: cation and anion dependence of self-diffusion coefficients of ions. *The journal of physical chemistry. B*, 113(31):10641–10649, 2009. doi: 10.1021/jp811128b.

[133] D. van der Spoel, E. Lindahl, B. Hess, G. Groenhof, A. E. Mark, and H. J. Berendsen. Gromacs: Fast, flexible, and free. *Journal of Computational Chemistry*, 26(16):1701–1718, 2005. doi: 10.1002/jcc.20291.

[134] F. J. van Eerden, D. H. de Jong, A. H. d. Vries, T. A. Wassenaar, and S. J. Marrink. Characterization of thylakoid lipid membranes from cyanobacteria and higher plants by molecular dynamics simulations. *Biochimica et Biophysica Acta (BBA) - Biomembranes*, 1848(6):1319–1330, 2015. doi: 10.1016/j.bbamem.2015.02.025.

[135] W. van Nieuwenhuyzen. Funktionalität von lecithinen. *Lipid / Fett*, 99(1):10–14, 1997. doi: 10.1002/lipi.2700990103.

[136] W. van Nieuwenhuyzen and M. C. Tomas. Update on vegetable lecithin and phospholipid technologies. *European Journal of Lipid Science and Technology*, 110(5):472–486, 2008. doi: 10.1002/ejlt.200800041.

[137] S. Vierros and M. Sammalkorpi. Phosphatidylcholine reverse micelles on the wrong track in molecular dynamics simulations of phospholipids in an organic solvent. *The Journal of Chemical Physics*, 142(9), 2015. doi: 10.1063/1.4914022.

[138] T. Vuorela, A. Catte, P. S. Niemelä, A. Hall, M. T. Hyvönen, S.-J. Marrink, M. Karttunen, and I. Vattulainen. Role of lipids in spheroidal high density lipoproteins. *PLOS Computational Biology*, 6(10):1–14, 2010. doi: 10.1371/journal.pcbi.1000964.

[139] R. C. Walker, M. F. Crowley, and D. A. Case. The implementation of a fast and accurate qm/mm potential method in amber. *Journal of Computational Chemistry*, 29(7):1019–1031, 2008. doi: 10.1002/jcc.20857.

[140] J. Wang and T. Hou. Application of molecular dynamics simulations in molecular property prediction II: Diffusion coefficient. *Journal of Computational Chemistry*, 32(16):3505–3519, 2011. doi: 10.1002/jcc.21939.

[141] J. Wang, W. Wang, P. A. Kollman, and D. A. Case. Antechamber: An accessory software package for molecular mechanical calculations. *Journal of the American Chemical Society*, 222:U403, 2001.

[142] J. Wang, W. Wang, P. A. Kollman, and D. A. Case. Automatic atom type and bond type perception in molecular mechanical calculations. *Journal of Molecular Graphics & Modelling*, 25(2):247–260, 2006. doi: 10.1016/j.jmgm.2005.12.005.

[143] J. M. Wang, R. M. Wolf, J. W. Caldwell, P. A. Kollman, and D. A. Case. Development and testing of a general amber force field. *Journal of Computational Chemistry*, 25(9):1157–1174, 2004. doi: 10.1002/jcc.20035.

[144] T. A. Wassenaar, H. I. Ingólfsson, R. A. Böckmann, D. P. Tieleman, and S. J. Marrink. Computational lipidomics with insane: A versatile tool for generating custom membranes for molecular simulations. *Journal of Chemical Theory and Computation*, 11(5):2144–2155, 2015. doi: 10.1021/acs.jctc.5b00209.

[145] S. J. Weiner, P. A. Kollman, D. A. Case, U. C. Singh, C. Ghio, G. Alagona, S. Profeta, and P. Weiner. A new force-field for molecular mechanical simulation of nucleic-acids and proteins. *Journal of the American Chemical Society*, 106(3):765–784, 1984. doi: 10.1021/ja00315a051.

[146] S. J. Weiner, P. A. Kollman, D. T. Nguyen, and D. A. Case. An all atom force field for simulations of proteins and nucleic acids. *Journal of Computational Chemistry*, 7(2):230–252, 1986. doi: 10.1002/jcc.540070216.

[147] E. J. Windhab. Rheology in food processing. In S. T. Beckett, editor, *Physico-Chemical Aspects of Food Processing*. Springer US, Boston, MA, 1995. ISBN 0751402400.

[148] E. J. Windhab. Fluid immobilization - a structure-related key mechanism for the viscous flow behavior of concentrated suspension systems. *Applied Rheology*, 10(3):133–144, 2000. doi: 10.3933/ApplRheol-10-134.

[149] Y. Zhang, A. Lervik, J. Seddon, and F. Bresme. A coarse-grained molecular dynamics investigation of the phase behavior of dppc/cholesterol mixtures. *Chemistry and Physics of Lipids*, 185: 88–98, 2015. doi: 10.1016/j.chemphyslip.2014.07.011.

[150] G. Ziegleder, G. Balimann, Mikle H., and Zaki H. Neue Erkenntnisse über das Conchieren: Teil 2: Aroma-Untersuchung. *Süsswaren*, 48(4):16–18, 2003.